Appendix 2:
Configuration Flexibility in HSX

A2.0 Introduction

The HSX auxiliary coils provide a substantial degree of flexibility to the device. It is possible to drastically change the magnetic field spectrum without substantially changing the well depth, rotational transform, or plasma boundary shape. Alternatively, the well depth can be changed without a significant change to the spectrum. Magnetic islands can be introduced or eliminated. As part of the research conducted for this dissertation, these different configurations were thoroughly studied. This appendix provides information on the different configurations available to HSX, in a format of use to somebody designing and performing experiments.

A detailed explanation of the information provided in the appendix is given in Section 2.1. The information on the Mirror and antiMirror configurations in given in Section 2.2. Data on the Well and Hill configurations if provided in Section 2.3. Two alternative Mirror configurations, designed to excite spectral components with toroidal mode numbers greater than 4 are briefly discussed in Section 2.4.

A2.1 Data Contained in this Appendix.

All calculations presented here were made using a Biot-Savart code to calculate the HSX magnetic field. The main coils are represented by 14 turns, 60 sticks per turn, and are closed at the feed block. The auxiliary coils are also closed, and are represented by a single turn. The single turn has between 41 and 45 sticks, depending on the coil. The various quantities that are presented in this appendix are described as follows:

Polynomial Fits to Profiles:

Both $dV/d\psi$ and ι are specified in polynomial form as a function of radius. All curves can be fit sufficiently well with polynomial of the form:

$$f(\xi) = \sum_{k=0} A_k \xi^k \tag{A2.1}$$

where ξ is a radial variable defined as

$$\xi = \sqrt{\frac{\psi}{\psi_{boundary}}} \tag{A2.2}$$

Profiles of the rotational transform, $dV/d\psi$, and well depth are shown in this appendix. They are plotted against an effective plasma radius (r_{eff}) defined as:

$$r_{eff} = \xi \sqrt{\frac{\psi_{boundary}}{\pi(.5\text{Tesla})}} \tag{A2.3}$$

This choice of independent variable has the advantage of illustrating the differences in size of the different configurations.

Machine Configurations:

In the following work, the machine configuration will be specified by a "stencil" specifying the auxiliary coil currents and an amp-turn percentage in the auxiliary coils. The amp turn percentage is divided by 100 and then multiplied by the stencil to give the auxiliary coil current configuration. The stencils used in this appendix are given in table A2.1

Configuration	Coil 1	Coil 2	Coil 3	Coil 4	Coil 5	Coil 6
Mirror, Type 1	1	1	1	-1	-1	-1
Mirror, Type 2	1	-1	1	-1	1	-1
Mirror, Type 3	1	-1	-1	1	1	-1
Hill/Well	1	1	1	1	1	1

Table A2.1: Stencils for various auxiliary coil configurations

Note that Type 1 Mirror is the standard Mirror configuration that HSX typically is operated in. Type 2 and 3 Mirrors are configurations where an attempt is made to excite a n>4 spectral components. The antiMirror configurations are accessed by multiplying the stencils by negative amp-turns, and Mirror configurations use positive amp-turns. The Hill configuration of the auxiliary coils adds toroidal field everywhere, leading to a drop in the rotational transform, while the Well configuration subtracts toroidal field everywhere.

Main Current:

Unless otherwise noted, current specified for a given configuration is that required to place the ECH resonance (|B|=0.5T) on the magnetic axis at the box port. For a given amp-turns percentage (%) and main coil current, the auxiliary coil current for central resonance can be calculated as

$$I_{aux} = \left(\frac{\%}{100}\right)\frac{14 I_{main}}{10} \tag{A2.4}$$

The required main current (for central resonance) for the different configurations can be fit to a polynomial of the form:

$$I(\%) = \sum_{k=0} A_k (\%)^k \tag{A2.5}$$

The fit coefficients are given in table A2.2, for the different configurations under discussion here. The term A_o is the current required for QHS central resonance. The two amp difference in the calculation below is indicative of the error in the fits.

Configuration	A_o	A_1	A_2
Type 1 Mirror	5360.20504969796	-44.19885742206	0.38820759802
Hill/Well	5362.39188177955	-66.03272438081	0.72693525977

Table A2.2: Main coil current fit coefficients for different configurations of HSX.

Edge at Box Port.

This is the coordinate of the edge of the plasma at $\Phi=0$, $Z=0$. It is selected by following field lines at closely spaced intervals, and judging whether a good surface is formed by the quality of the Poincarre plot, the quality of the flux calculation, and the convergence of the dV/dψ calculation. In the end, this determination is a judgment call, and the error in this calculation is of the order (+0.001,-0). This error leads to an error in the determination of the total volume, the edge rotational transform, and the boundary flux. Note that in a few cases, the plasma is limited by the vessel wall, i.e. the LCFS intersects the vacuum vessel.

ɫ(r/a=0) & ɫ(r/a=1):

These are the rotational transform at the axis and at the boundary. They are computed based on the Hamada spectrum, using techniques described in Chapter 5. The rotational transform on the axis changes smoothly as the configuration is scanned. The edge transform is not a smooth function of the amp-turns in the auxiliary coil set.

Toroidal Flux:

The flux (ψ) is the total toroidal flux passing through a vertical cut at the joint flange. In general, the joint flange is easier for area integration than the box port, as the surfaces there are not as corrugated near the boundary.

dV/dψ:

This quantity is computed as $\frac{dV}{d\psi} = \frac{1}{N}\int \frac{dl}{B}$, as part of both the initial surface calculation and when computing the Hamada spectrum. It is used to calculate the volume of the LCFS, and can be used to calculate the well depth of the different configurations.

Volume:

This is the volume enclosed by the last closed flux surface, in m^3. The volume is calculated by two different methods. The method involves integrating the calculated values of $dV/d\psi$ outward from the magnetic axis, using the calculated values of flux. The second method involves a Monte Carlo integration method. Note that the volume is not a smooth function of the amp-turns percentage or the magnet currents. The calculated volume is also dependent upon the decision made in locating the LCFS.

Magnetic Axis Location:

This is the value of the R coordinate at the magnetic axis, at the box port (Φ=0, π/2, π, 3π/2, Z=0), and at the joint flange (Φ=π/4, 3π/4, 5π/4, 7π/4, Z=0). The magnetic axis shifts as the configuration is changed but is independent of the resonance location.

Well Depth:

This well depth is calculated as

$$\text{W.D.} = \frac{\frac{dV}{d\psi}\left(\frac{r}{a}=0\right) - \frac{dV}{d\psi}}{\frac{dV}{d\psi}\left(\frac{r}{a}=0\right)} \qquad \text{(A2.6)}$$

Note that this can be calculated by the user, based on the fits to $dV/d\psi$ presented in this appendix.

Magnetic Shear:

The magnetic shear parameter is defined in this appendix as

$$s = -\frac{r_{eff}}{\iota\!\!\!-}\frac{\partial \iota\!\!\!-}{\partial r_{eff}} = -\frac{\xi}{\iota\!\!\!-}\frac{\partial \iota\!\!\!-}{\partial \xi} \qquad \text{(A2.7)}$$

This definition can be derived from the standard tokamak shear parameter,[1] when that expression is written in terms of $\iota\!\!-$ instead of q. Plots of this parameter are shown for the for the different configurations. It can be easily calculated from the polynomial fits of $\iota\!\!-$ vs ξ.which are provided in this appendix.

***Resonance Shifting*:**

For any given configuration of HSX, the ECH resonance (location where |B|=.5T) can be shifted along the midplane at the boxport, leading to a shift of the heating location. The resonance location is specified by the flux surface label ξ of the surface on which resonance sits $\left(\xi = \sqrt{\frac{\psi}{\psi_{\text{boundary}}}}\right)$. The main coil current to achieve the resonance location can be related to the shift by a 5th order polynomial:

$$I_{\text{main}}(\zeta) = \sum_{k=0}^{5} A_k \zeta^k \tag{A2.8}$$

Note that negative values of ζ correspond to inboard resonance, with positive values implying outboard resonance. The auxiliary current can then be specified using equation (A2.4). These fit coefficients are tabulated for the different configurations in the sections below.

The currents for shifting the resonance are also provided in graphic form. In each case, the graph presents the quantity $I_{graph}=I_{main}-C_{main}$, where C_{main} is a constant in the legend. Hence, the actual coil current is $I_{main}=I_{graph}+C_{main}$. The auxiliary coil current is specified as $I_{graph}=(I_{aux}-C_{aux})/10$, so that the actual auxiliary current is specified as $I_{aux}=10I_{graph}+C_{aux}$.

As an example, if it were desired to calculate the currents to place the resonance at r/a=0.5 in the Mirror configuration, the main coil current would be I_{main}=4962+300=5262A. The auxiliary current would be I_{aux}=695+420/10=737A.

Puncture Plots

Puncture plots are given for many different configurations of HSX. These plots graphically illustrate the changes in volume and shifts of the axis as the configuration is scanned, as well as the presence of various resonances and island chains. The puncture plots are in vertical planes at Φ=0 (box port) and $\Phi=\pi/4$ (joint flange). Vertical cuts are chosen because they are computationally simpler than helical cuts. Field lines are followed typically 300 field periods, and the points are reflected over the midplane to fill in the surfaces. At each integration step, a check is made if the field line has wandered outside the vessel; the integration is stopped when this occurs.

A2.2 The Type 1 Mirror-QHS-antiMirror Continuum of Configurations

This continuum of configurations mainly represents a scan of the amplitude of the n=4, m=0 spectral component. A few relevant points are as follows:

1) For antiMirror percentages larger than ~13%, the LCFS is determined by the intersection of the magnetic surfaces at the outboard side with the vacuum vessel. This intersection occurs at the toroidal angle of the box port.

2) These is a large discrete jump in volume at between 12.5% and 12.75% Mirror, corresponding to the ι=8/7 islands entering the LCFS.

3) The LCFS for the QHS case is at R=1.5161m, somewhat larger than usually taken by J.N. Talmadge or K.M. Likin.

Amp Turns %	R_{axis}, BP (m)	R_{axis}, JF (m)	R_{edge} (m)	I_{main} (A)	I_{aux} (A)
0	1.4454	1.032	1.5161	5361	0
0.5	1.4449	1.0314	1.5141	5339	37
1	1.4444	1.0309	1.5154	5318	74
1.5	1.4439	1.0304	1.5139	5296	111
2	1.4434	1.0299	1.5126	5276	148
2.5	1.443	1.0295	1.5107	5254	184
3	1.4425	1.0289	1.5095	5234	220
3.5	1.442	1.0285	1.5080	5213	255
4	1.4416	1.028	1.5079	5193	291
4.5	1.4411	1.0275	1.5061	5173	326
5	1.4407	1.0271	1.5048	5152	361
5.5	1.4402	1.0265	1.5032	5133	395
6	1.4398	1.0261	1.5012	5114	430
6.5	1.4394	1.0256	1.5004	5094	464
7	1.4389	1.025	1.4987	5074	497
7.5	1.4385	1.0246	1.4987	5055	531
8	1.438	1.0241	1.4980	5036	564
8.5	1.4376	1.0236	1.4966	5017	597
9	1.4372	1.0231	1.4958	4999	630
9.5	1.4368	1.0227	1.4938	4980	662
10	1.4364	1.0222	1.4928	4961	695
10.5	1.436	1.0218	1.4922	4944	727
11	1.4355	1.0213	1.4905	4926	759
11.5	1.4351	1.0208	1.4881	4907	790
12	1.4347	1.0203	1.4878	4890	822
12.5	1.4343	1.0199	1.4885	4871	852
13	1.4339	1.0194	1.4899	4854	883
13.5	1.4335	1.0189	1.4885	4837	914
14	1.4331	1.0184	1.4881	4819	945
14.5	1.4327	1.0179	1.4847	4802	975
15	1.4324	1.0175	1.4858	4785	1005
15.5	1.432	1.017	1.4850	4769	1035
16	1.4316	1.0166	1.4836	4752	1064
16.5	1.4312	1.0161	1.4822	4735	1094
17	1.4308	1.0156	1.4808	4718	1123
17.5	1.4305	1.0151	1.4800	4701	1152
18	1.4301	1.0147	1.4791	4685	1181
19	1.4294	1.0138	1.4764	4653	1238
20	1.4287	1.0128	1.4727	4621	1294
17.25	1.4306	1.0153	1.4806	4710	1137
17.375	1.4306	1.0153	1.4806	4706	1145
17.625	1.4304	1.015	1.4794	4698	1159
17.75	1.4303	1.0149	1.4793	4694	1166
14.25	1.4329	1.0182	1.4859	4810	960
14.75	1.4326	1.0177	1.4866	4794	990
12.75	1.4341	1.0196	1.4891	4863	868

Table A2.3: Axis locations, plasma edge, and central resonant currents, for the Type 1 Mirror continuum.

Amp Turns %	R_{axis}, BP (m)	R_{axis}, JF (m)	R_{edge} (m)	I_{main} (A)	I_{aux} (A)
0	1.4454	1.032	1.5161	5361	0
-0.5	1.4458	1.0324	1.5168	5382	-38
-1	1.4464	1.0329	1.5184	5404	-76
-1.5	1.4468	1.0334	1.5198	5427	-114
-2	1.4473	1.0338	1.5220	5449	-153
-2.5	1.4478	1.0344	1.5232	5471	-191
-3	1.4483	1.0349	1.5237	5494	-231
-3.5	1.4489	1.0354	1.5239	5518	-270
-4	1.4494	1.0359	1.5224	5540	-310
-4.5	1.4499	1.0364	1.5249	5564	-351
-5	1.4505	1.0369	1.5256	5587	-391
-5.5	1.451	1.0374	1.5280	5612	-432
-6	1.4515	1.0379	1.5295	5635	-473
-6.5	1.452	1.0384	1.5310	5660	-515
-7	1.4526	1.0389	1.5328	5684	-557
-7.5	1.4531	1.0394	1.5347	5709	-599
-8	1.4537	1.0399	1.5363	5734	-642
-8.5	1.4543	1.0405	1.5383	5760	-685
-9	1.4548	1.041	1.5398	5785	-729
-9.5	1.4554	1.0415	1.5404	5811	-773
-10	1.4559	1.042	1.5430	5836	-817
-10.5	1.4565	1.0425	1.5445	5862	-862
-11	1.4571	1.043	1.5470	5889	-907
-11.5	1.4577	1.0435	1.5479	5916	-952
-12	1.4583	1.0441	1.5493	5943	-998
-12.5	1.4589	1.0446	1.5487	5969	-1045
-13	1.4595	1.0451	1.5500	5998	-1092
-13.5	1.4601	1.0456	1.5500	6025	-1139
-14	1.4607	1.0462	1.5500	6054	-1187
-14.5	1.4613	1.0467	1.5500	6082	-1235
-15	1.462	1.0473	1.5500	6110	-1283
-15.5	1.4626	1.0478	1.5500	6139	-1332
-16	1.4632	1.0483	1.5500	6169	-1382
-16.5	1.4639	1.0488	1.5500	6198	-1432
-17	1.4645	1.0493	1.5500	6229	-1483
-17.5	1.4652	1.0499	1.5500	6258	-1533
-18	1.4658	1.0504	1.5500	6288	-1585
-19	1.4671	1.0515	1.5500	6350	-1689
-20	1.4685	1.0526	1.5500	6413	-1796
-3.75	1.4491	1.0356	1.5261	5528	-290
-9.75	1.4557	1.0418	1.5427	5823	-795
-10.25	1.4562	1.0422	1.5432	5849	-839

Table A2.4: Axis locations, plasma edge, and central resonant currents, for the Type 1 antiMirror continuum.

Amp Turns %	Boundary Flux (Tm^2)	ɨ(0)	ɨ(0)	Volume ($dV/d\psi$) (m^3)	Volume (MC) (m^3)
0	0.0212	1.0500	1.1091	0.378	0.381
0.5	0.0205	1.0509	1.1071	0.368	0.371
1	0.0212	1.0519	1.1143	0.380	0.381
1.5	0.0209	1.0527	1.1149	0.376	0.379
2	0.0206	1.0543	1.1161	0.371	0.375
2.5	0.0201	1.0558	1.1159	0.364	0.367
3	0.0198	1.0555	1.1161	0.362	0.362
3.5	0.0195	1.0562	1.1165	0.356	0.360
4	0.0197	1.0568	1.1231	0.361	0.364
4.5	0.0193	1.0579	1.1211	0.355	0.349
5	0.0189	1.0576	1.1230	0.350	0.351
5.5	0.0185	1.0597	1.1214	0.344	-1.000
6	0.0179	1.0621	1.1182	0.333	0.336
6.5	0.0178	1.0613	1.1220	0.333	-1.000
7	0.0174	1.0622	1.1213	0.326	0.326
7.5	0.0175	1.0629	1.1250	-1.000	0.334
8	0.0174	1.0637	1.1293	0.330	0.333
8.5	0.0171	1.0645	1.1294	0.325	0.328
9	0.0169	1.0653	1.1325	0.322	0.321
9.5	0.0164	1.0661	1.1296	0.314	-1.000
10	0.0162	1.0670	1.1301	0.310	0.314
10.5	0.0160	1.0677	1.1356	0.308	0.307
11	0.0156	1.0685	1.1334	0.302	0.307
11.5	0.0150	1.0692	1.1293	0.290	-1.000
12	0.0150	1.0700	1.1338	0.291	0.296
12.5	0.0179	1.0702	1.1562	0.349	-1.000
13	0.0189	1.0714	1.1717	0.372	0.376
13.5	0.0184	1.0720	1.1702	0.362	-1.000
14	0.0178	1.0728	1.1690	0.353	0.376
14.5	0.0166	1.0736	1.1607	0.330	-1.000
15	0.0180	1.0758	1.1822	0.359	0.365
15.5	0.0181	1.0751	1.1872	0.361	-1.000
16	0.0174	1.0757	1.1833	0.350	0.354
16.5	0.0168	1.0763	1.1808	0.338	-1.000
17	0.0162	1.0770	1.1782	0.327	0.332
17.5	0.0161	1.0778	1.1829	0.328	-1.000
18	0.0160	1.0784	1.1880	0.330	0.332
19	0.0148	1.0796	1.1809	0.304	0.308
20	0.0128	1.0809	1.1649	0.265	-1.000
17.25	0.0163	1.0774	1.1830	0.331	-1.000
17.375	0.0166	1.0776	1.1888	0.337	-1.000
17.625	0.0157	1.0779	1.1787	0.320	-1.000
17.75	0.0158	1.0781	1.1813	0.322	-1.000
14.25	0.0173	1.0732	1.1651	0.342	-1.000
14.75	0.0184	1.0740	1.1829	0.366	-1.000
12.75	0.0183	1.0711	1.1626	0.358	-1.000

Table A2.5: Boundary flux, rotational transform, and volume information for Type 1 Mirror continuum.

Amp Turns %	Boundary Flux (Tm^2)	$\iota(0)$	$\iota(0)$	Volume ($dV/d\psi$) (m^3)	Volume (MC) (m^3)
0	0.0212	1.0500	1.1091	0.378	0.381
-0.5	0.0212	1.0491	1.1056	0.376	0.378
-1	0.0216	1.0483	1.1056	0.382	0.384
-1.5	0.0219	1.0473	1.1051	0.386	0.388
-2	0.0226	1.0463	1.1072	0.397	0.399
-2.5	0.0227	1.0442	1.1045	0.398	-1.000
-3	0.0226	1.0445	1.1018	0.395	0.395
-3.5	0.0225	1.0434	1.0984	0.391	-1.000
-4	0.0206	1.0425	1.0863	0.357	0.358
-4.5	0.0211	1.0416	1.0882	0.365	-1.000
-5	0.0213	1.0416	1.0843	0.366	0.368
-5.5	0.0219	1.0396	1.0868	0.375	-1.000
-6	0.0222	1.0386	1.0859	0.380	0.381
-6.5	0.0226	1.0377	1.0853	0.384	-1.000
-7	0.0230	1.0366	1.0852	0.389	0.390
-7.5	0.0234	1.0363	1.0842	0.394	-1.000
-8	0.0237	1.0346	1.0846	0.399	0.397
-8.5	0.0242	1.0336	1.0849	0.405	-1.000
-9	0.0245	1.0325	1.0840	0.409	0.412
-9.5	0.0246	1.0315	1.0815	0.408	-1.000
-10	0.0251	1.0302	1.0829	0.417	0.418
-10.5	0.0254	1.0295	1.0820	0.420	-1.000
-11	0.0256	1.0284	1.0800	0.422	0.422
-11.5	0.0261	1.0273	1.0804	0.427	-1.000
-12	0.0263	1.0262	1.0791	0.430	0.431
-12.5	0.0259	1.0241	1.0757	0.422	-1.000
-13	0.0261	1.0240	1.0728	0.424	0.423
-13.5	0.0259	1.0230	1.0694	0.419	-1.000
-14	0.0250	1.0220	1.0630	0.403	0.404
-14.5	0.0247	1.0208	1.0593	0.396	-1.000
-15	0.0242	1.0191	1.0565	0.388	0.389
-15.5	0.0237	1.0187	1.0512	0.378	-1.000
-16	0.0233	1.0175	1.0476	0.370	0.369
-16.5	0.0228	1.0162	1.0440	0.361	-1.000
-17	0.0222	1.0154	1.0403	0.351	0.352
-17.5	0.0217	1.0141	1.0367	0.341	-1.000
-18	0.0211	1.0127	1.0333	0.331	0.333
-19	0.0200	1.0107	1.0266	0.311	-1.000
-20	0.0186	1.0085	1.0201	0.288	-1.000
-3.75	0.0232	1.0429	1.1017	0.403	-1.000
-9.75	0.0251	1.0310	1.0840	0.416	-1.000
-10.25	0.0251	1.0300	1.0810	0.416	-1.000

Table A2.6: Boundary flux, rotational transform, and volume Information for Type 1 antiMirror continuum.

Amp Turn %	A_0	A_1	A_2	A_3	A_4	A_5
16	1.0757	.0016766	.016385	0.11941	-.16938	0.13959
14	1.0728	.0020299	.018291	0.063059	-.059575	0.567899
12	1.0699	.0058833	-.041832	0.23814	-.30742	0.16871
10	1.0668	.0077317	-.054029	0.24963	-.30516	0.16543
8	1.0635	.017081	-.13938	0.49097	-.58778	0.28416
6	1.0604	.0044137	-.03179	0.15173	-0.16937	00.10378
4	1.0571	.0014223	-.0075576	0.064649	-.05274	0.056654
2	1.0536	.0062623	-.059927	0.22501	-.26148	0.15213
0	1.05	.0024	-.02381	0.086768	-.07433	0.0060676
-2	1.0462	.0082105	-.080862	0.25771	-.28714	0.16271
-4	1.0425	.0042069	-.045399	0.13238	-.13066	0.083238
-6	1.0385	.0065992	-.071717	0.2081	.22489	0.1291
-8	1.0345	.0086805	-.094307	.27106	-.30294	.16742
-10	1.0304	.0031904	-.046077	.11165	-.10064	.076335
-12	1.0261	.0083832	-.097152	.26379	-.29065	.16824
-14	1.0219	.0041728	-.05785	.13098	-.12135	.085102
-16	1.0175	.0012673	-.02964	.037352	-.006245	.027021

Table A2.7: Polynomial fits to iota for Type 1 antiMirror/Mirror

Amp Turn %	A_0	A_1	A_2	A_3	A_4	A_5
16	20.2624	.0353066	-.627721	.11941	-.16938	.13959
14	19.9599	.0289731	-.579056	.872478	-.945249	.567899
12	19.6555	.0160435	-.355825	.288513	-.191075	.145936
10	19.3668	0.0107499	-.336105	.236419	-.131108	.122344
8	19.0811	.0125419	-.363404	.310281	-.210956	.153974
6	18.7915	.0074275	-.307311	.16345	-.0325986	.0690117
4	18.5168	.0112364	-.331214	.188056	-.0285341	.0635264
2	18.243	.0110681	-.328151	.207064	-.0593807	.0740951
0	17.9739	.00882552	-.283691	.134405	.0144549	.0304803
-2	17.7166	.00573446	-.284157	.136399	.0135928	0.394491
-4	17.4604	.0108015	-.269027	.179492	-.0639652	.0552748
-6	17.2071	.00963139	-.264397	.188132	-.0804959	.0665737
-8	16.9566	.0116079	-.273556	.235814	-.139361	.0932145
-10	16.7127	.00488742	-.203333	.092949	.0114351	.0283453
-12	16.4695	.00967796	-.234282	.195803	-.112276	.0885321
-14	16.2312	.0036887	-.162773	.076634	-.0023121	.0382809
-16	15.9978	.0009629	-.112228	.013708	.043213	.0147294

Table A2.8: Polynomial fits to $\frac{dV}{d\psi} = \frac{1}{N}\int \frac{dl}{B}$ **for Type 1 antiMirror/Mirror**

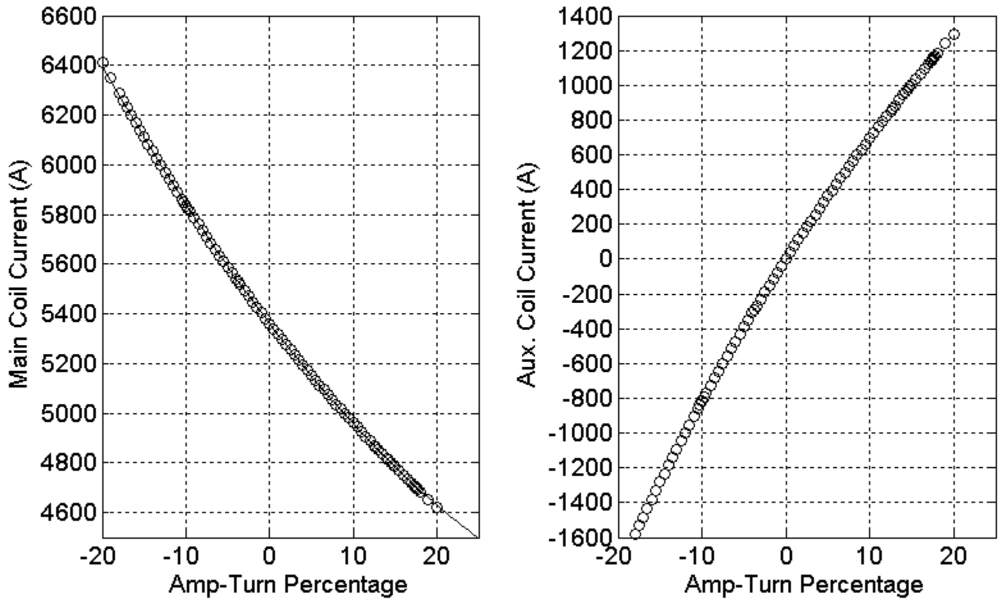

Figure A2.1: Main coil current (left) and Aux. coil current (right) to keep the ECH resonance on axis in the Type 1 Mirror/antiMirror configurations.

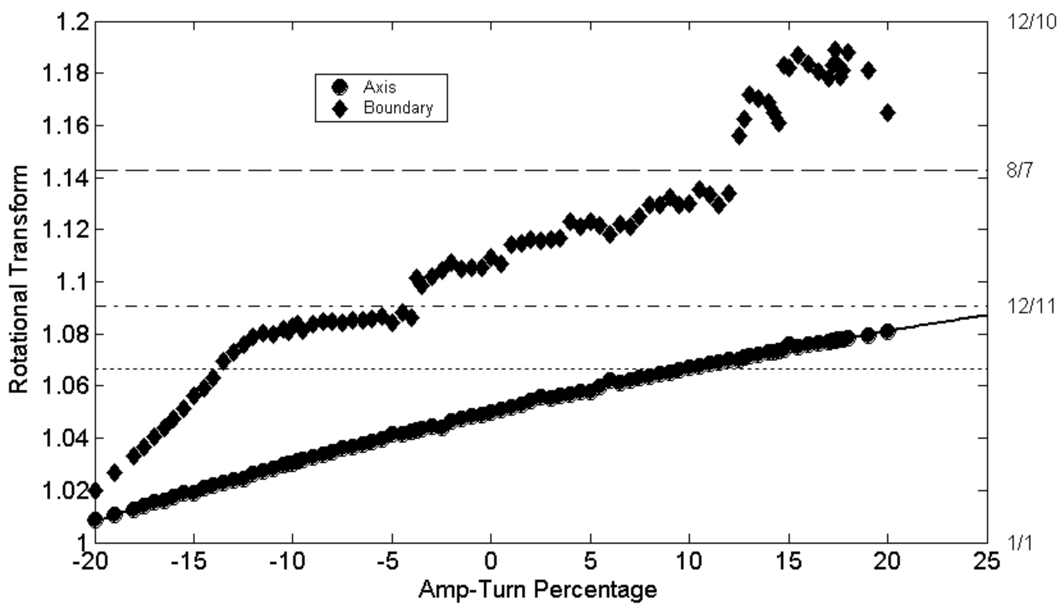

Figure A2.2: Edge and core rotational transform values in the Type 1 Mirror/antiMirror configurations.

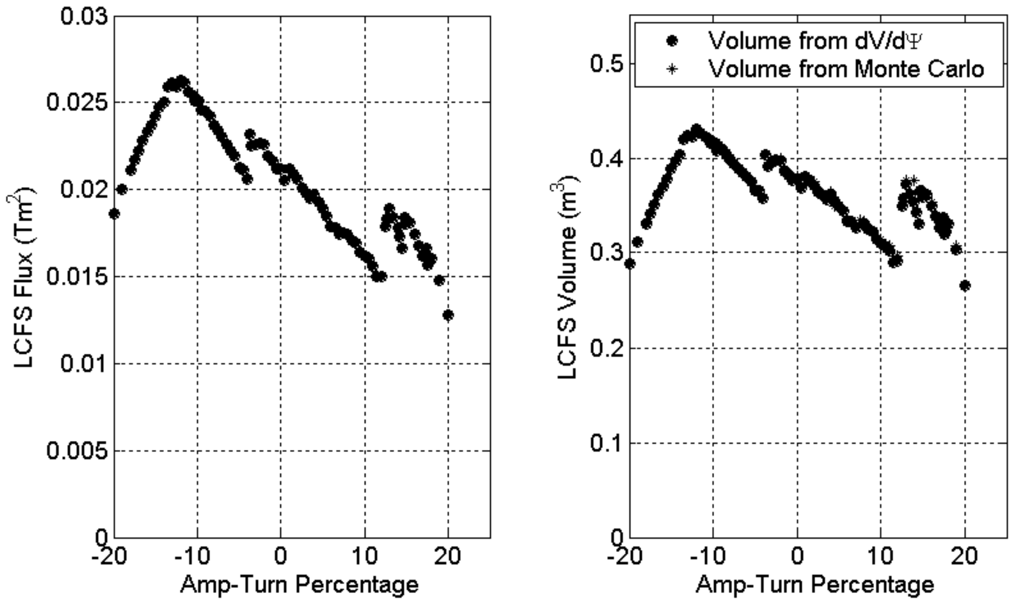

Figure A2.3: Boundary toroidal flux (left) and total volume (right) in the Type 1 Mirror/antiMirror configurations.

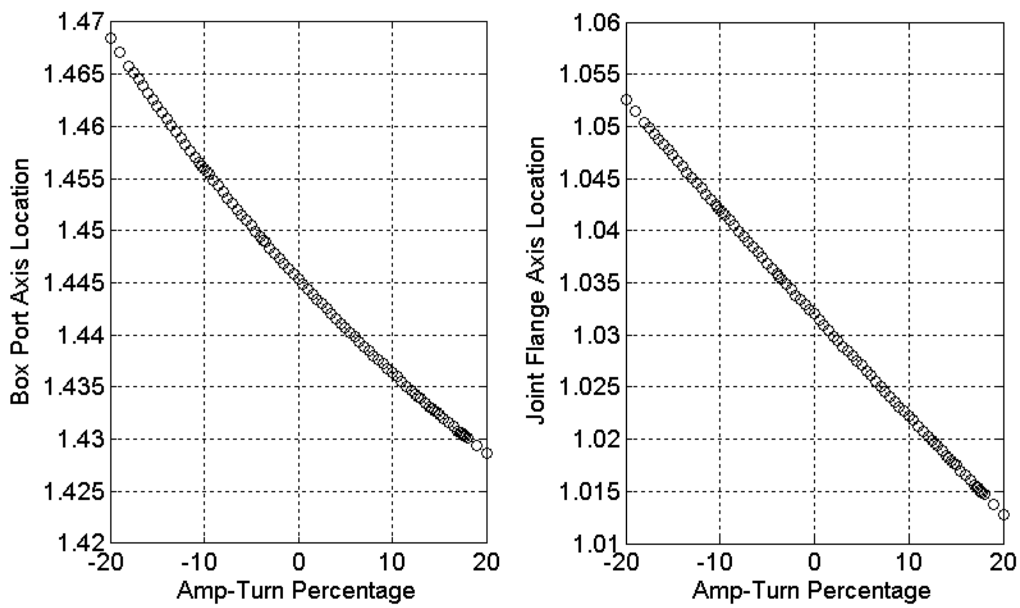

Figure A2.4: Major radius of the magnetic axis at the box port (left) and joint flange (right) in the Type 1 Mirror/antiMirror configurations.

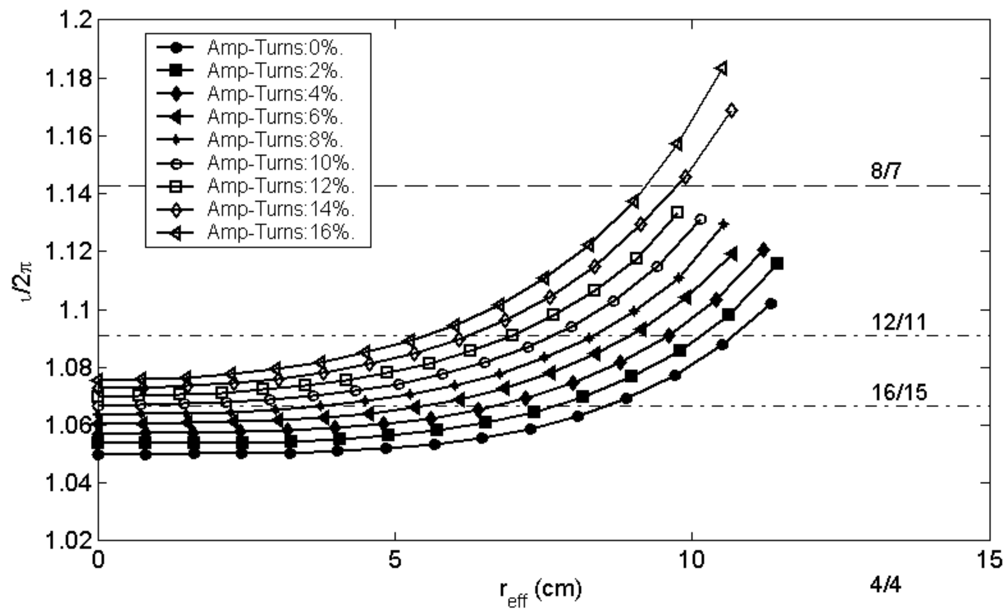

Figure A2.5: Rotational transform profiles in the Type 1 Mirror configurations.

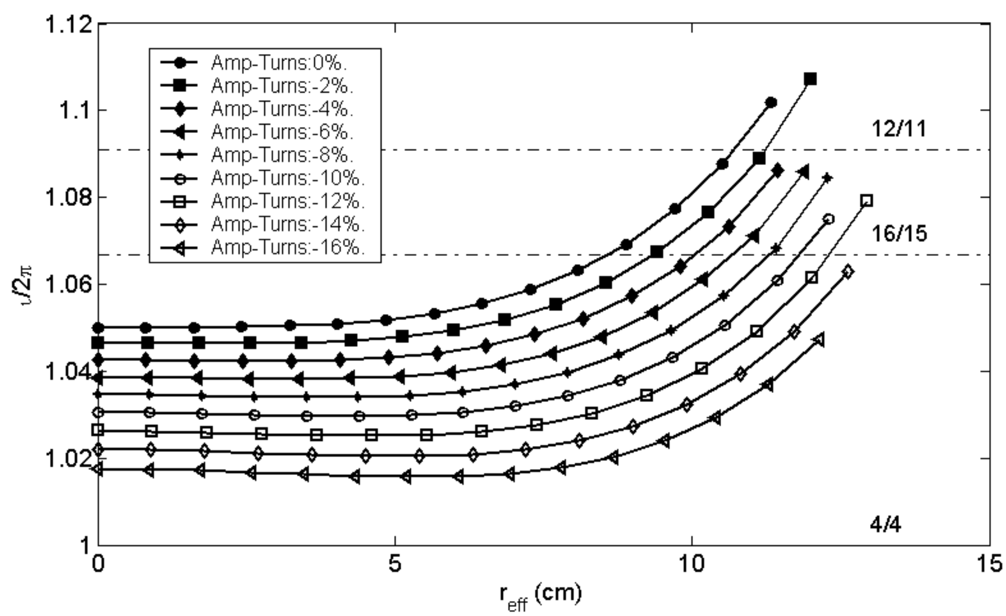

Figure A2.6: Rotational transform profiles in the Type 1 antiMirror configurations.

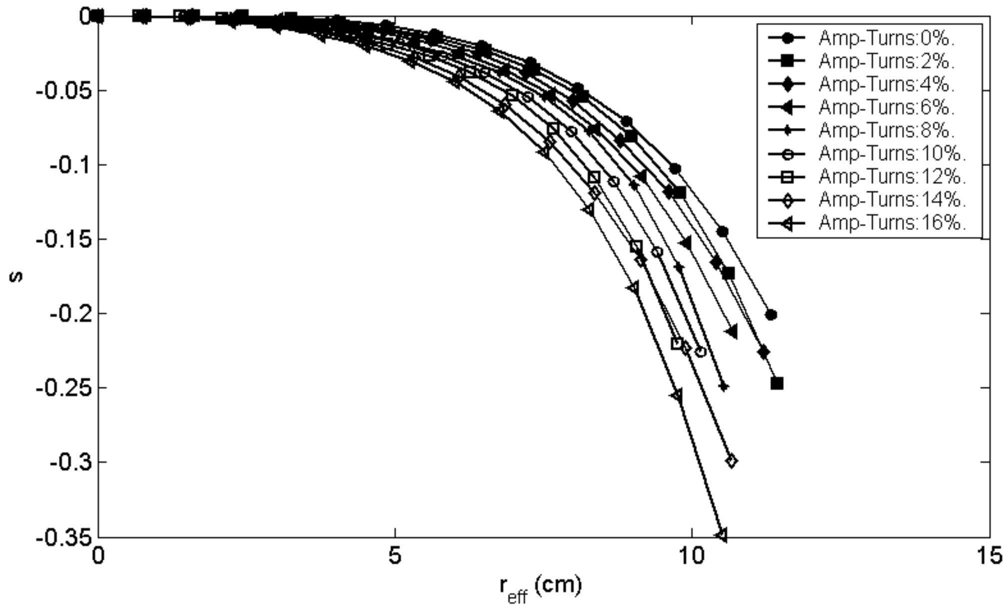

Figure A2.7: Magnetic shear profiles in the Type 1 Mirror configurations.

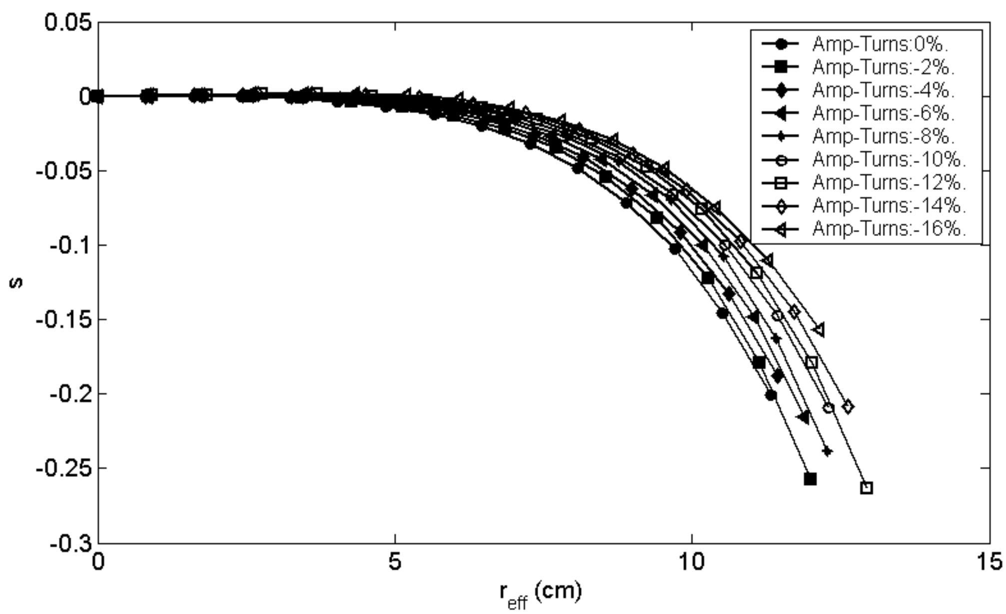

Figure A2.8: Magnetic shear profiles in the Type 1 antiMirror configurations.

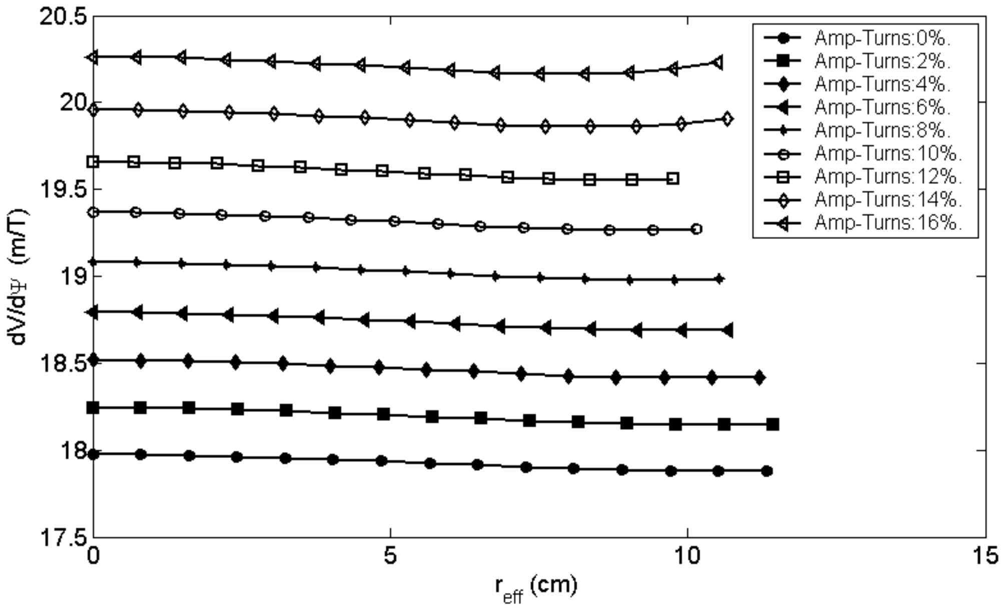

Figure A2.9: dV/dψ profiles in the Type 1 Mirror configurations.

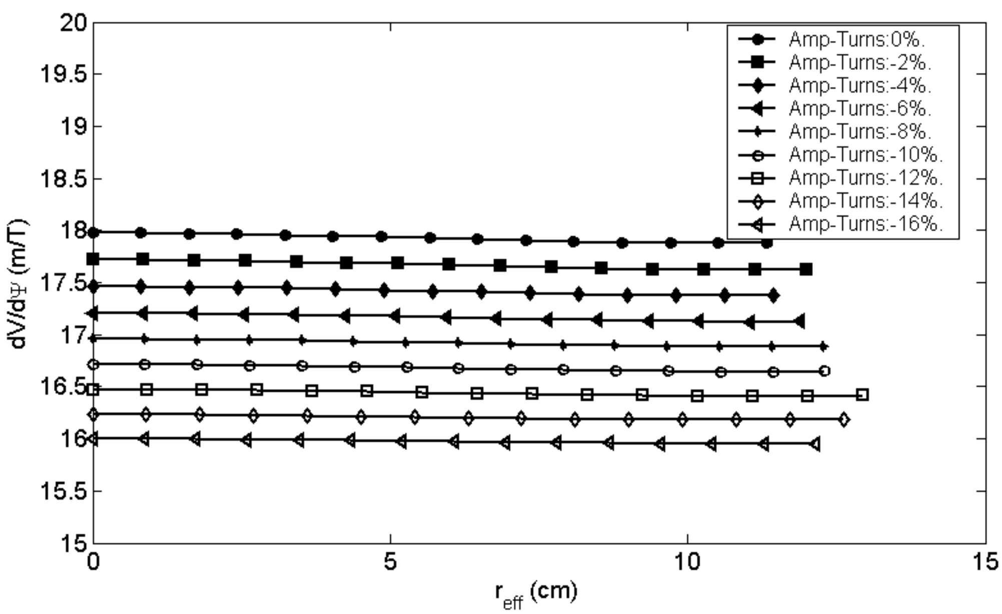

Figure A2.10: dV/dψ profiles in the Type 1 antiMirror configurations.

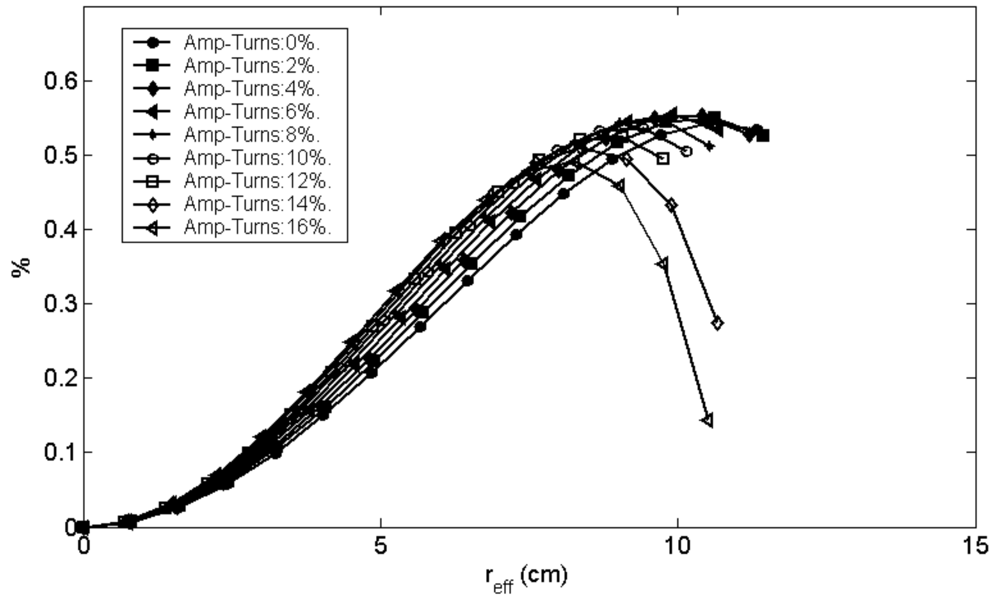

Figure A2.11: Well depth profiles in the Type 1 Mirror configurations.

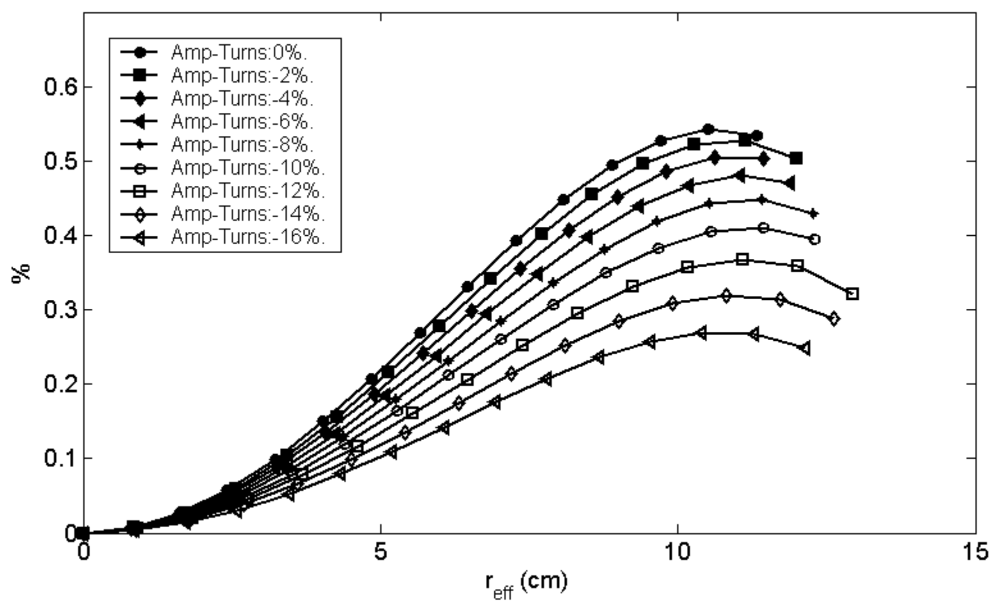

Figure A2.12: Well depth profiles in the Type 1 antiMirror configurations.

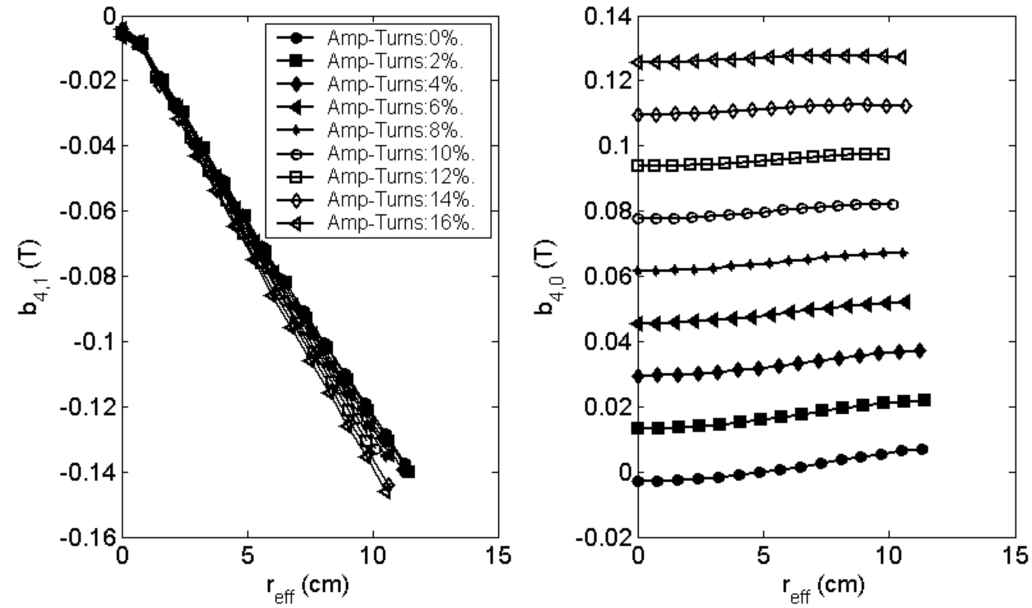

Figure A2.13: Profiles of the (n,m)=(4,1) and (n,m)=(4,0) Hamada spectrum component amplitudes in the Type1 Mirror configuration.

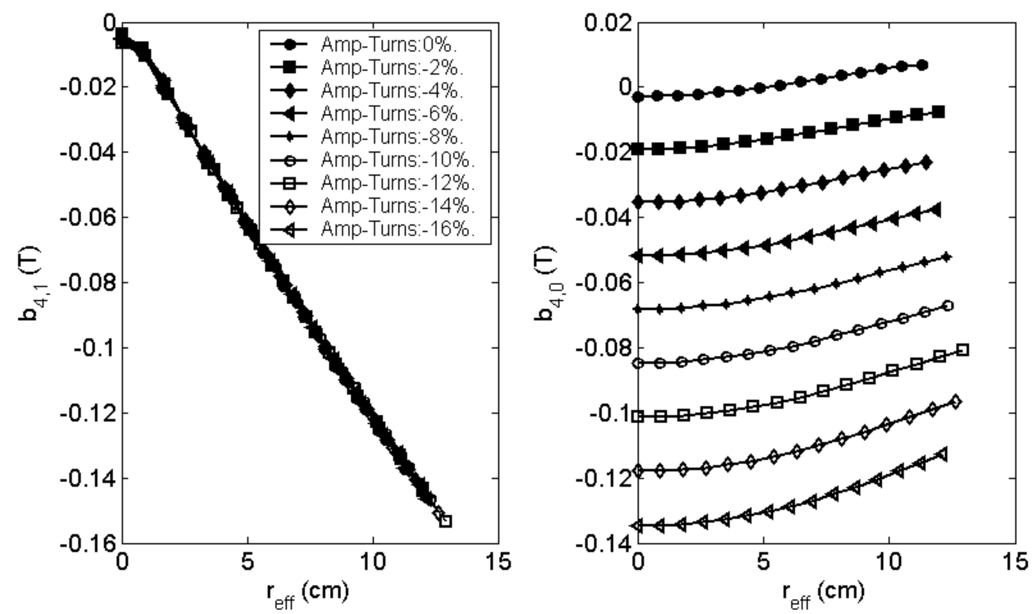

Figure A2.14: Profiles of the (n,m)=(4,1) and (n,m)=(4,0) spectral component amplitudes in the Type1 antiMirror configuration.

Amp-Turn %	A_0	A_1	A_2	A_3	A_4
17	4718.6437	577.99107	-65.65623	-9.7735568	47.923427
15	4785.3436	621.42999	-62.426293	-6.5466785	56.071296
14	4819.3694	623.14803	-54.872234	-4.1418995	51.435373
12	4889.8987	583.02715	-47.264134	0.54479146	48.731614
10	4962.2596	614.9662	-43.417841	1.4570856	53.694679
8	5036.887	656.28388	-38.7909	4.8125103	61.58452
6	5113.9084	679.819	-31.024302	9.5457597	63.145586
5	5153.3265	707.55085	-26.290553	10.767385	64.79281
4	5193.4959	730.5974	-22.336756	11.521956	68.638671
2	5275.9117	763.0311	-14.078008	19.106259	74.36585
0	5361.2313	770.59662	-5.17344	29.956348	73.27219
-2	5449.1698	835.47074	11.08986	44.080608	81.371731
-4	5541.4017	817.19047	10.914138	46.92811	81.968905
-5	5588.3661	841.9258	17.751917	53.818432	85.96951
-6	5636.4652	871.85415	21.415152	60.362612	97.798462
-8	5734.9277	924.70685	36.659154	76.5534425	110.05599
-10	5837.5977	979.03442	47.675095	95.798052	134.01949
-12	5944.0343	1031.2634	65.06143	120.88919	152.76818

Table A2.9: Fit coefficients for I_{main} as a function of flux surface where the resonance resides, for the Mirror/antiMirror continuum of configurations.

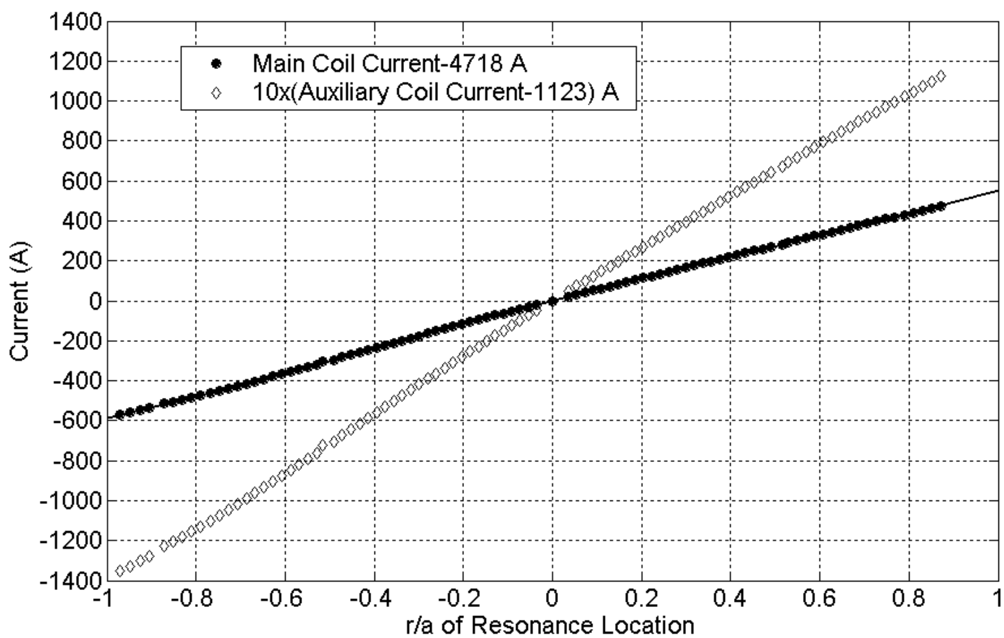

Figure A2.15: Magnet currents for shifting the resonance in the 17% Mirror configuration.

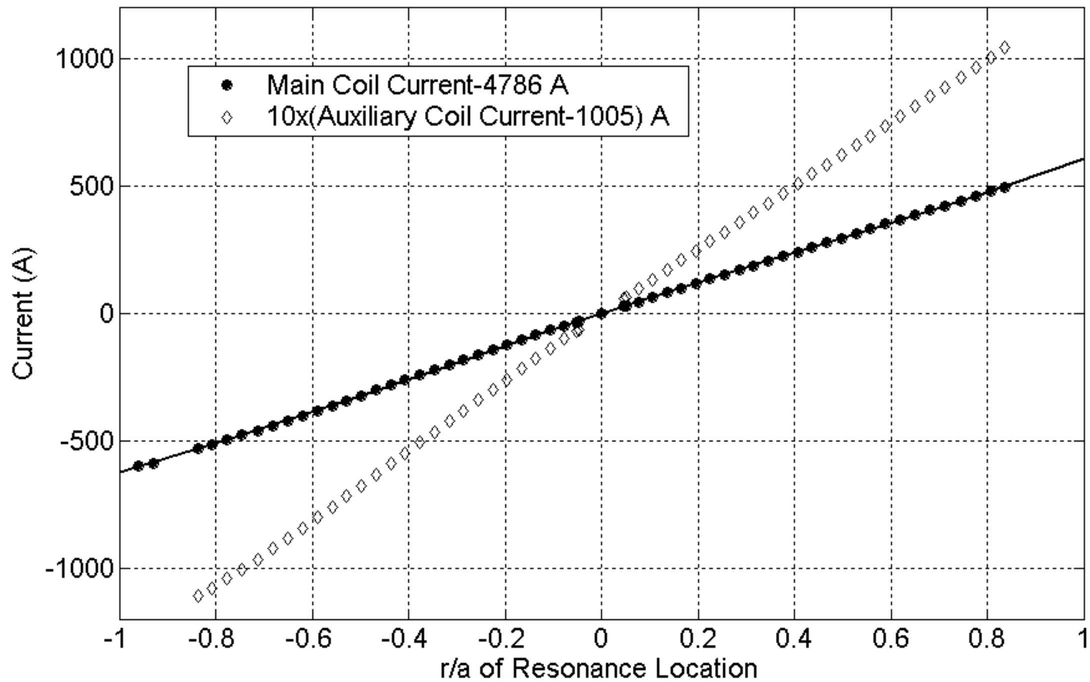

Figure A2.16: Magnet currents for shifting the resonance in the 15% Mirror configuration.

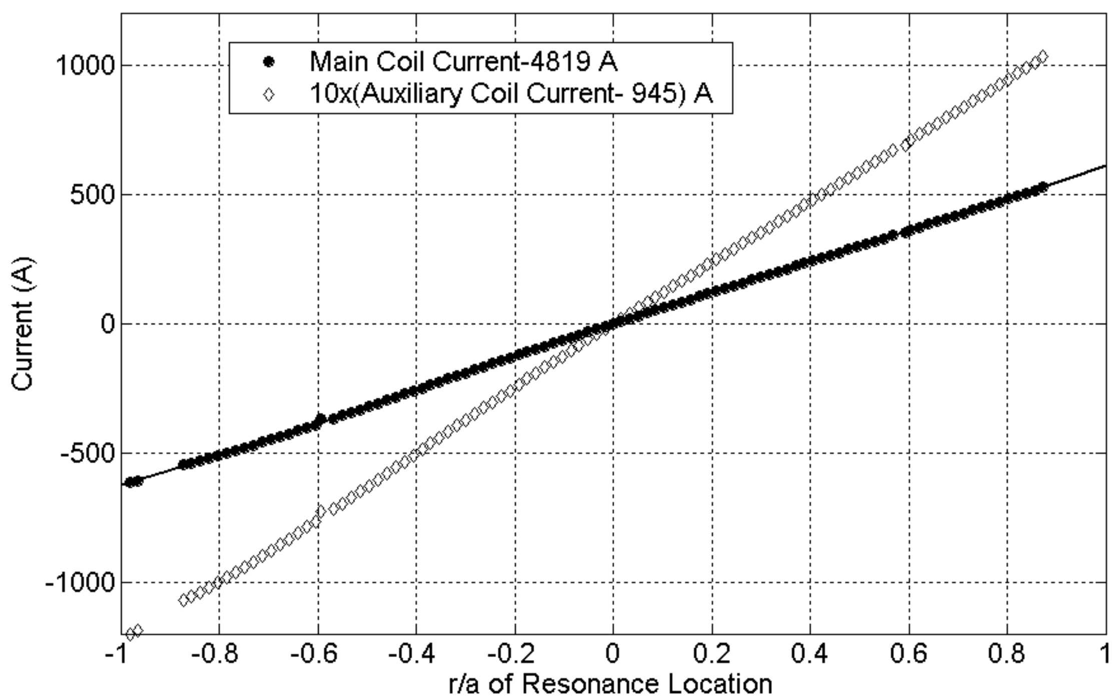

Figure A2.17: Magnet currents for shifting the resonance in the 14% Mirror configuration.

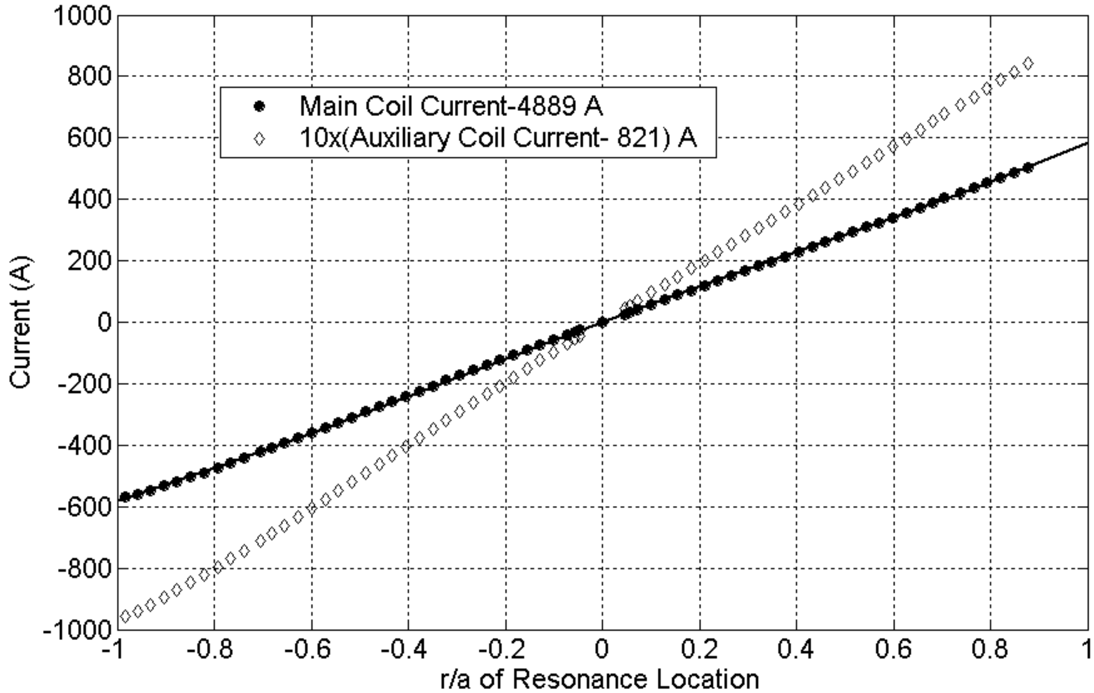

Figure A2.18: Magnet currents for shifting the resonance in the 12% Mirror configuration.

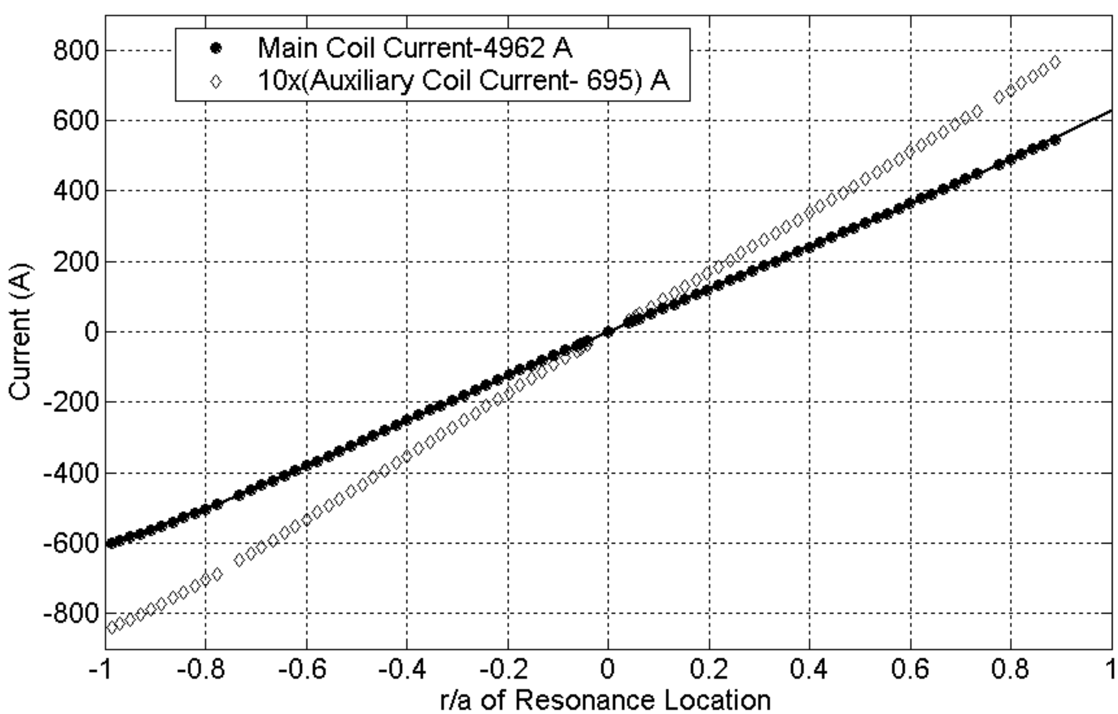

Figure A2.19: Magnet currents for shifting the resonance in the 10% Mirror configuration.

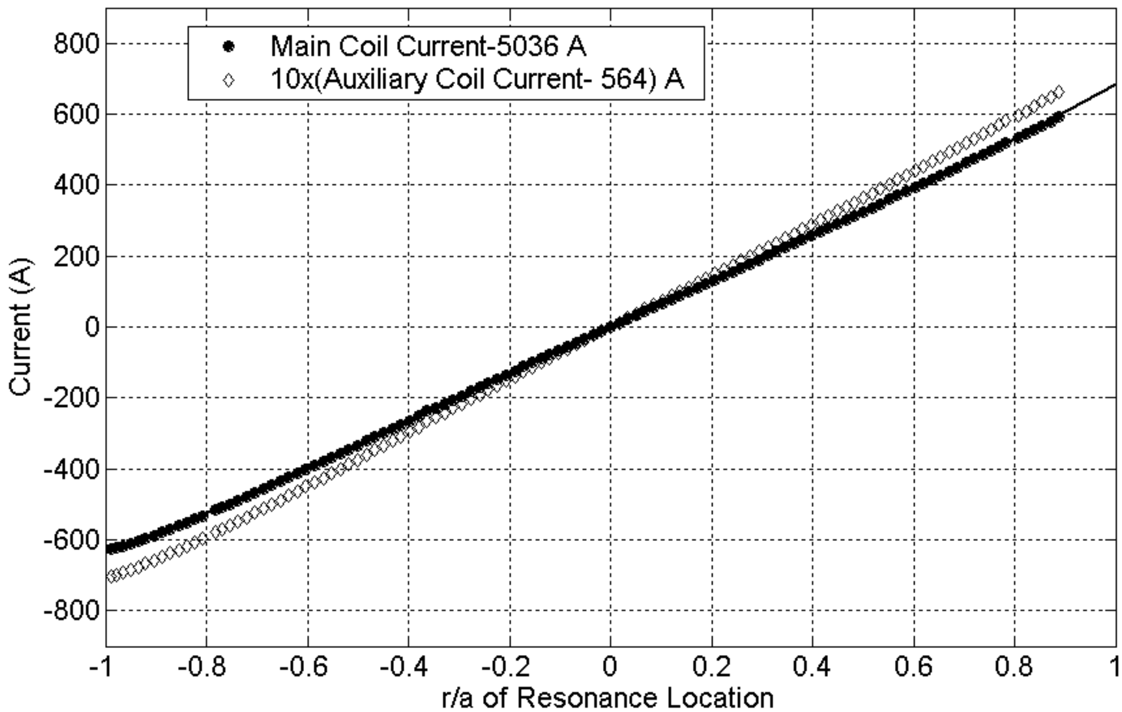

Figure A2.20: Magnet currents for shifting the resonance in the 8% Mirror configuration.

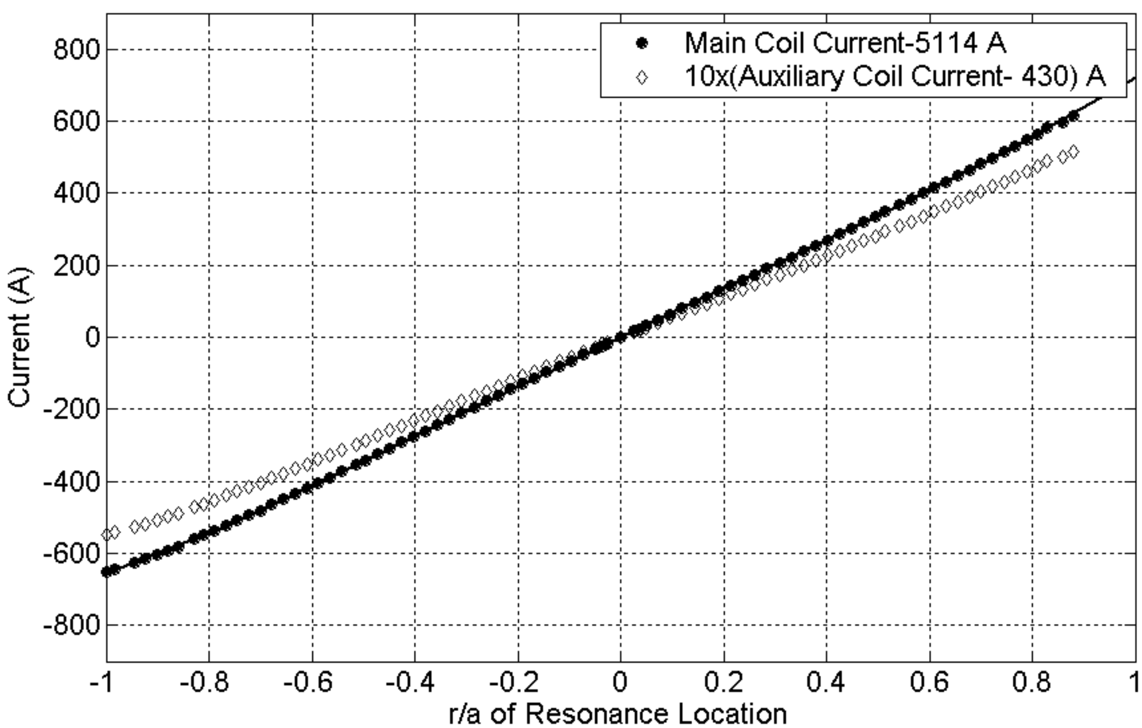

Figure A2.21: Magnet currents for shifting the resonance in the 6% Mirror configuration.

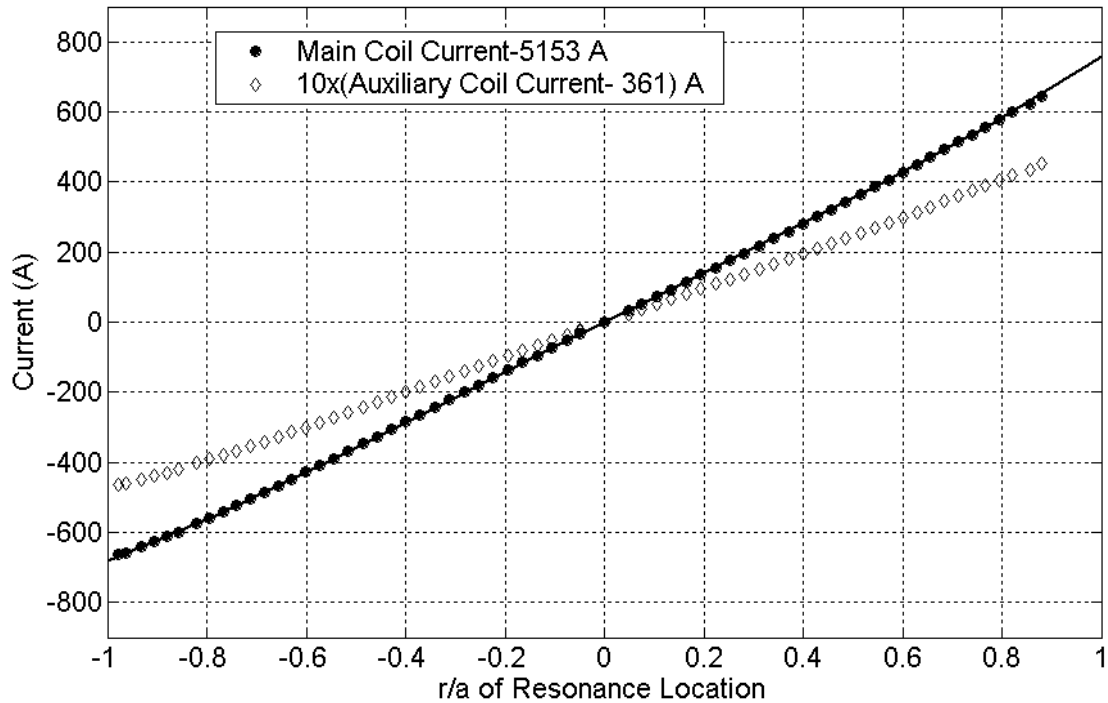

Figure A2.22: Magnet currents for shifting the resonance in the 5% Mirror configuration.

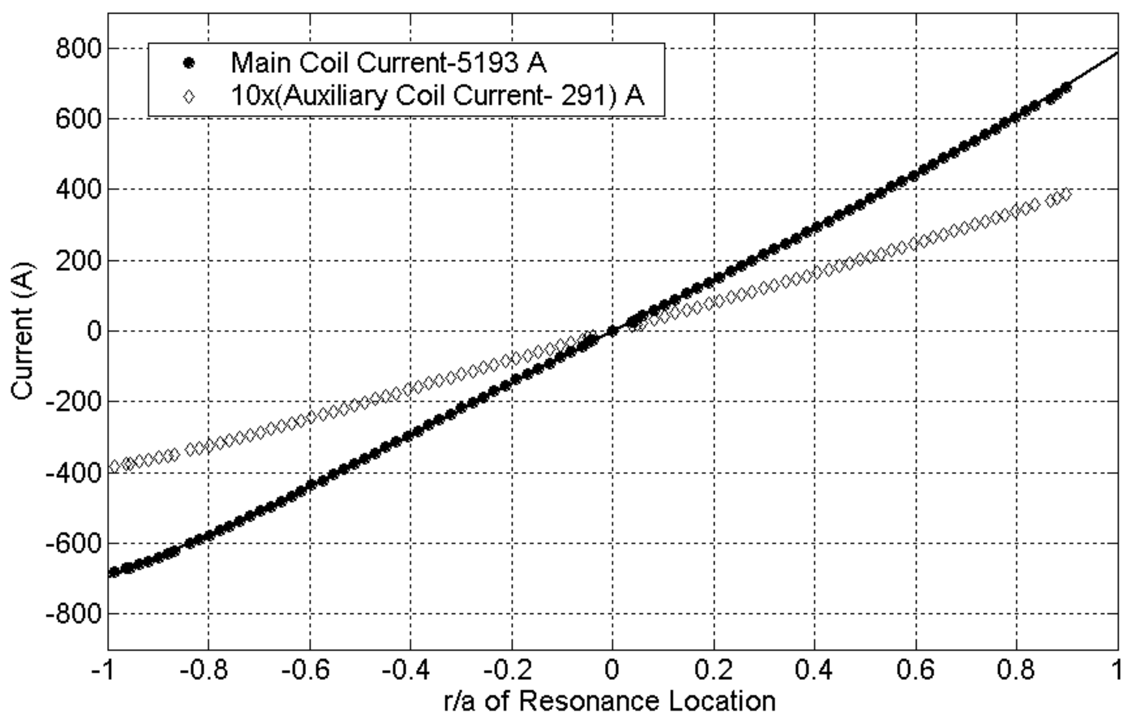

Figure A2.23: Magnet currents for shifting the resonance in the 4% Mirror configuration.

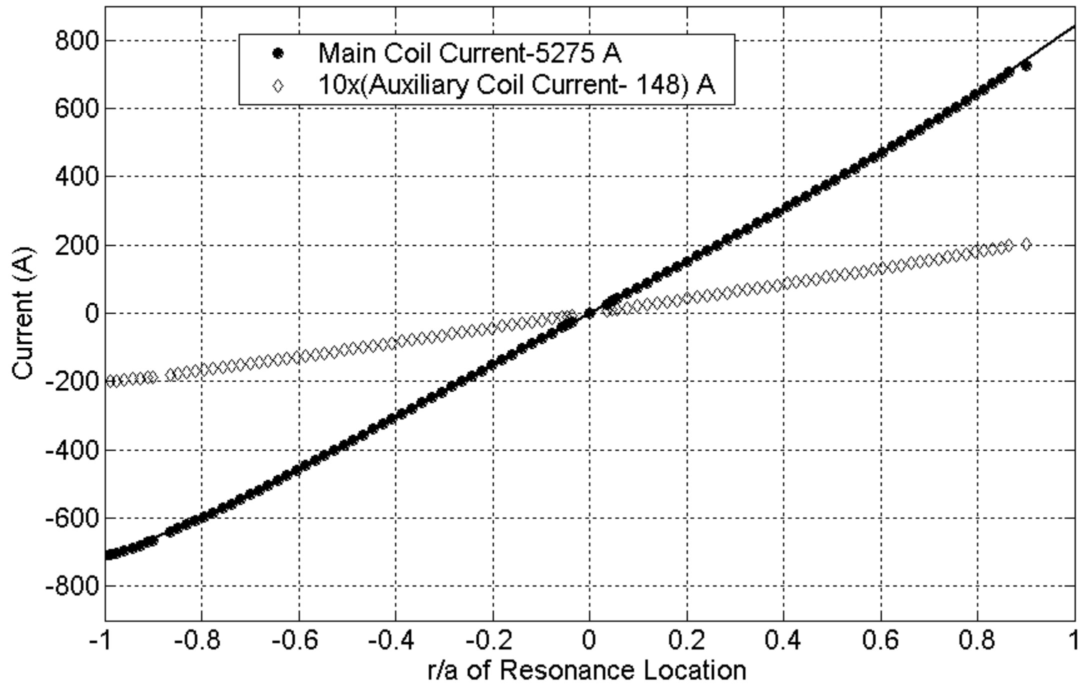

Figure A2.24: Magnet currents for shifting the resonance in the 2% Mirror configuration.

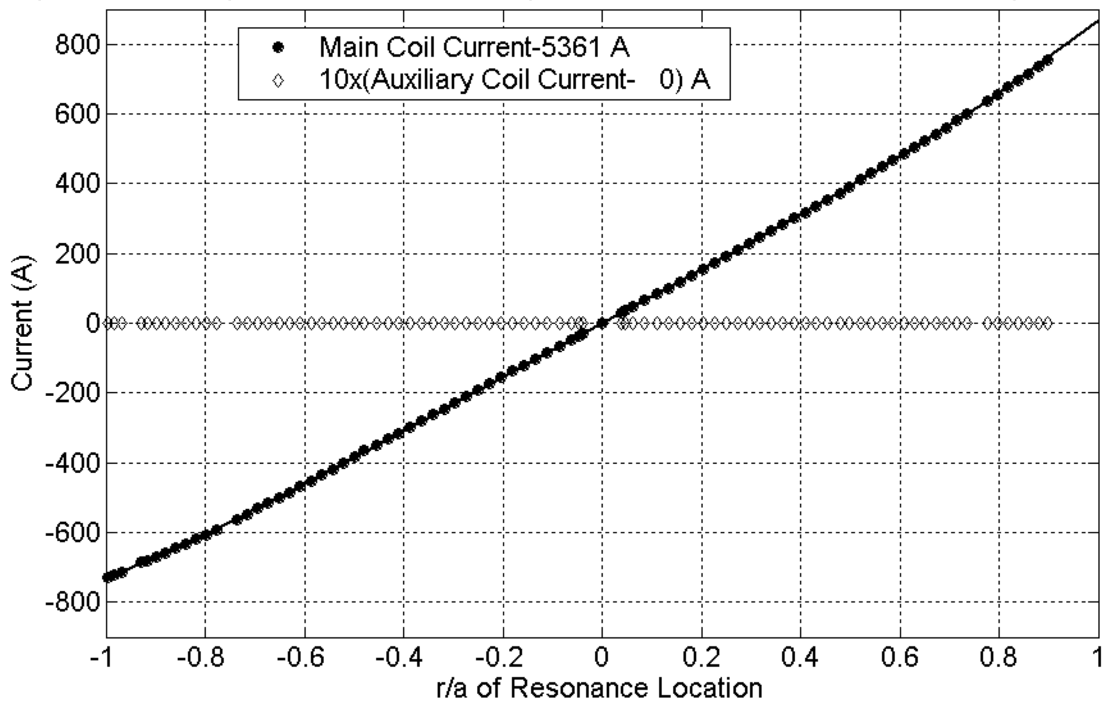

Figure A2.25: Magnet currents for shifting the resonance in the QHS configuration.

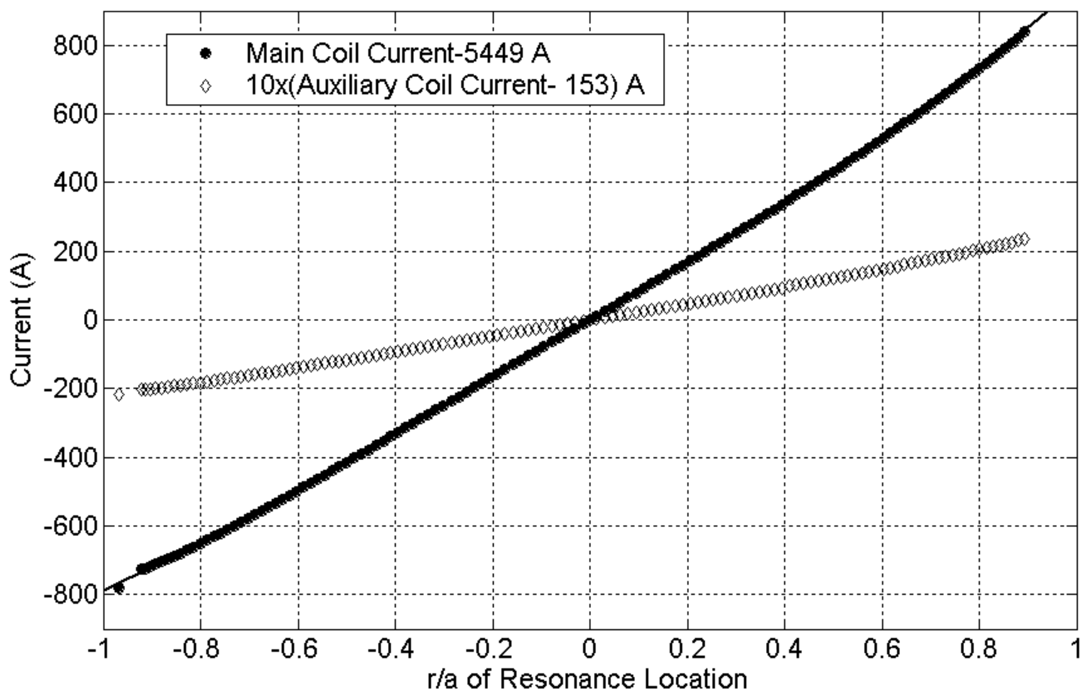

Figure A2.26: Magnet currents for shifting the resonance in the 2% antiMirror configuration.

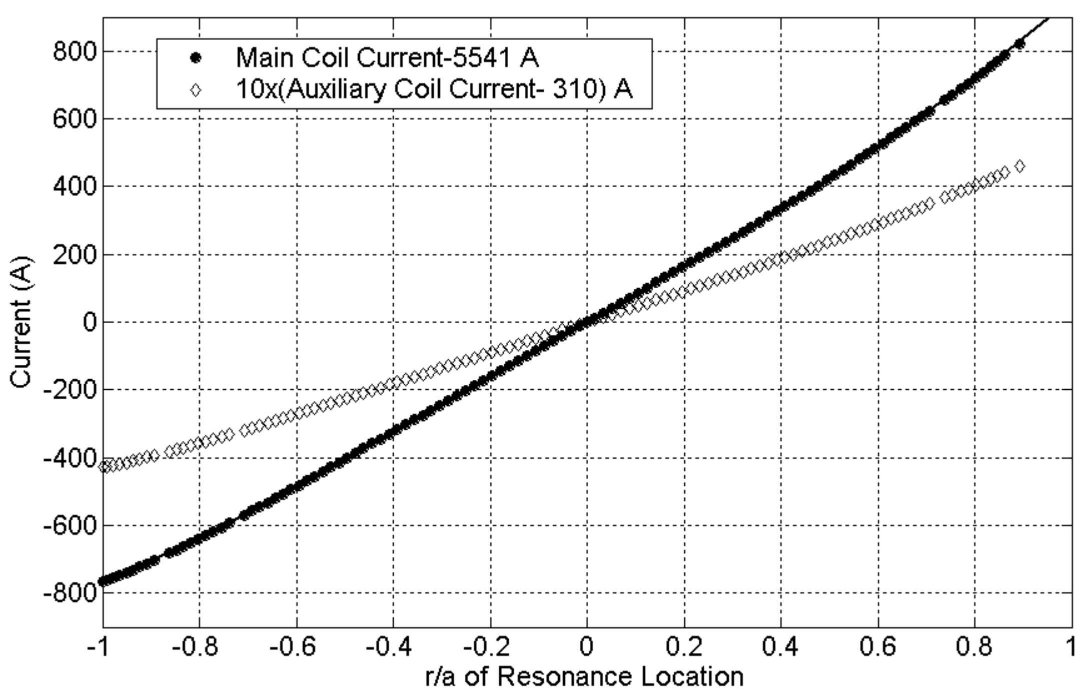

Figure A2.27: Magnet currents for shifting the resonance in the 4% antiMirror configuration.

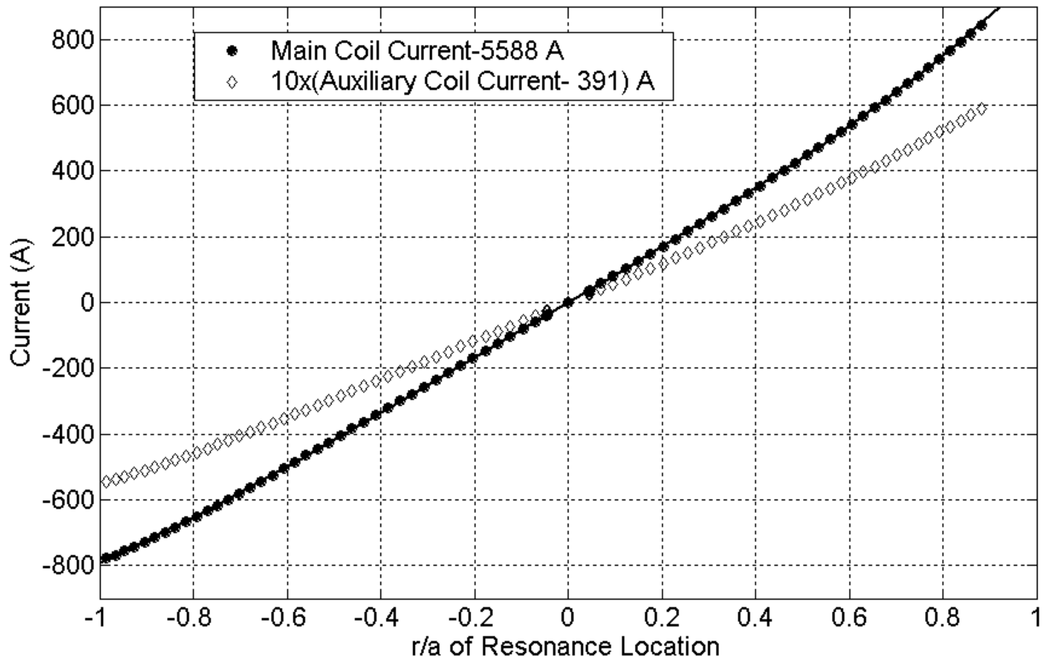

Figure A2.28: Magnet currents for shifting the resonance in the 5% antiMirror configuration.

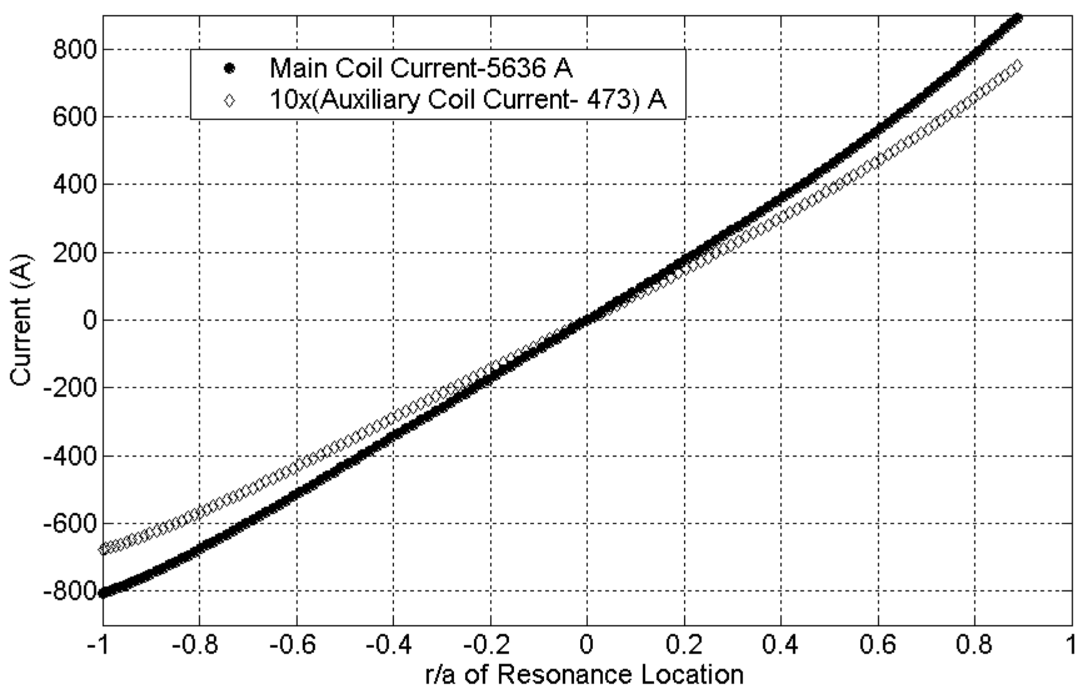

Figure A2.29: Magnet currents for shifting the resonance in the 6% antiMirror configuration.

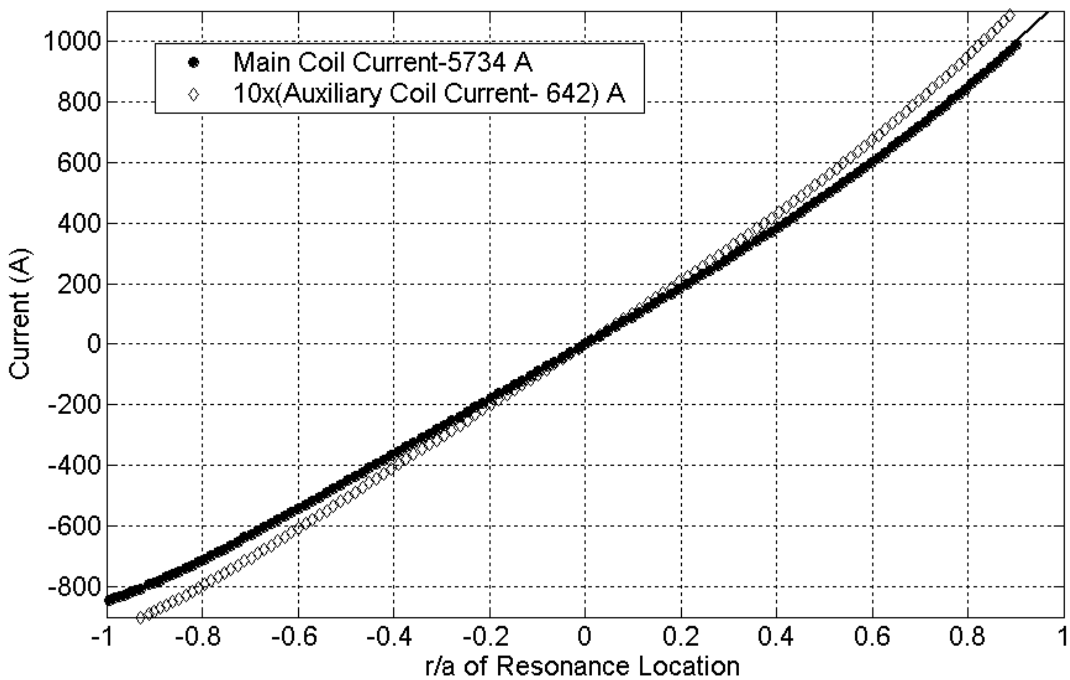

Figure A2.30: Magnet currents for shifting the resonance in the 8% antiMirror configuration.

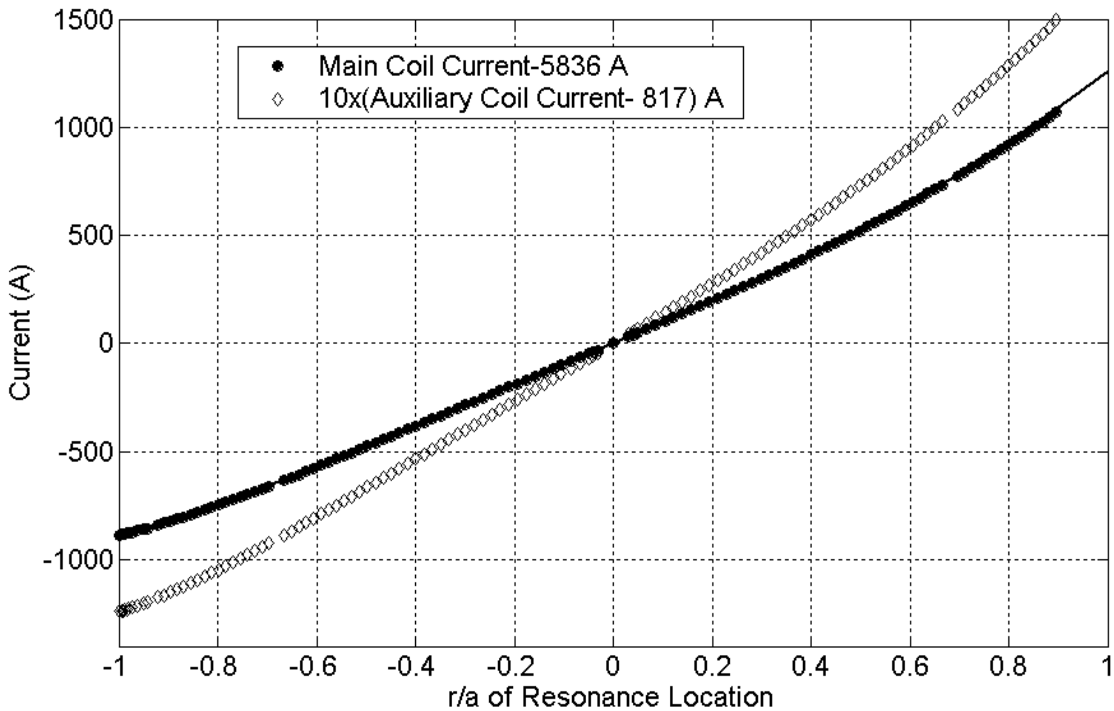

Figure A2.31: Magnet currents for shifting the resonance in the 10% antiMirror configuration.

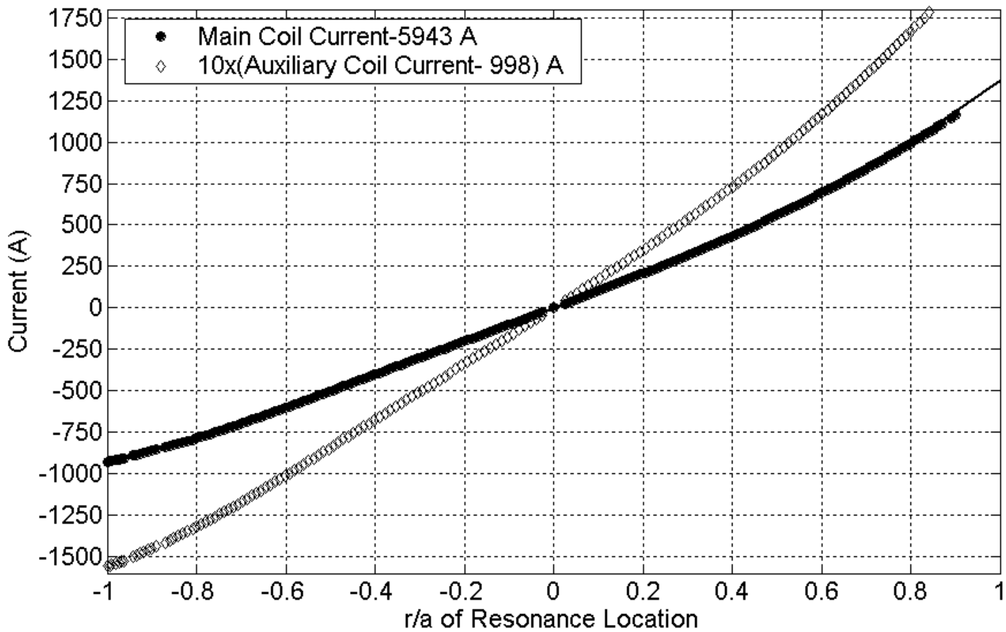

Figure A2.32: Magnet currents for shifting the resonance in the 12% antiMirror configuration.

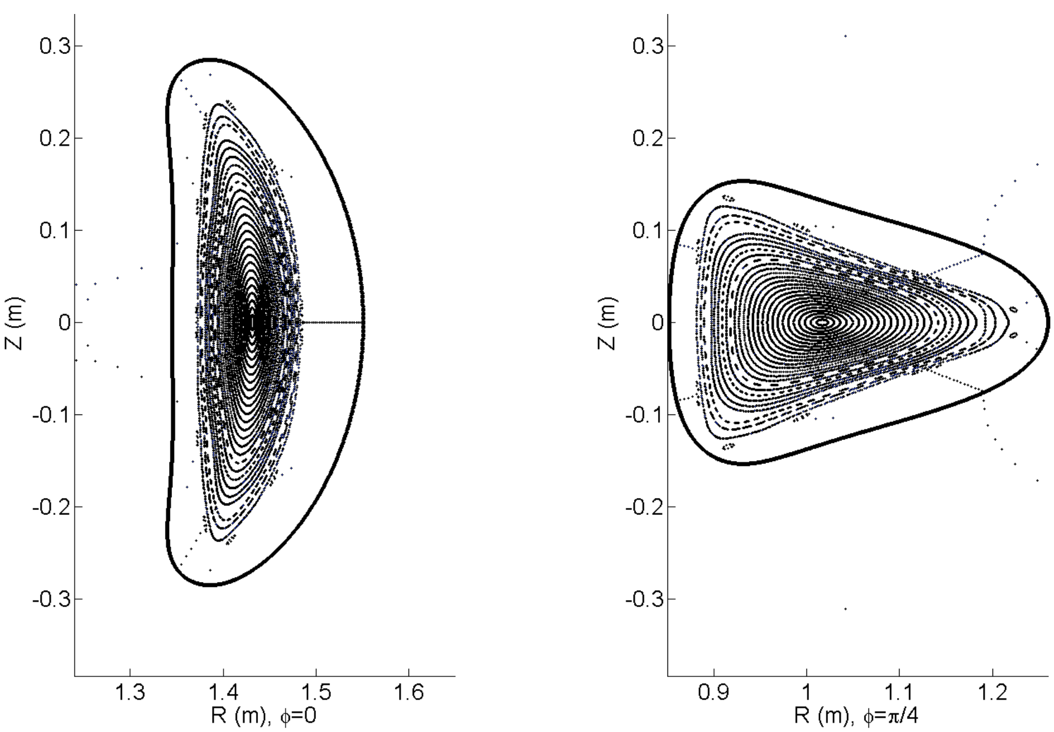

Figure A2.33: Flux Surfaces in 16% Mirror Configuration.

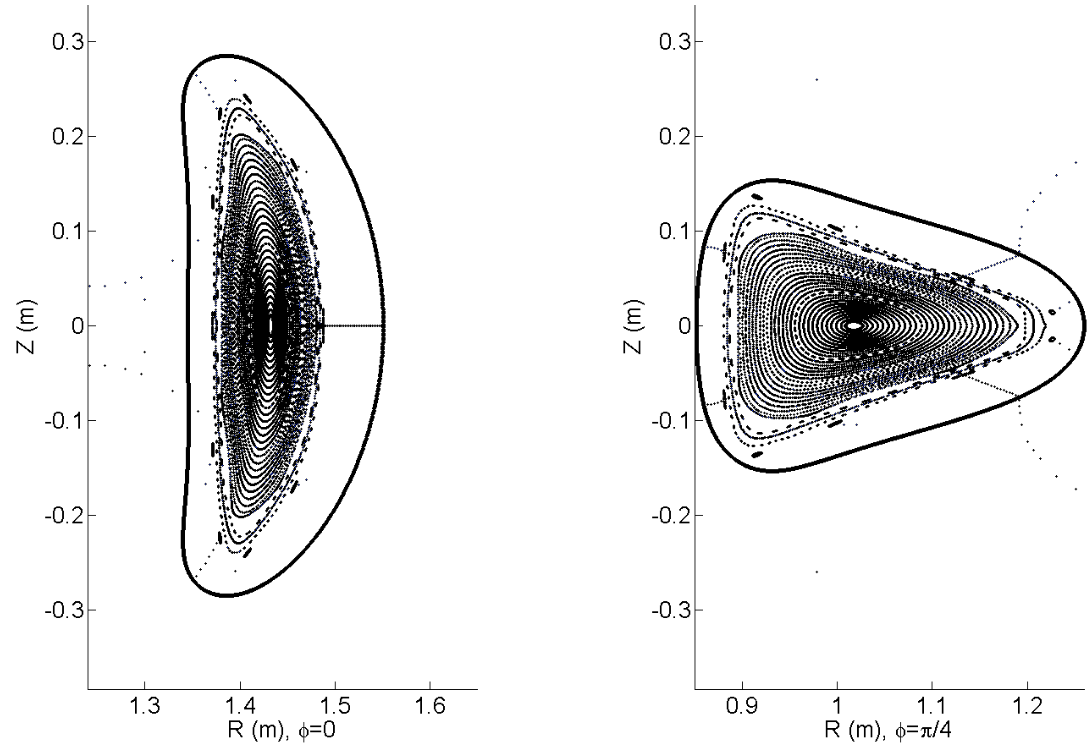

Figure A2.34: Flux Surfaces in 15% Mirror Configuration.

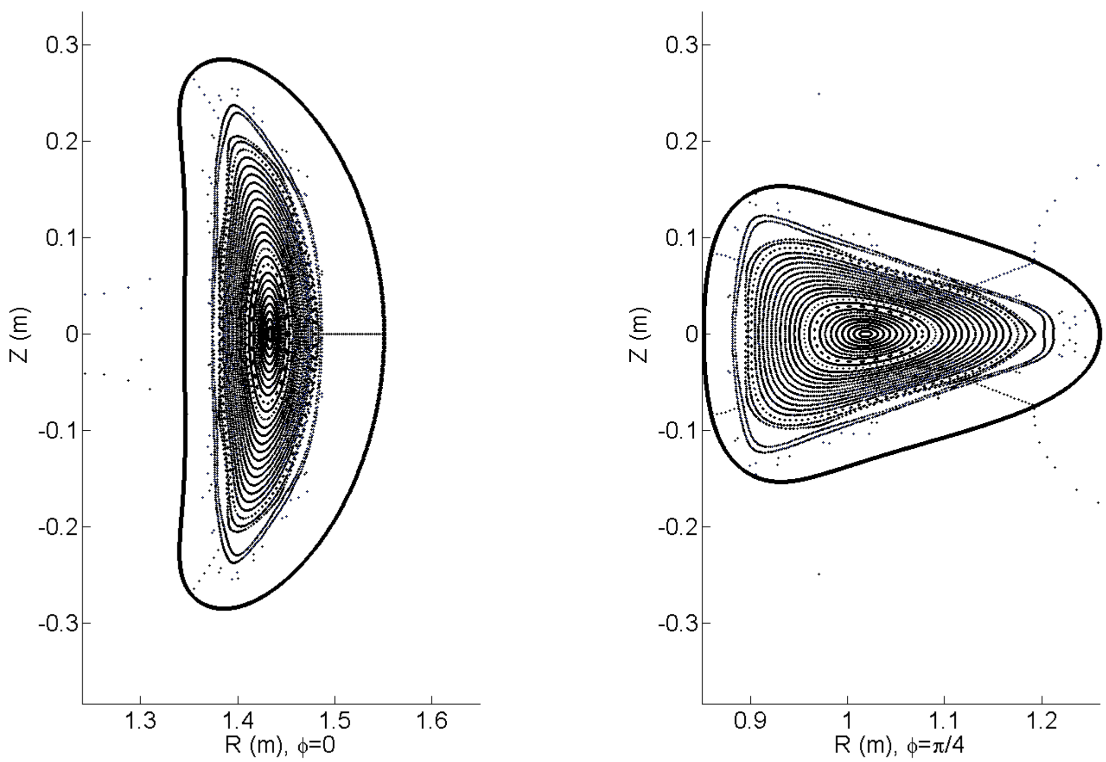

Figure A2.35: Flux Surfaces in 14% Mirror Configuration.

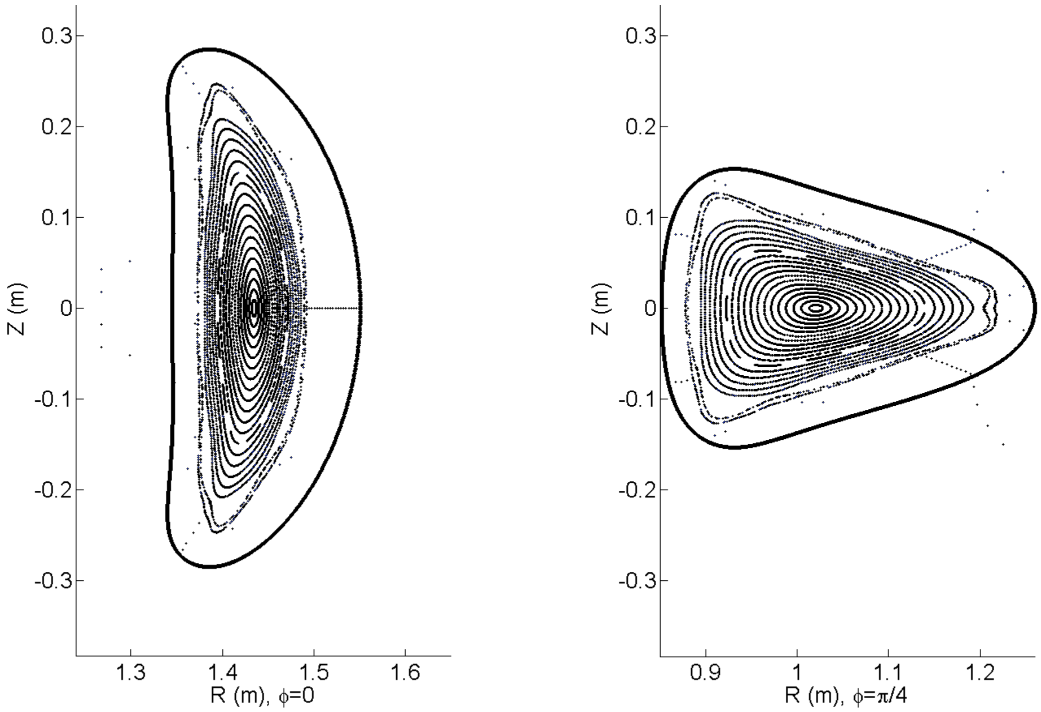

Figure A2.36: Flux Surfaces in 12% Mirror Configuration.

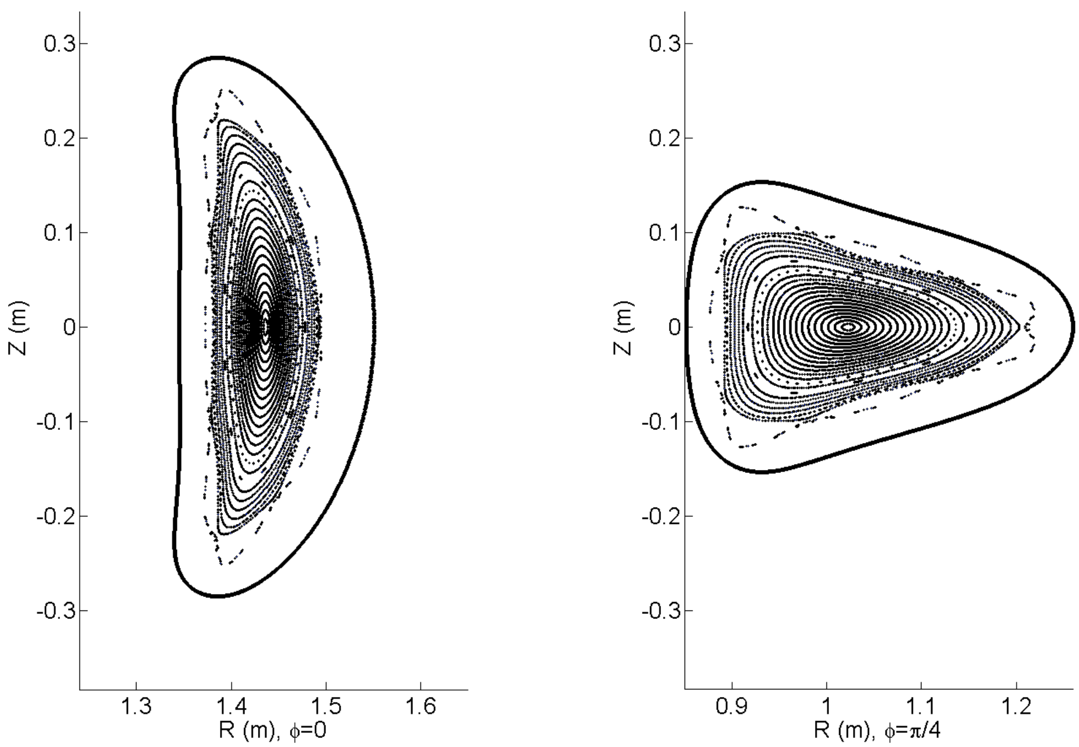

Figure A2.37: Flux Surfaces in 10% Mirror Configuration.

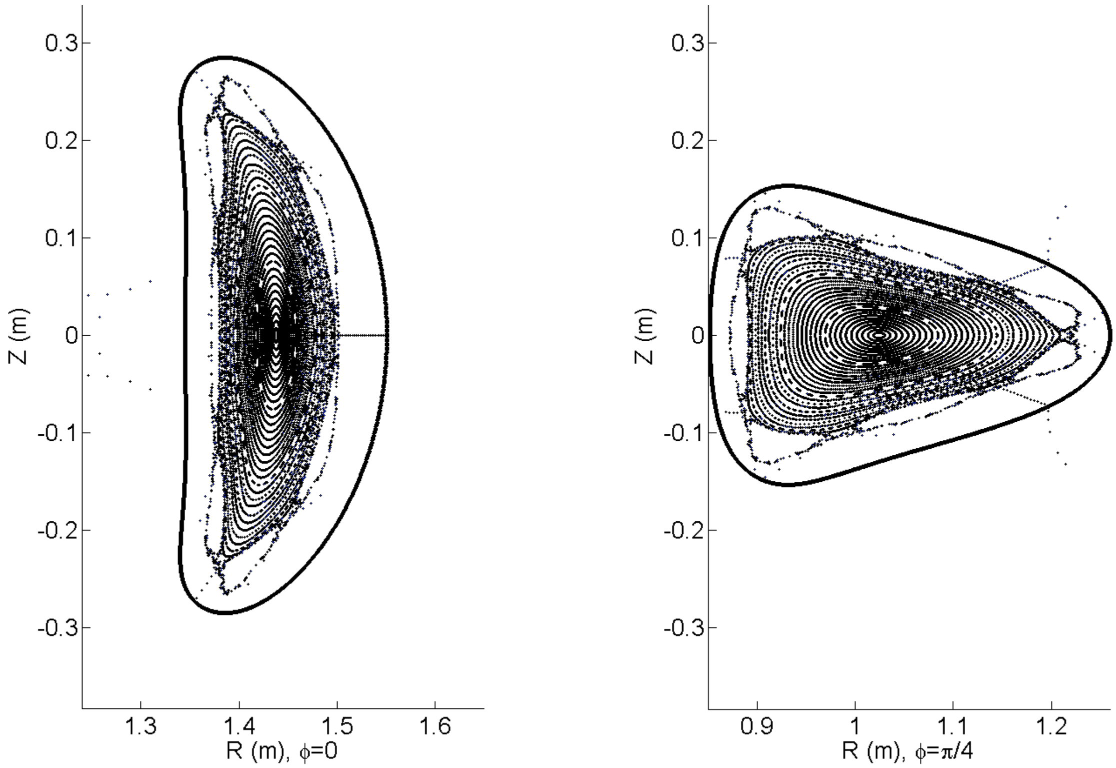

Figure A2.38: Flux Surfaces in 8% Mirror Configuration.

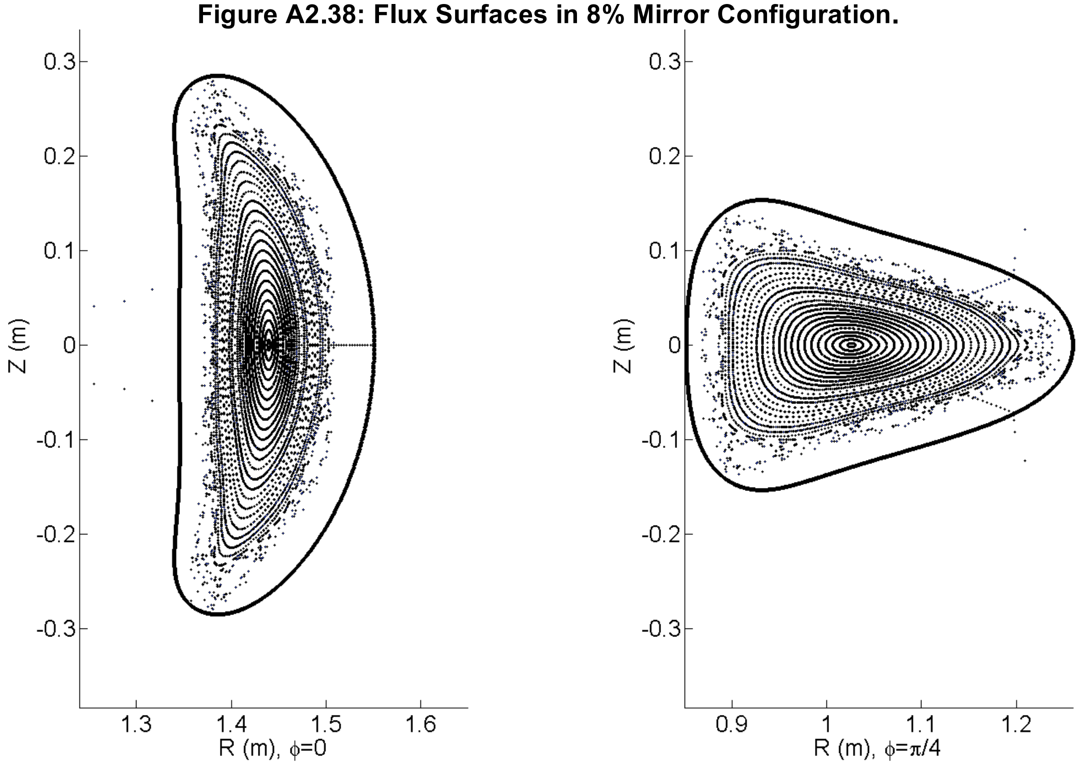

Figure A2.39: Flux Surfaces in 6% Mirror Configuration.

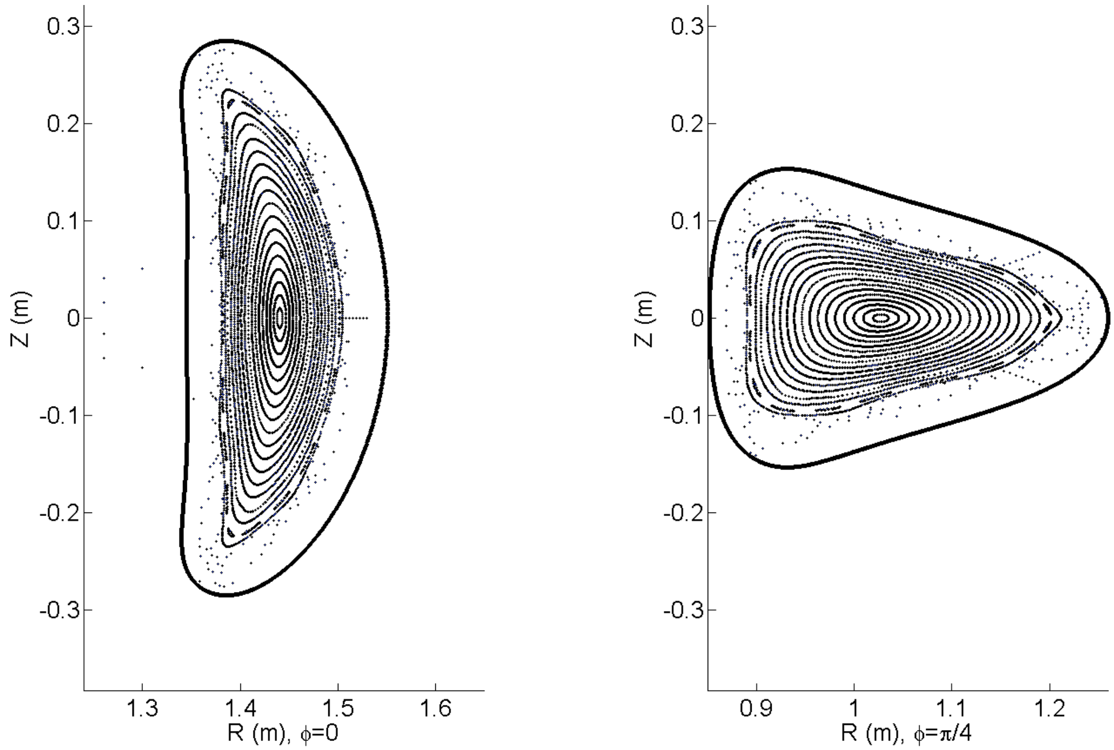

Figure A2.40: Flux Surfaces in 5% Mirror Configuration.

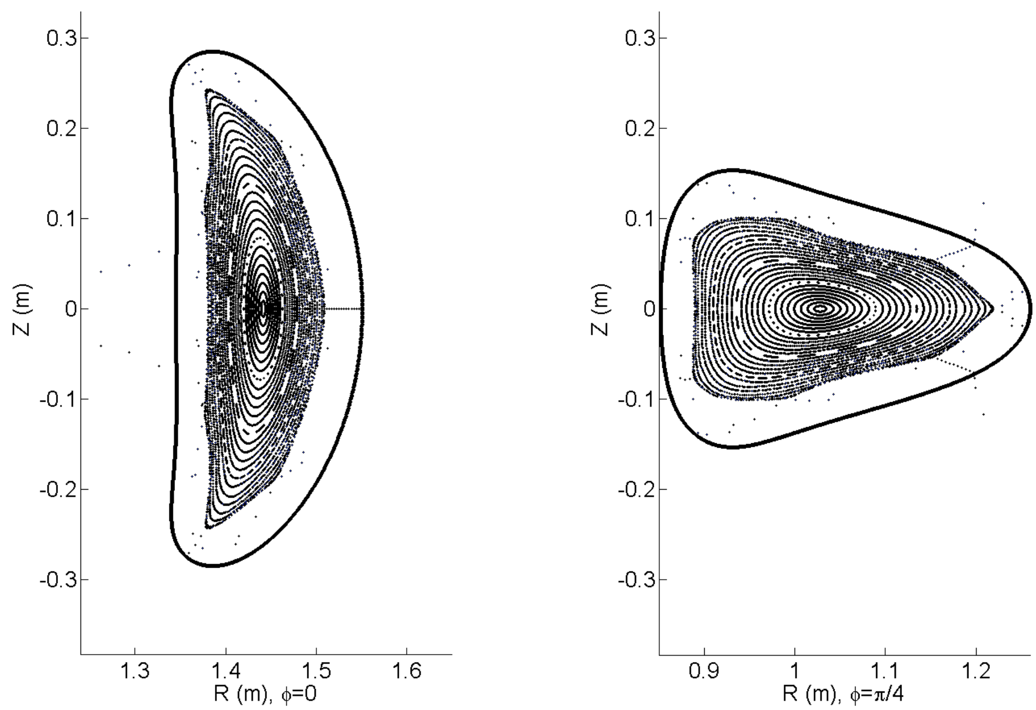

Figure A2.41: Flux Surfaces in 4% Mirror Configuration.

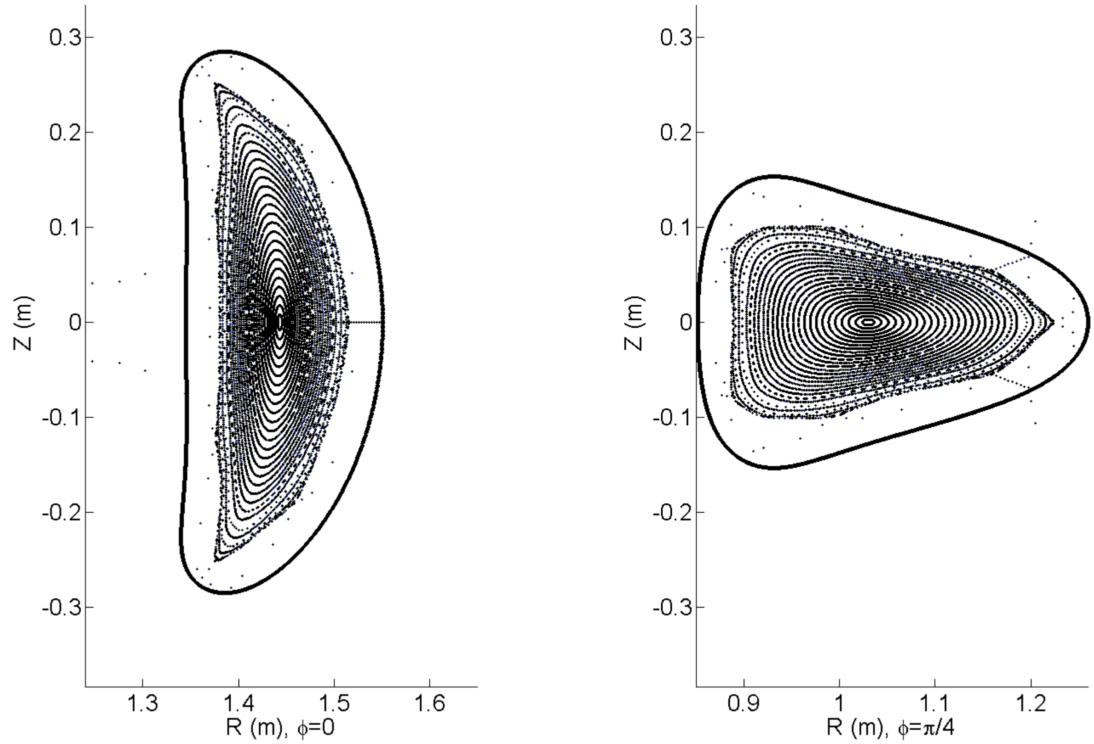

Figure A2.42: Flux Surfaces in 2% Mirror Configuration.

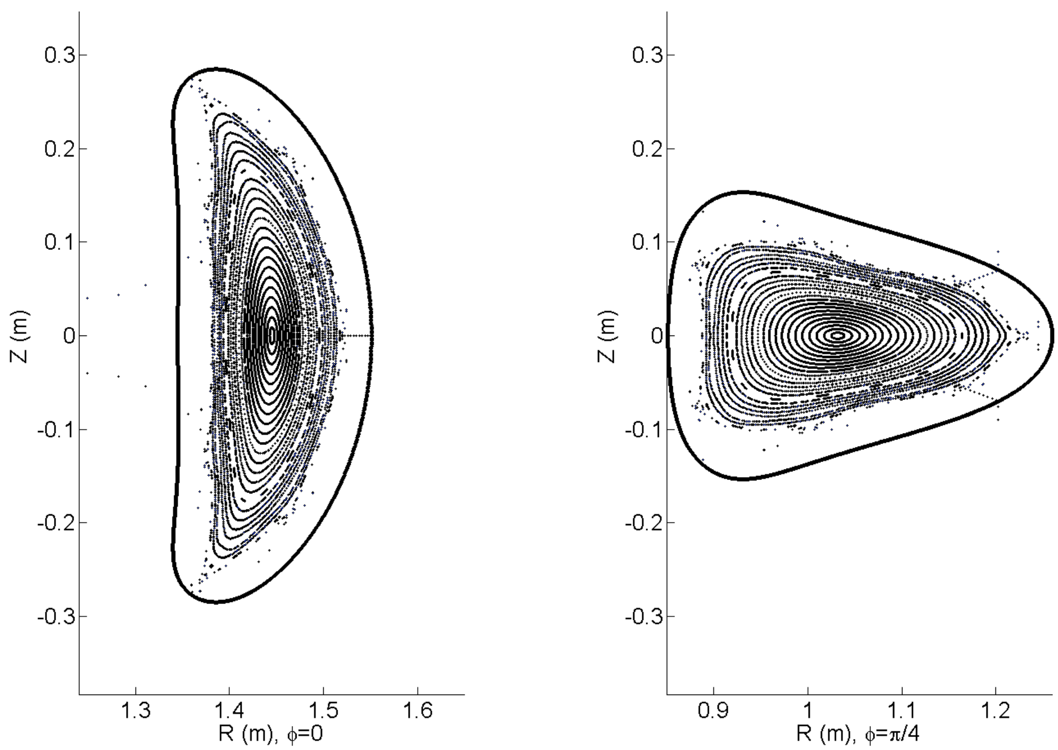

Figure A2.43: Flux Surfaces in QHS (0% Mirror) Configuration.

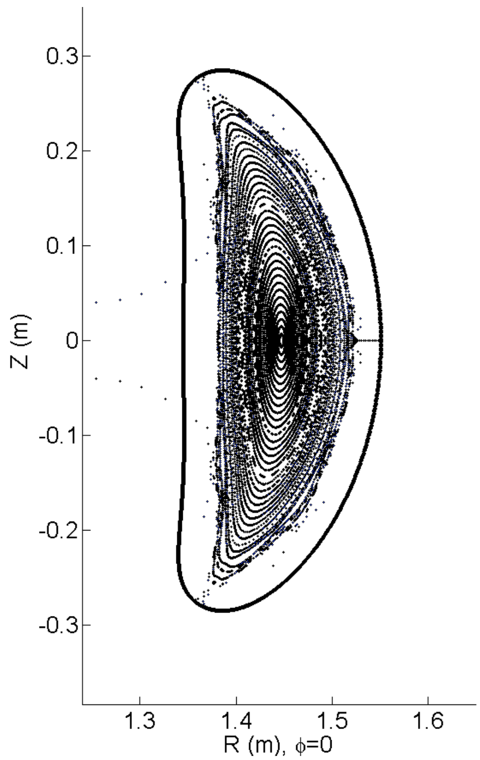

Figure A2.44: Flux Surfaces in 2% Type 1 antiMirror Configuration.

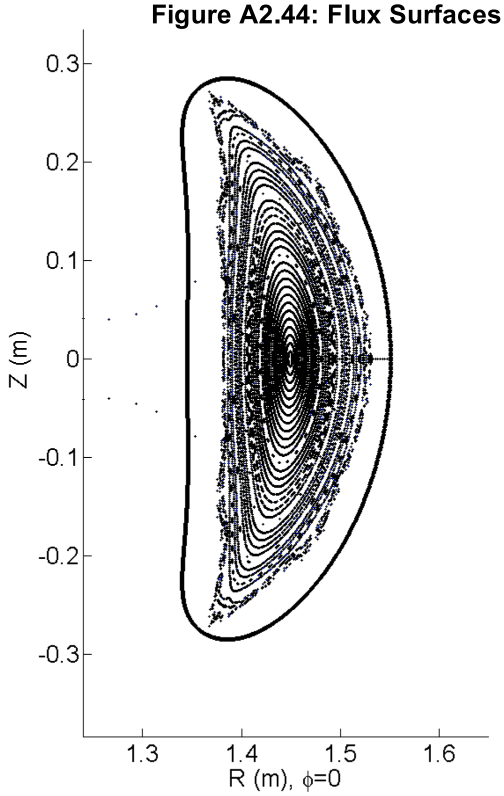

Figure A2.45: Flux Surfaces in 4% Type 1 antiMirror Configuration.

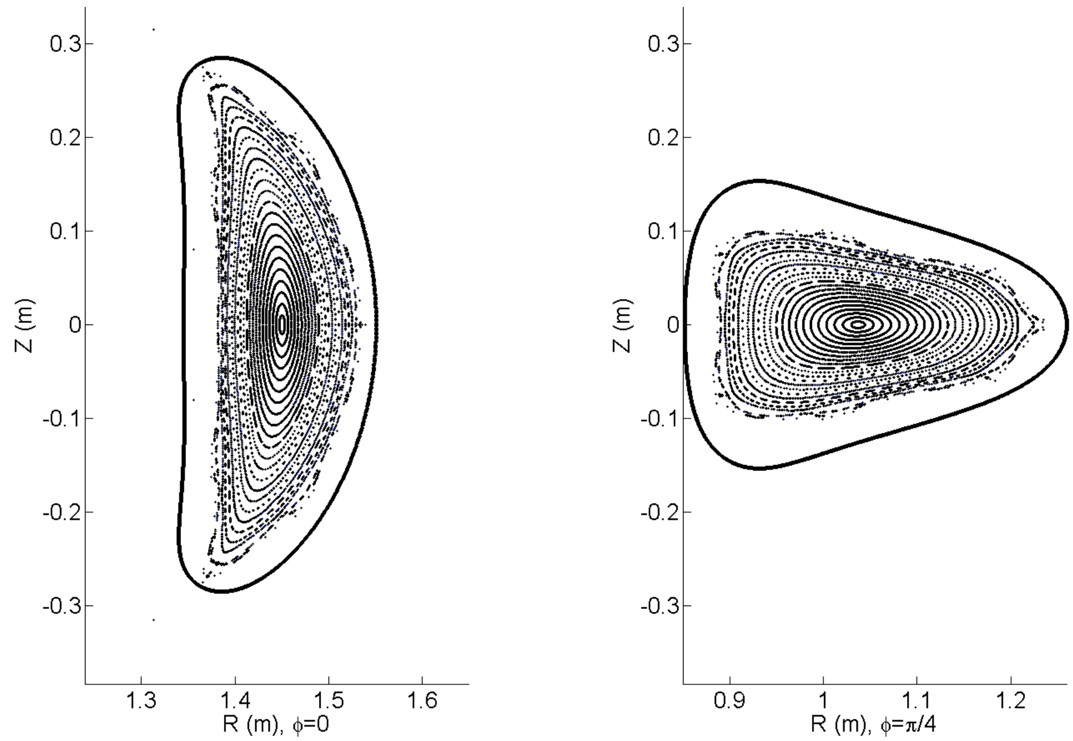

Figure A2.46: Flux Surfaces in 5% Type 1 antiMirror Configuration.

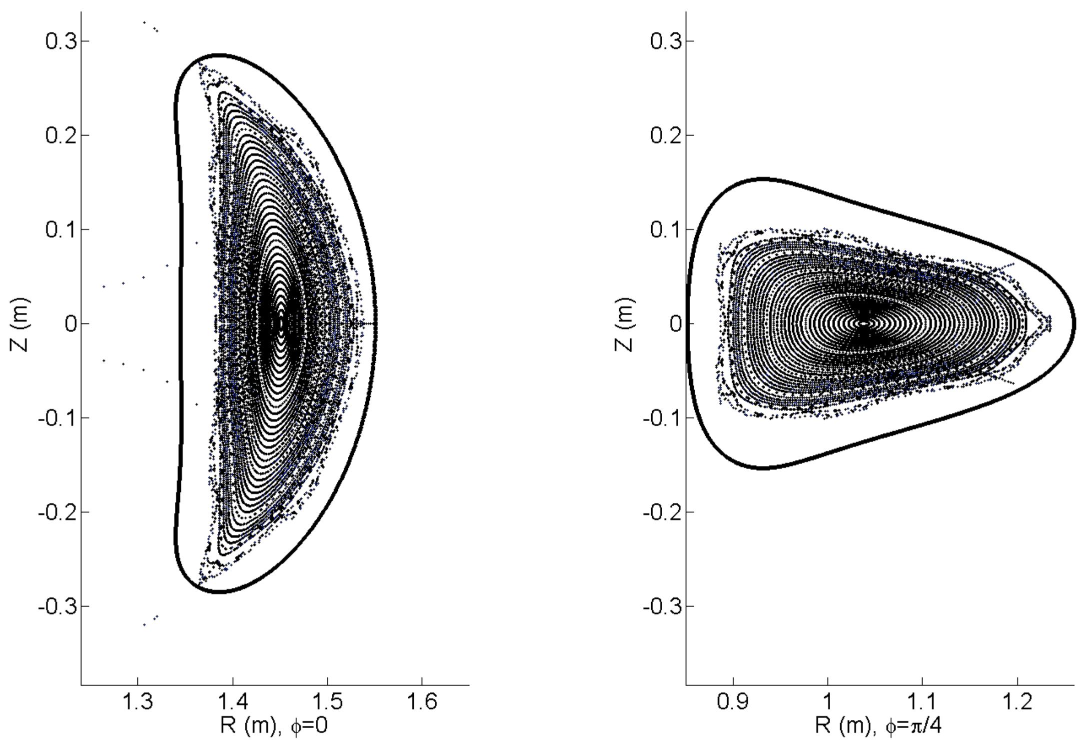

Figure A2.47: Flux Surfaces in 6% Type 1 antiMirror Configuration.

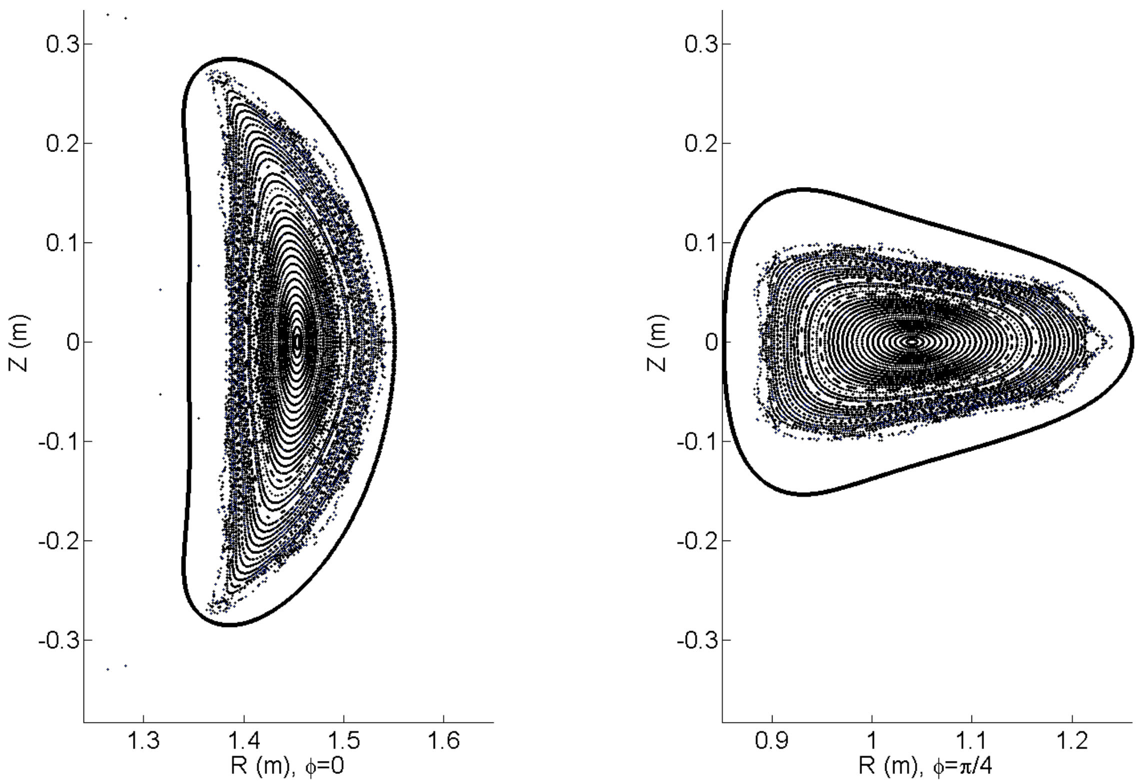

Figure A2.48: Flux Surfaces in 8% Type 1 antiMirror Configuration.

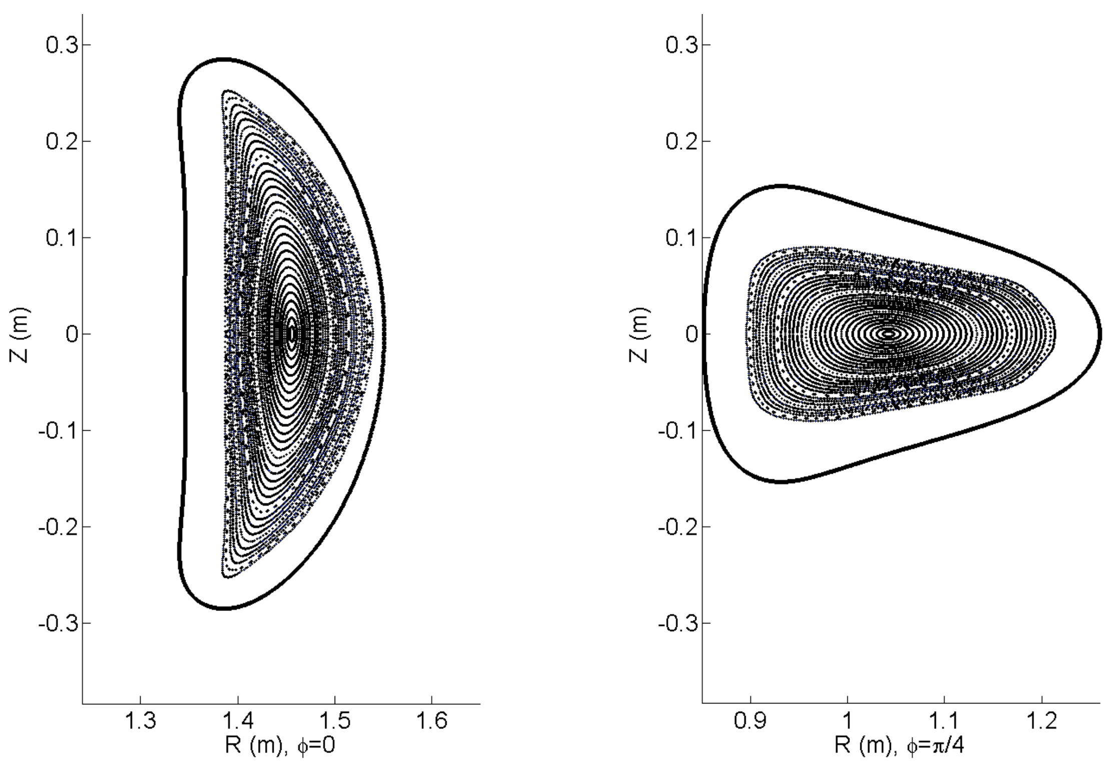

Figure A2.49: Flux Surfaces in 10% Type 1 antiMirror Configuration.

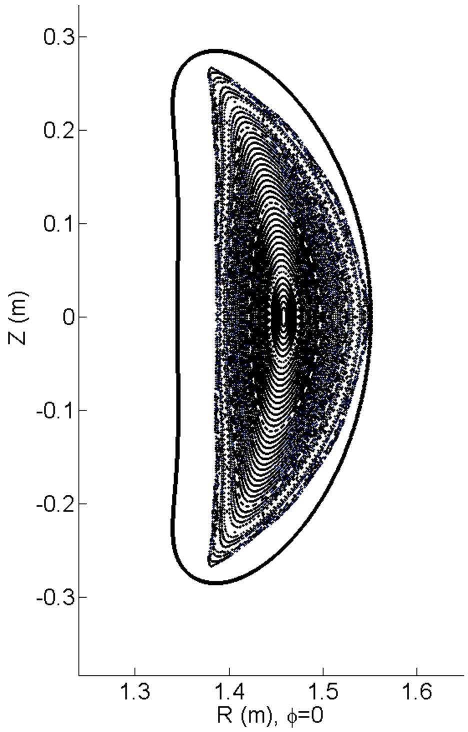

Figure A2.50: Flux Surfaces in 12% Type 1 antiMirror Configuration.

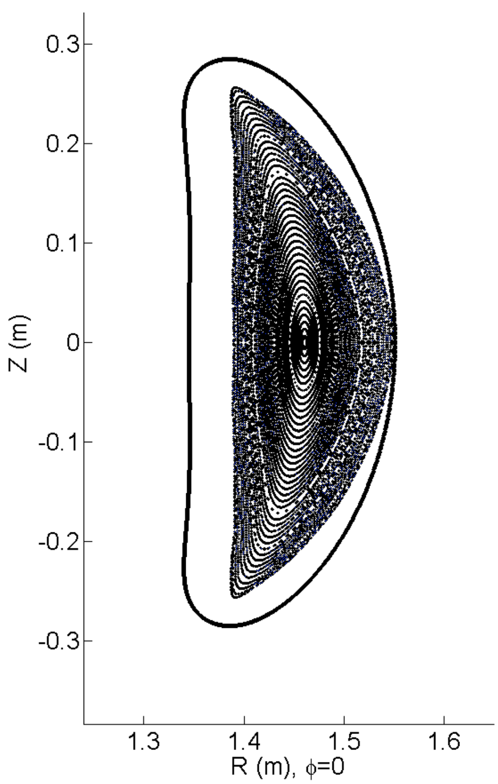

Figure A2.51: Flux Surfaces in 14% Type 1 antiMirror Configuration.

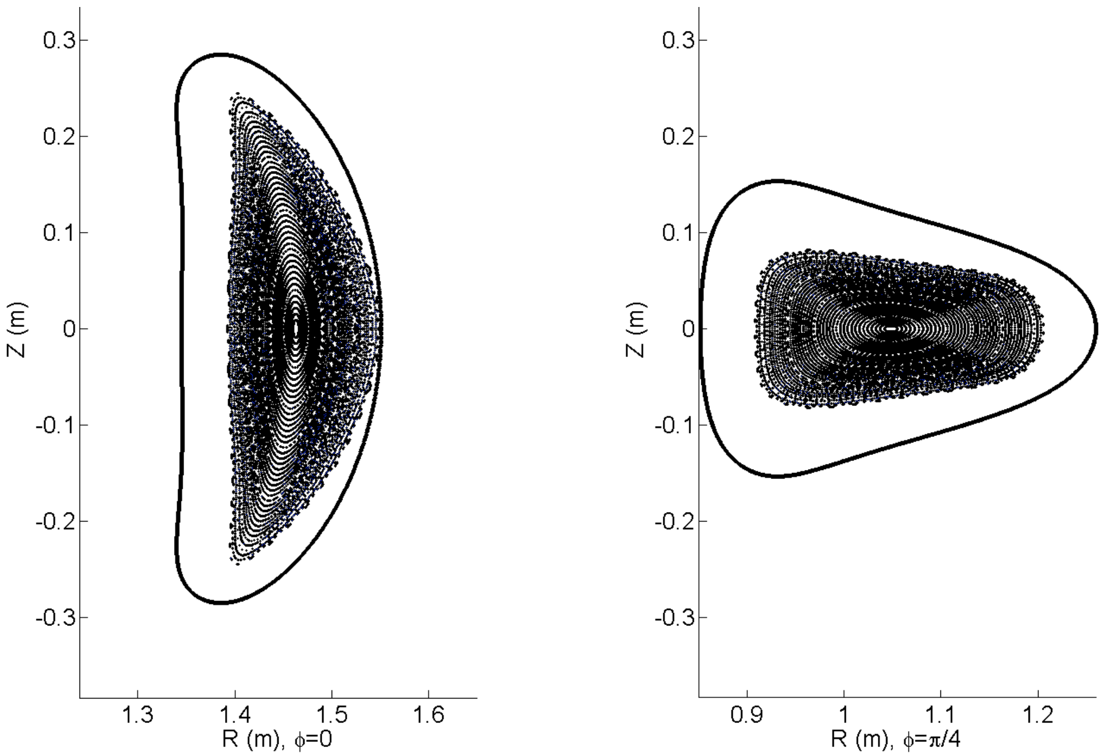

Figure A2.52: Flux Surfaces in 16% Type 1 antiMirror Configuration.

A2.3 The Hill-QHS-Well Continuum of Configurations

Comments Regarding this Configuration:

1) The $\iota\!\!\!-$=4/4 island chain enters the plasma core at a Hill mode percentage of between 5.0% and 5.25%.

2) There are closed flux surfaces outside of the $\iota\!\!\!-$=4/4 island chain until some percentage between 7.0% and 7.25% Hill

3) The $\iota\!\!\!-$=8/7 resonance enters the LCFS at a percentage well percentage between 4 and 4.25%

4) The $\iota\!\!\!-$=8/7 island chain exits the plasma at a percentage between 7 and 7.5%

5) The $\iota\!\!\!-$=4/3 island chain determines the plasma boundary Well percentages greater than ~9%.

6) The $\iota\!\!\!-$=8/9 island chain enters the plasma for Hill percentages greater than 21%.

Amp Turns %	R_{axis}, BP (m)	R_{axis}, JF (m)	R_{edge} (m)	I_{main} (A)	I_{aux} (A)
0	1.4454	1.0320	1.5161	5361	0
-0.5	1.4460	1.0322	1.5166	5393	-38
-1	1.4465	1.0324	1.5158	5425	-76
-1.5	1.4471	1.0327	1.5141	5458	-115
-2	1.4478	1.0331	1.5119	5492	-154
-2.5	1.4484	1.0334	1.5134	5525	-193
-3	1.4490	1.0337	1.5110	5560	-234
-3.5	1.4496	1.0339	1.5096	5594	-274
-4	1.4502	1.0343	1.5065	5629	-315
-4.5	1.4509	1.0346	1.5133	5665	-357
-5	1.4515	1.0349	1.5122	5700	-399
-5.5	1.4521	1.0352	1.5121	5736	-442
-6	1.4528	1.0355	1.5110	5773	-485
-6.5	1.4534	1.0358	1.5144	5810	-529
-7	1.4541	1.0361	1.5142	5847	-573
-7.5	1.4548	1.0365	1.5131	5886	-618
-8	1.4554	1.0368	1.5109	5924	-663
-8.5	1.4561	1.0371	1.5131	5963	-710
-9	1.4568	1.0375	1.5112	6002	-756
-9.5	1.4575	1.0378	1.5105	6043	-804
-10	1.4582	1.0381	1.5086	6083	-852
-10.5	1.4589	1.0385	1.5069	6125	-900
-11	1.4595	1.0388	1.5055	6165	-949
-11.5	1.4603	1.0392	1.5033	6208	-999
-12	1.4610	1.0395	1.5010	6250	-1050
-12.5	1.4617	1.0399	1.4977	6294	-1101
-13	1.4624	1.0403	1.4952	6338	-1154
-13.5	1.4631	1.0406	1.4931	6382	-1206
-14	1.4639	1.0410	1.4895	6427	-1260
-14.5	1.4647	1.0414	1.4877	6472	-1314
-15	1.4654	1.0417	1.4830	6519	-1369
-16	1.4669	1.0424	1.4760	6613	-1481
-17	1.4685	1.0433	-1.0000	6711	-1597
-18	1.4701	1.0440	-1.0000	6810	-1716
-19	1.4717	1.0449	-1.0000	6913	-1839
-20	1.4733	1.0456	-1.0000	7018	-1965
-0.25	1.4457	1.0321	1.5177	5377	-19
-4.25	1.4505	1.0344	1.5115	5647	-336
-8.25	1.4558	1.0370	1.5138	5944	-687
-11.75	1.4606	1.0393	1.5016	6229	-1025

Table A2.10: Axis locations, plasma edge, and central resonant currents, for the Well continuum.

Amp Turns %	Raxis, BP (m)	Raxis, JF (m)	Redge (m)	Imain (A)	Iaux (A)
0	1.4454	1.0320	1.5161	5361	0
0.5	1.4448	1.0316	1.5168	5329	37
1	1.4442	1.0313	1.5162	5297	74
1.5	1.4436	1.0311	1.5166	5267	111
2	1.4431	1.0308	1.5178	5236	147
2.5	1.4425	1.0305	1.5195	5205	182
3	1.4419	1.0302	1.5202	5175	217
3.5	1.4414	1.0300	1.5204	5146	252
4	1.4408	1.0297	1.5212	5116	286
4.5	1.4403	1.0295	1.5213	5087	320
5	1.4397	1.0292	1.5216	5058	354
5.5	1.4392	1.0290	1.5212	5029	387
6	1.4386	1.0286	1.5207	5001	420
6.5	1.4381	1.0284	1.5221	4974	453
7	1.4375	1.0282	1.5232	4946	485
7.5	1.4370	1.0279	1.4734	4918	516
8	1.4365	1.0277	1.4765	4892	548
8.5	1.4360	1.0274	1.4790	4865	579
9	1.4355	1.0272	1.4810	4839	610
9.5	1.4350	1.0270	1.4830	4812	640
10	1.4345	1.0267	1.4848	4787	670
10.5	1.4339	1.0265	1.4859	4761	700
11	1.4334	1.0262	1.4885	4735	729
11.5	1.4330	1.0260	1.4900	4711	758
12	1.4325	1.0258	1.4915	4685	787
12.5	1.4320	1.0255	1.4922	4661	816
13	1.4315	1.0253	1.4934	4637	844
13.5	1.4310	1.0251	1.4960	4613	872
14	1.4305	1.0249	1.4975	4589	899
14.5	1.4300	1.0246	1.4990	4565	927
15	1.4296	1.0244	1.5001	4542	954
15.5	1.4291	1.0242	1.5021	4519	981
16	1.4286	1.0240	1.5026	4495	1007
16.5	1.4282	1.0238	1.5042	4473	1033
17	1.4277	1.0236	1.5057	4451	1059
17.5	1.4273	1.0233	1.5063	4428	1085
18	1.4268	1.0232	1.5078	4407	1111
19	1.4259	1.0227	1.5079	4363	1161
20	1.4250	1.0223	1.5090	4320	1210
21	1.4242	1.0219	1.5102	4278	1258
22	1.4233	1.0215	1.5103	4237	1305
24	1.4216	1.0208	-1.0000	4157	1397
0.25	1.4451	1.0318	1.5161	5345	19
5.25	1.4394	1.0290	1.5224	5043	371
7.25	1.4373	1.0281	1.4273	4933	501

Table A2.11: Axis locations, plasma edge, and central resonant currents, for the Hill continuum.

Amp Turns %	Boundary Flux (Tm^2)	$\iota(0)$	$\iota(a)$	Volume ($dV/d\psi$) (m^3)	Volume (MC) (m^3)
0	0.0212	1.0500	1.1091	0.378	0.381
-0.5	0.0210	1.0554	1.1147	0.374	0.376
-1	0.0211	1.0620	1.1175	0.375	0.366
-1.5	0.0196	1.0662	1.1209	0.349	0.351
-2	0.0185	1.0707	1.1220	0.329	0.331
-2.5	0.0185	1.0777	1.1327	0.329	-1.000
-3	0.0171	1.0835	1.1301	0.305	0.312
-3.5	0.0165	1.0895	1.1345	0.293	-1.000
-4	0.0152	1.0964	1.1308	0.269	0.278
-4.5	0.0187	1.1019	1.1728	0.362	0.371
-5	0.0198	1.1090	1.1760	0.353	0.355
-5.5	0.0200	1.1148	1.1841	0.356	-1.000
-6	0.0194	1.1227	1.1900	0.341	0.342
-6.5	0.0208	1.1283	1.2090	0.369	-1.000
-7	0.0210	1.1363	1.2225	0.372	0.373
-7.5	0.0202	1.1425	1.2251	0.360	-1.000
-8	0.0189	1.1499	1.2227	0.335	0.336
-8.5	0.0209	1.1572	1.2560	0.372	-1.000
-9	0.0198	1.1638	1.2568	0.372	0.353
-9.5	0.0197	1.1717	1.2697	0.350	-1.000
-10	0.0185	1.1821	1.2705	0.328	0.330
-10.5	0.0175	1.1891	1.2741	0.311	-1.000
-11	0.0170	1.1976	1.2931	0.302	0.305
-11.5	0.0156	1.2067	1.2938	0.276	-1.000
-12	0.0140	1.2165	1.2698	0.248	0.251
-12.5	0.0115	1.2245	1.2714	0.203	-1.000
-13	0.0099	1.2354	1.2723	0.175	0.183
-13.5	0.0088	1.2437	1.2827	0.157	-1.000
-14	0.0067	1.2554	1.2766	0.118	0.120
-14.5	0.0522	1.2643	1.3054	0.093	-1.000
-15	0.0030	1.2715	1.3000	0.070	0.072
-16	0.0009	1.2984	1.3228	0.012	-1.000
-17	-1.0000	-1.0000	-1.0000	-1.000	-1.000
-18	-1.0000	-1.0000	-1.0000	-1.000	-1.000
-19	-1.0000	-1.0000	-1.0000	-1.000	-1.000
-20	-1.0000	-1.0000	-1.0000	-1.000	-1.000
-0.25	0.0215	1.0527	1.1146	0.382	-1.000
-4.25	0.0202	1.0987	1.1633	0.359	0.359
-8.25	0.0213	1.1534	1.2535	0.377	0.378
-11.75	0.0141	1.2108	1.2763	0.250	-1.000

Table A2.12: Boundary flux, rotational transform, and volume information for Well continuum of configurations.

Amp Turns %	Boundary Flux (Tm^2)	$\iota(0)$	$\iota(0)$	Volume ($dV/d\psi$) (m^3)	Volume (MC) (m^3)
0	0.0212	1.0500	1.1091	0.378	0.381
0.5	0.0217	1.0449	1.1046	0.387	0.385
1	0.0217	1.0397	1.0972	0.387	0.387
1.5	0.0207	1.0347	1.0873	0.370	0.373
2	0.0215	1.0299	1.0840	0.384	0.387
2.5	0.0224	1.0250	1.0830	0.400	-1.000
3	0.0228	1.0207	1.0772	0.407	0.410
3.5	0.0232	1.0157	1.0742	0.414	-1.000
4	0.0238	1.0103	1.0765	0.424	0.428
4.5	0.0231	1.0061	1.0621	0.413	-1.000
5	0.0233	1.0026	1.0574	0.417	0.422
5.5	0.0228	0.9979	1.0488	-1.000	0.412
6	0.0221	0.9936	1.0414	-1.000	0.401
6.5	0.0224	0.9891	1.0361	-1.000	0.404
7	0.0224	0.9840	1.0306	-1.000	0.405
7.5	0.0069	0.9820	0.9899	0.122	-1.000
8	0.0082	0.9770	0.9890	0.147	0.147
8.5	0.0095	0.9731	0.9882	0.169	-1.000
9	0.0104	0.9697	0.9854	0.186	0.186
9.5	0.0114	0.9654	0.9844	0.204	-1.000
10	0.0124	0.9627	0.9829	0.221	0.218
10.5	0.0129	0.9579	0.9781	0.230	-1.000
11	0.0147	0.9554	0.9890	0.263	0.259
11.5	0.0155	0.9507	0.9809	0.277	-1.000
12	0.0164	0.9472	0.9793	0.294	0.294
12.5	0.0167	0.9434	0.9711	0.298	-1.000
13	0.0175	0.9407	0.9699	0.312	0.308
13.5	0.0194	0.9369	0.9764	0.347	-1.000
14	0.0204	0.9339	0.9763	0.366	0.363
14.5	0.0215	0.9303	0.9759	0.386	-1.000
15	0.0222	0.9276	0.9705	0.397	0.397
15.5	0.0239	0.9238	0.9807	0.429	-1.000
16	0.0239	0.9207	0.9670	0.428	0.427
16.5	0.0251	0.9175	0.9676	0.451	-1.000
17	0.0263	0.9145	0.9676	0.472	0.470
17.5	0.0265	0.9115	0.9617	0.476	-1.000
18	0.0277	0.9085	0.9617	0.497	0.496
19	0.0274	0.9027	0.9498	0.492	0.492
20	0.0280	0.8970	0.9432	0.504	0.502
21	0.0291	0.8915	0.9382	0.523	0.523
22	0.0291	0.8860	0.9304	0.523	-1.000
24	0.0281	0.8757	0.9137	0.506	0.507
0.25	0.0212	1.0475	1.1053	0.379	-1.000
5.25	0.0237	0.9997	1.0562	0.418	0.428
7.25	0.0065	0.9832	0.9913	0.115	0.115

Table A2.13: Boundary flux, rotational transform, and volume information for Hill continuum of configurations.

Amp Turn %	A_0	A_1	A_2	A_3	A_4	A_5
16	.92057	.010124	-.096467	.35519	-.45754	.23503
14	.93346	.007563	-.078286	.31048	-.43095	.23332
12	.94695	.016133	-.15413	.52991	-.6931	.33291
10	.96158	.0028441	-.031595	.1361	-.19654	.11065
8	.97697	.0028472	-.030588	.12045	-.16982	.089346
4	1.0109	.0039992	-.035687	.12356	-.11399	.083315
2	1.0297	.0045141	-.041935	.14563	-.15022	.093516
0	1.05	.0024	-.02381	0.086768	-.07433	0.0060676
-2	1.0719	.004437	-.04608	.15748	-.17024	.10335
-4	1.0956	.003841	-.042568	.14652	-.16999	.098697
-6	1.1214	.0030485	-.034037	.11107	-.098245	.085118
-8	1.1496	.0025067	-.028079	.089798	-.073656	.082514
-10	1.1806	.013461	-.14053	.48012	-.61305	.34845
-12	1.2148	.061182	-.62127	2.108	-2.8156	1.3464
-14	1.2539	-.0007863	.016331	.017937	-.074965	.065572

Table A2.14: Polynomial fits to iota for Well/Hill configurations.

Amp Turn %	A_0	A_1	A_2	A_3	A_4	A_5
16	17.9609	.0504748	-.516157	1.73124	-2.21668	1.13758
14	17.9600	.0328993	-.379633	1.26552	-1.71791	.929827
12	17.9655	.0512113	-.538125	1.63887	-2.10636	1.01716
10	17.9643	.0093334	-.142022	.338378	-.44649	.254245
8	17.9674	.00694115	-.100735	.186101	-.228857	.121279
4	17.9725	.0185849	-.299904	.25222	-.0748278	.094142
2	17.5513	.020591	-.321244	.307269	-.181478	.115952
0	17.9739	.00882552	-.283691	.134405	.0144549	.0304803
-2	17.9728	.0321413	-.413986	.369889	-.215692	.100604
-4	19.9828	.00982538	-.2773	.0709789	.067942	-.0215529
-6	17.9831	.0402654	-.540415	.402868	-.171942	.0639968
-8	17.9872	.0233493	-.511926	.2891	-.0852557	.0363059
-10	17.9891	.0196717	-.526283	.198424	.0320826	-.0213293
-12	17.9906	-.0315936	.209383	-2.24951	3.32497	-1.57114
-14	17.9917	.0150401	-.266651	.0907513	-.0055136	-.0332601

Table A2.15: Polynomial fits to $\frac{dV}{d\psi} = \frac{1}{N}\int\frac{dl}{B}$ for Well/Hill configurations.

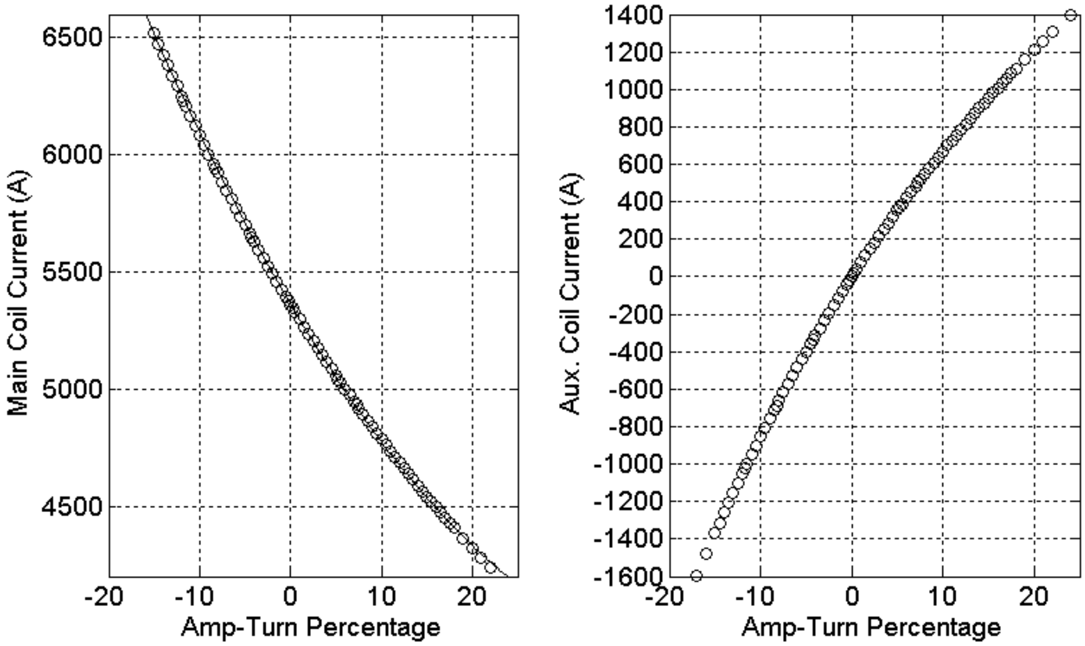

Figure A2.53: Main coil current (left) and Aux. coil current (right) to keep the ECH resonance on axis in the Well/Hill configurations.

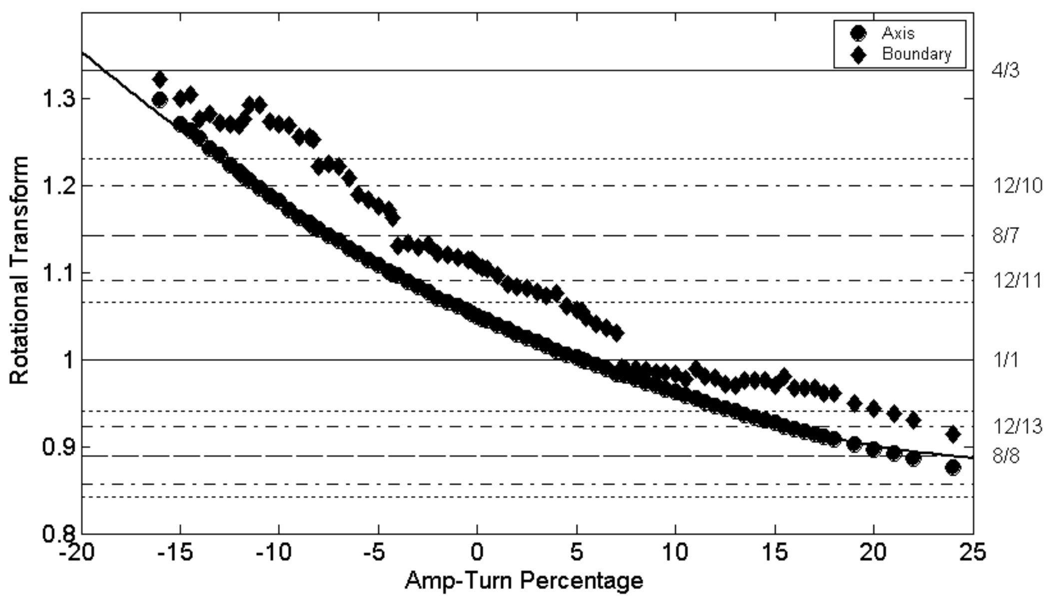

Figure A2.54: Edge and core rotational transform values in the Well/Hill configurations.

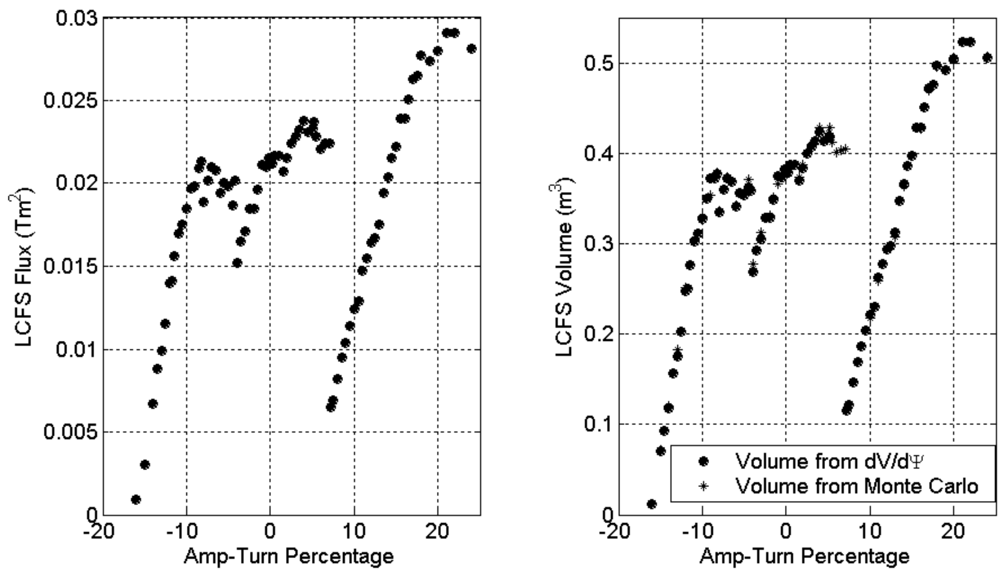

Figure A2.55: Boundary toroidal flux (left) and total volume (right) in the Type 1 Well/Hill configurations.

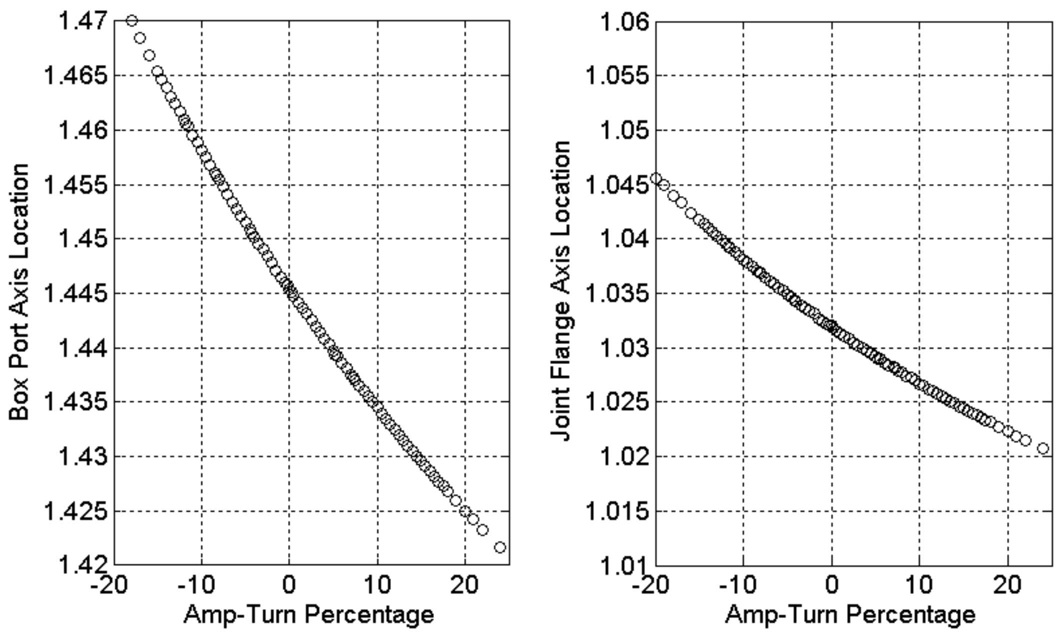

Figure A2.56: Major radius of the magnetic axis at the box port (left) and joint flange (right) in the Well/Hill configurations.

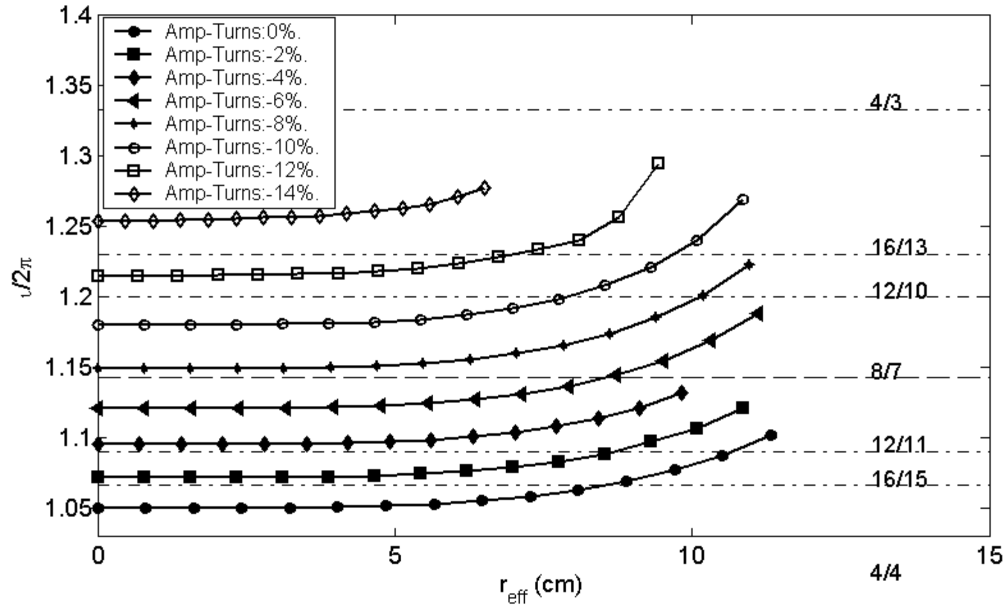

Figure A2.57: Rotational transform profiles in the Well configurations.

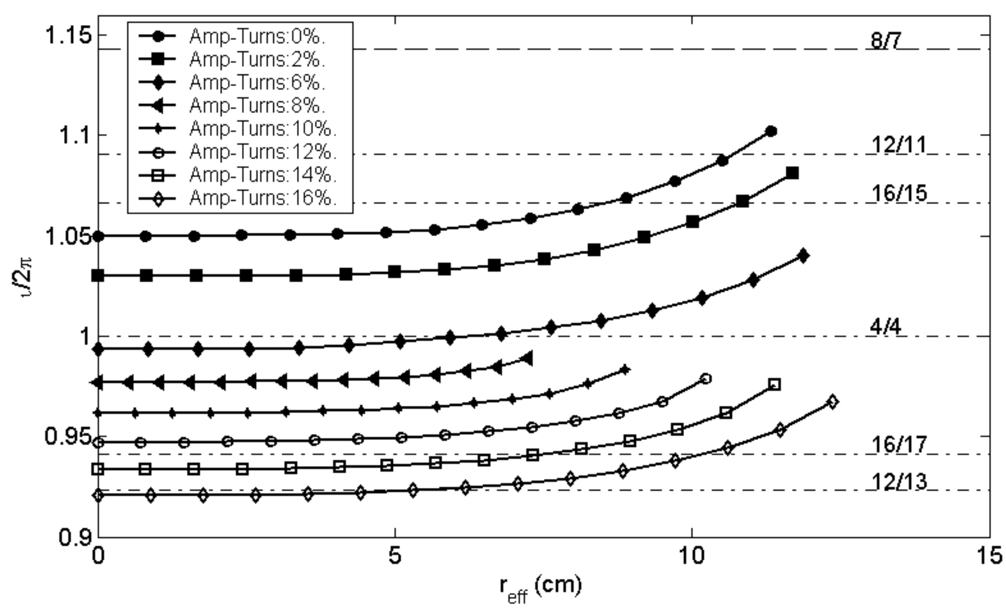

Figure A2.58: Rotational transform profiles in the Hill configurations.

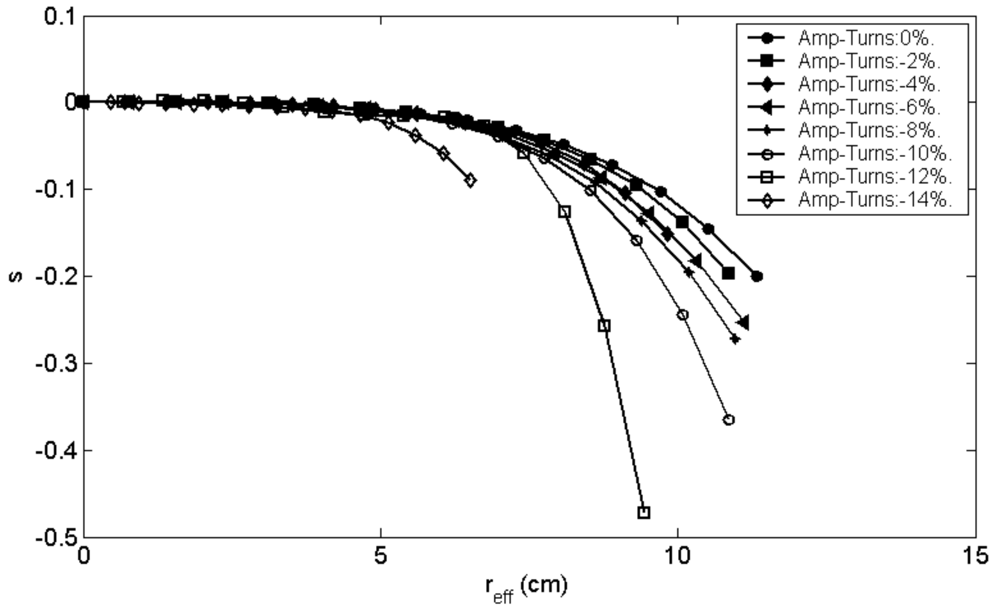

Figure A2.59: Magnetic shear profiles in the Well configurations.

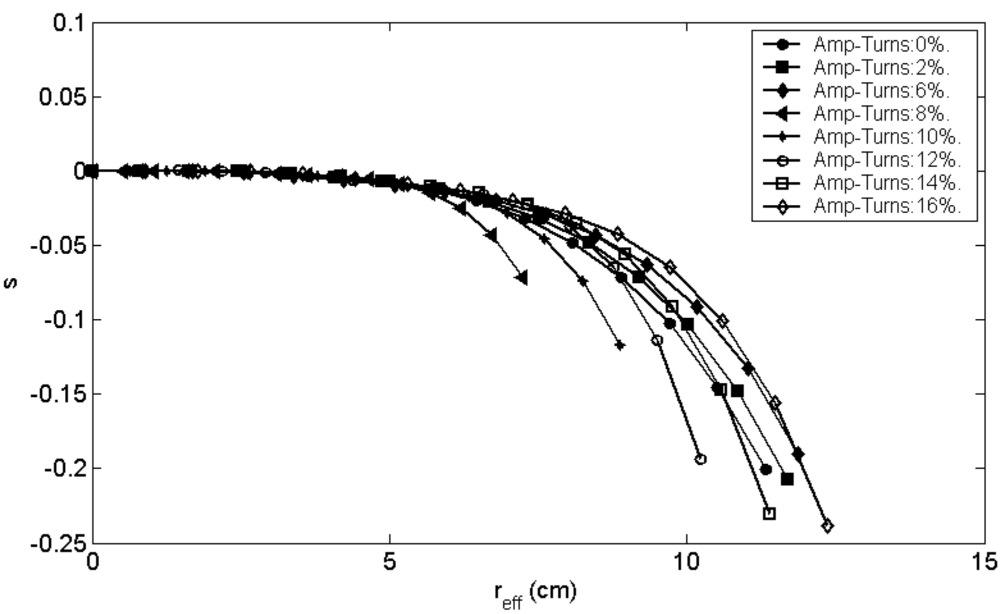

Figure A2.60: Magnetic shear profiles in the Hill configurations.

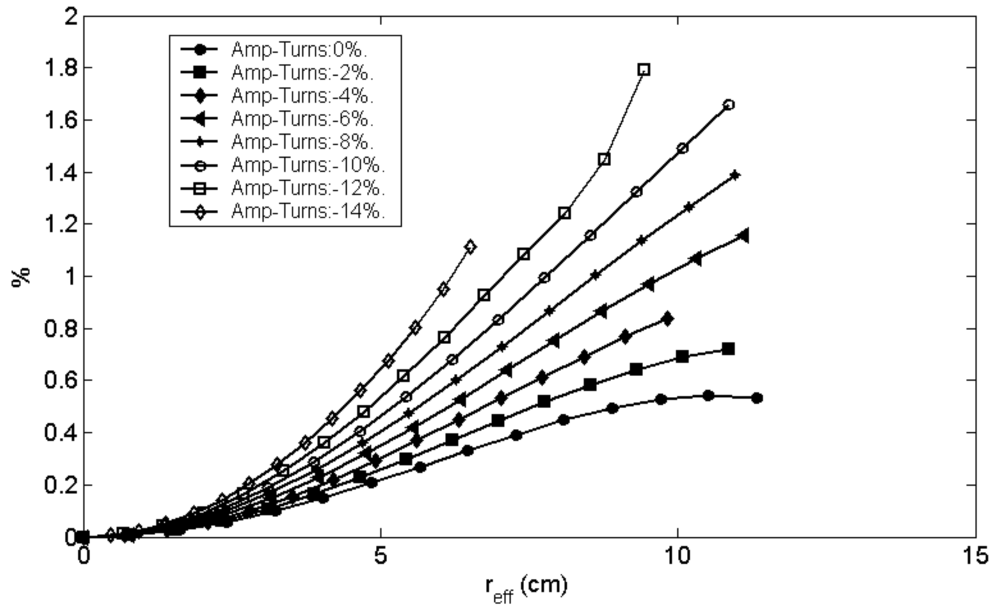

Figure A2.61: Well depth profiles in the Well configurations.

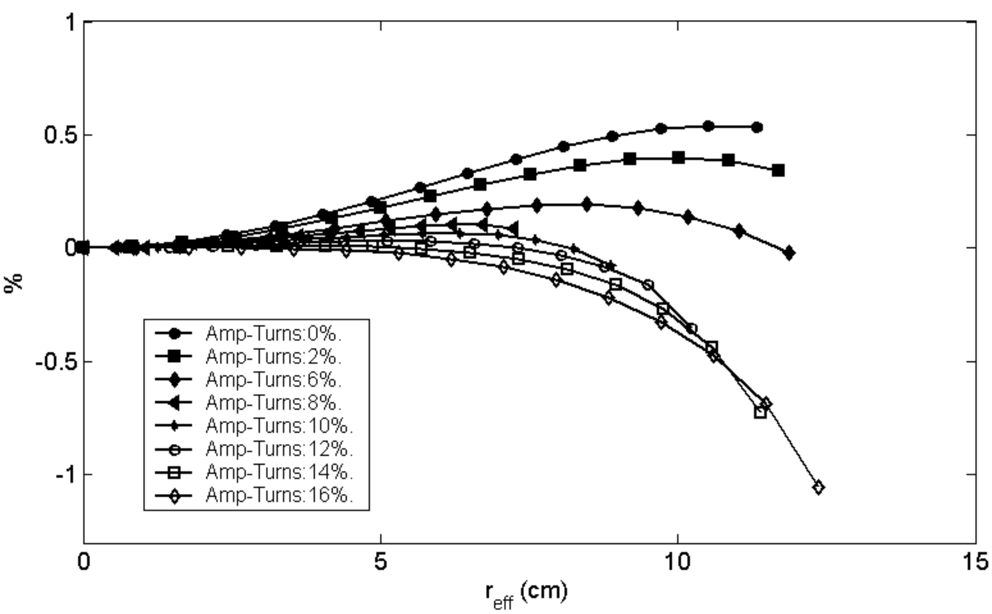

Figure A2.62: Well depth profiles in the Hill configurations.

Amp-Turn %	A_0	A_1	A_2	A_3	A_4
14	4589.0961	716.81786	45.007868	-52.341371	14.727537
12	4685.9862	649.52835	32.693796	-46.637953	11.70104
10	4787.0062	570.82659	19.460927	-42.468796	11.775286
8	4892.0209	469.89982	11.34611	-36.519783	5.9854209
4	5116.6163	870.01179	17.824357	17.297191	96.010043
2	5236.395	797.46601	1.7838349	35.399528	84.69277
-2	5492.3316	743.28421	-17.473452	21.016165	69.548888
-4	5629.3508	676.44988	-24.611627	15.122999	51.708197
-6	5771.7631	775.85184	-15.51015	1.1690291	15.423898
-8	5924.2321	769.71016	-69.909039	1.9185307	69.384808
-10	6083.0703	766.31327	-104.31327	-1.2842034	76.949356
-12	6250.2181	666.57914	-127.80641	11.393555	50.544482
-14	6426.8773	458.26024	-117.51357	24.450845	13.738153

Table A2.16: Fit coefficients for I_{main} as a function of flux surface where the resonance resides, for the Hill/Well continuum of configurations.

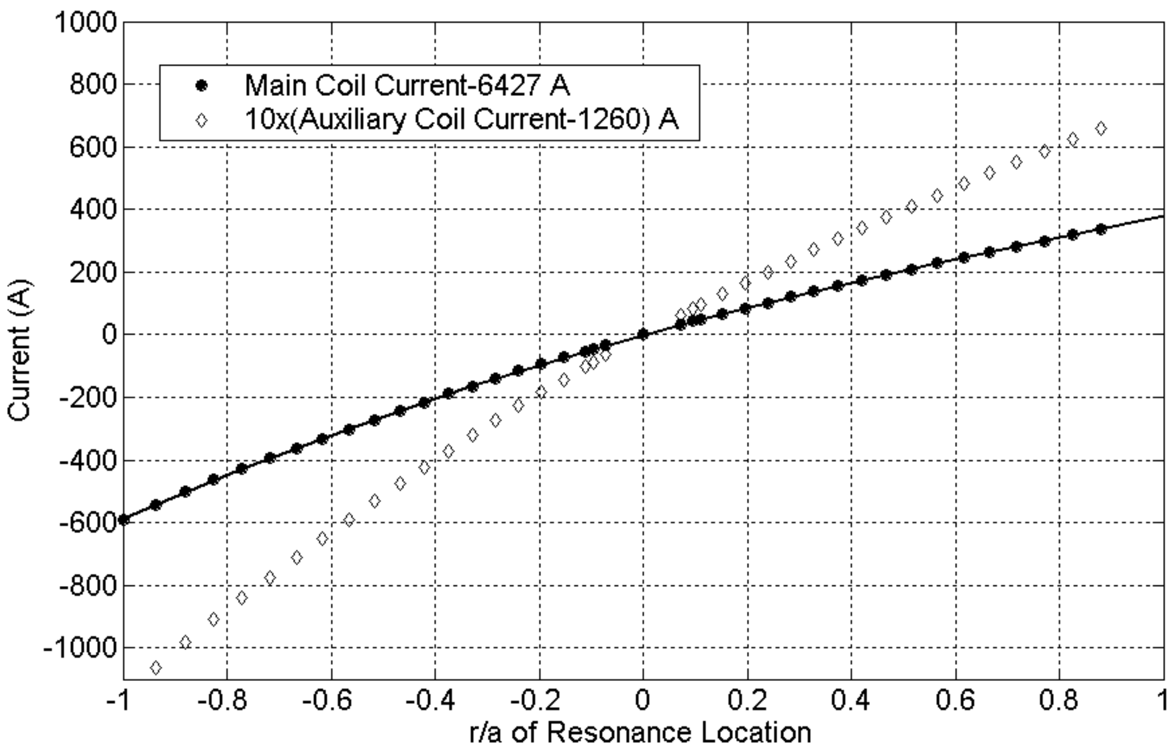

Figure A2.63: Magnet currents for shifting the resonance in the 14% Well configuration.

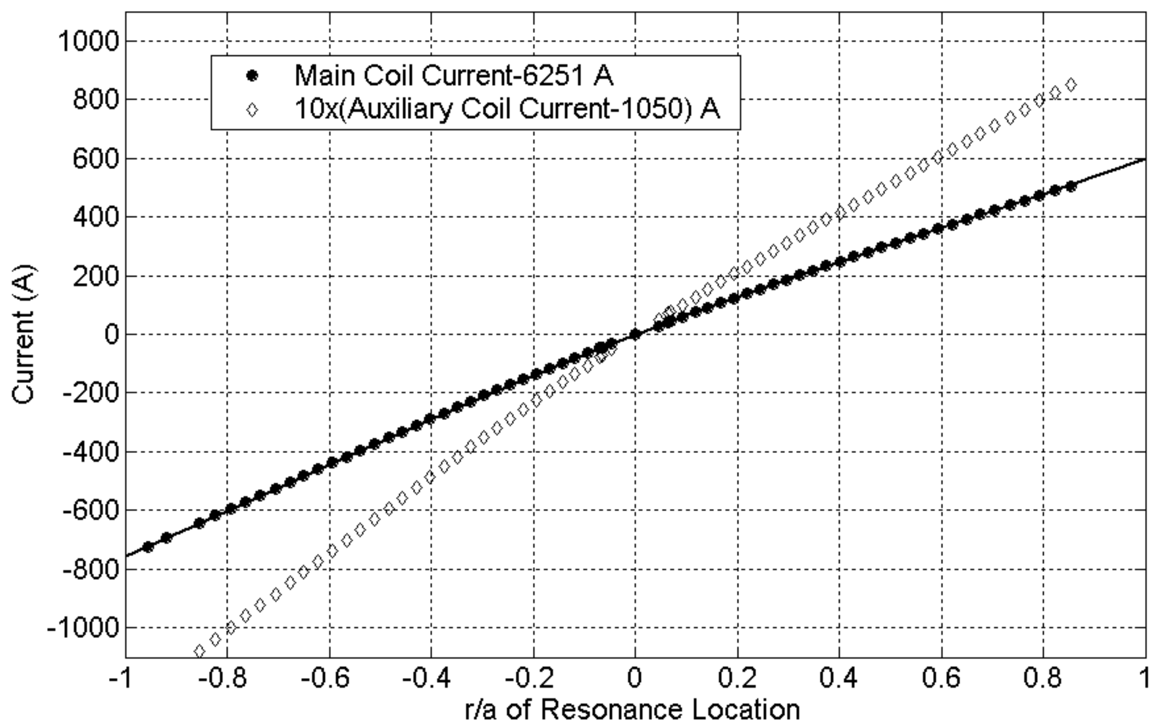

Figure A2.64: Magnet currents for shifting the resonance in the 12% Well configuration.

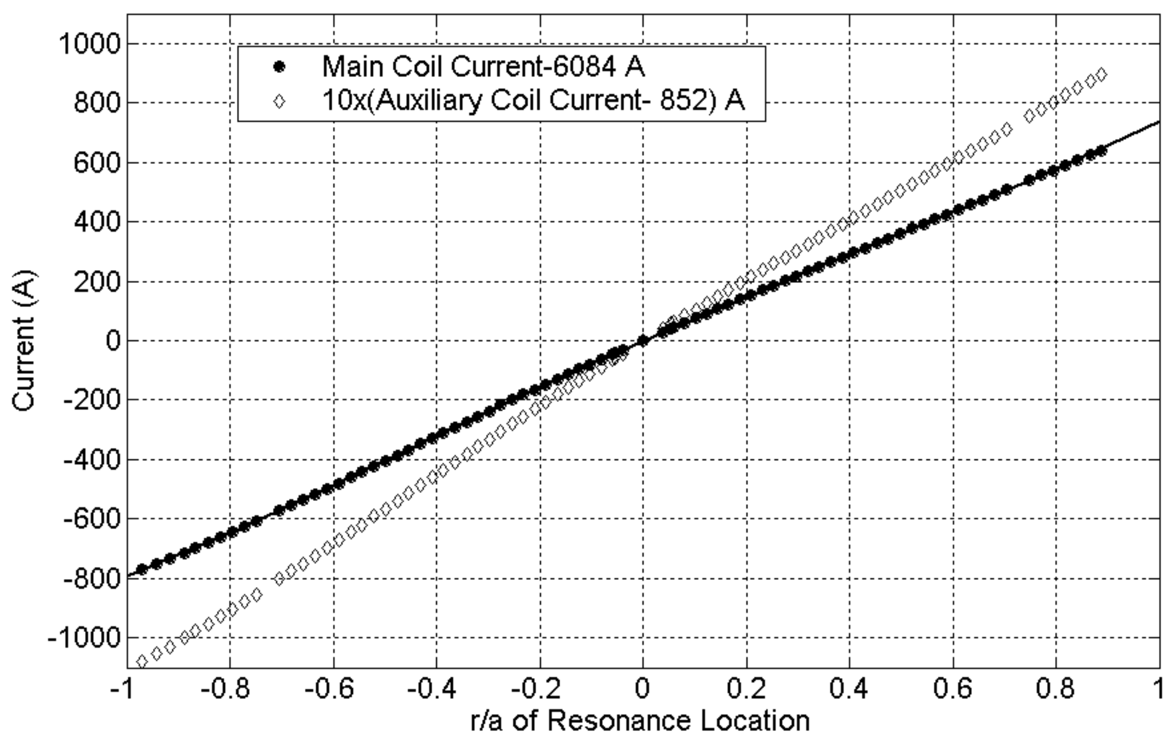

Figure A2.65: Magnet currents for shifting the resonance in the 10% Well configuration.

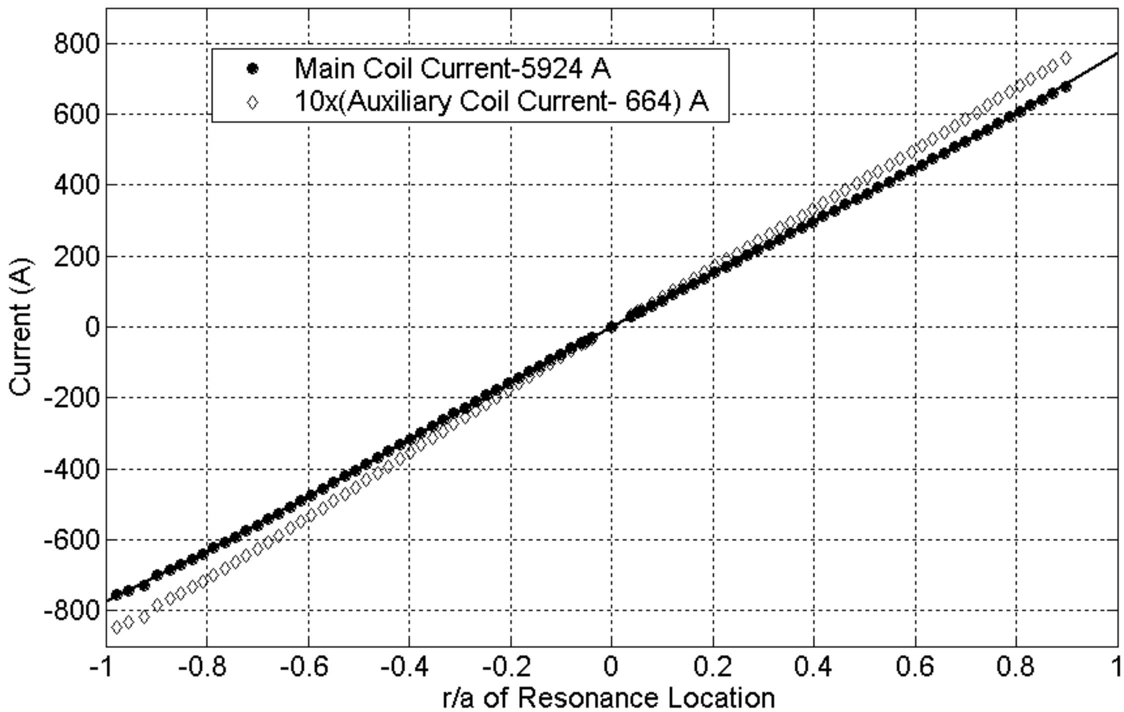

Figure A2.66: Magnet currents for shifting the resonance in the 8% Well configuration.

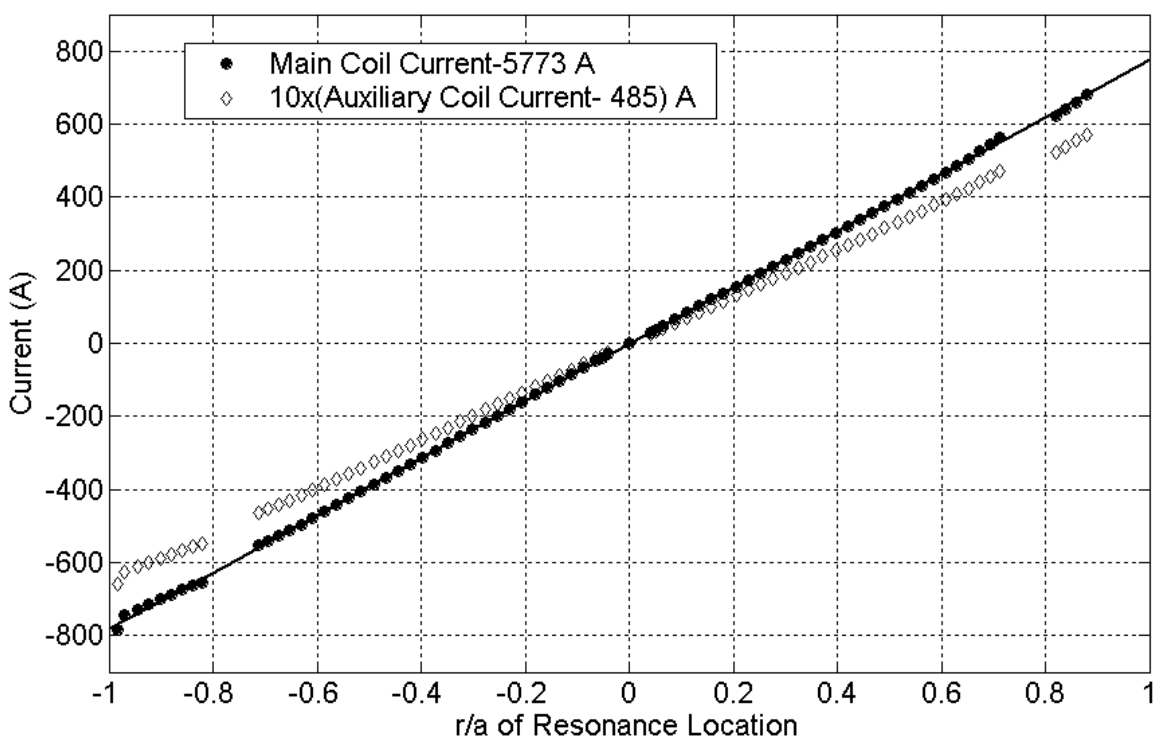

Figure A2.67: Magnet currents for shifting the resonance in the 6% Well configuration.

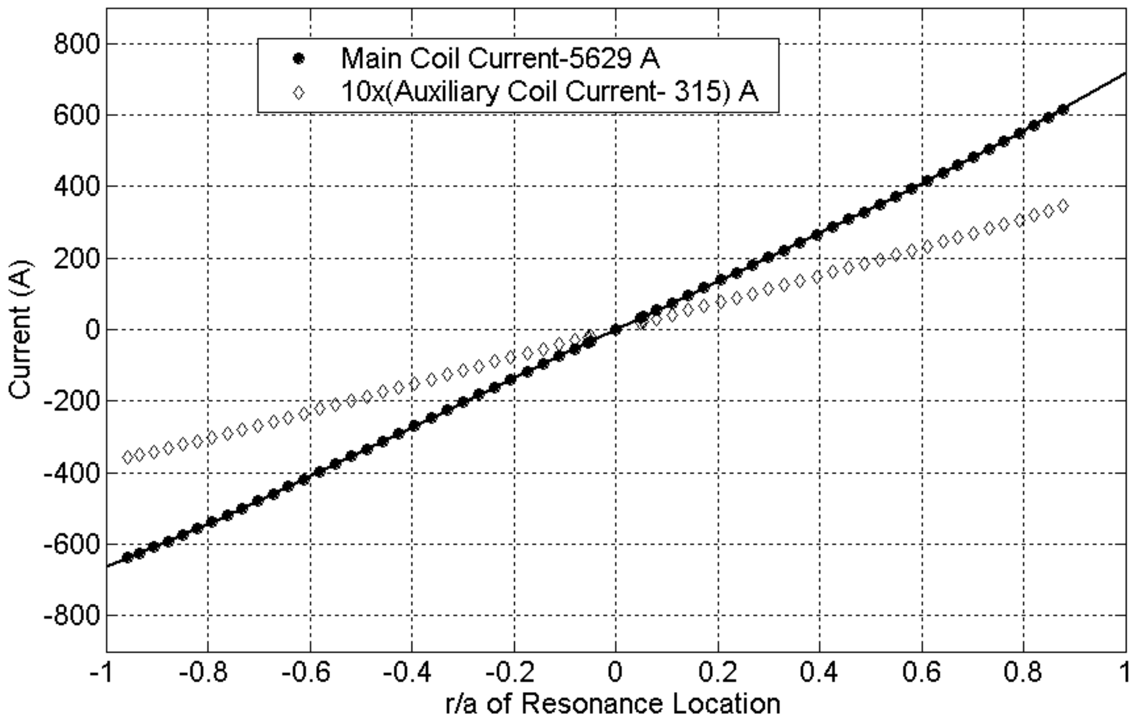

Figure A2.68: Magnet currents for shifting the resonance in the 4% Well configuration.

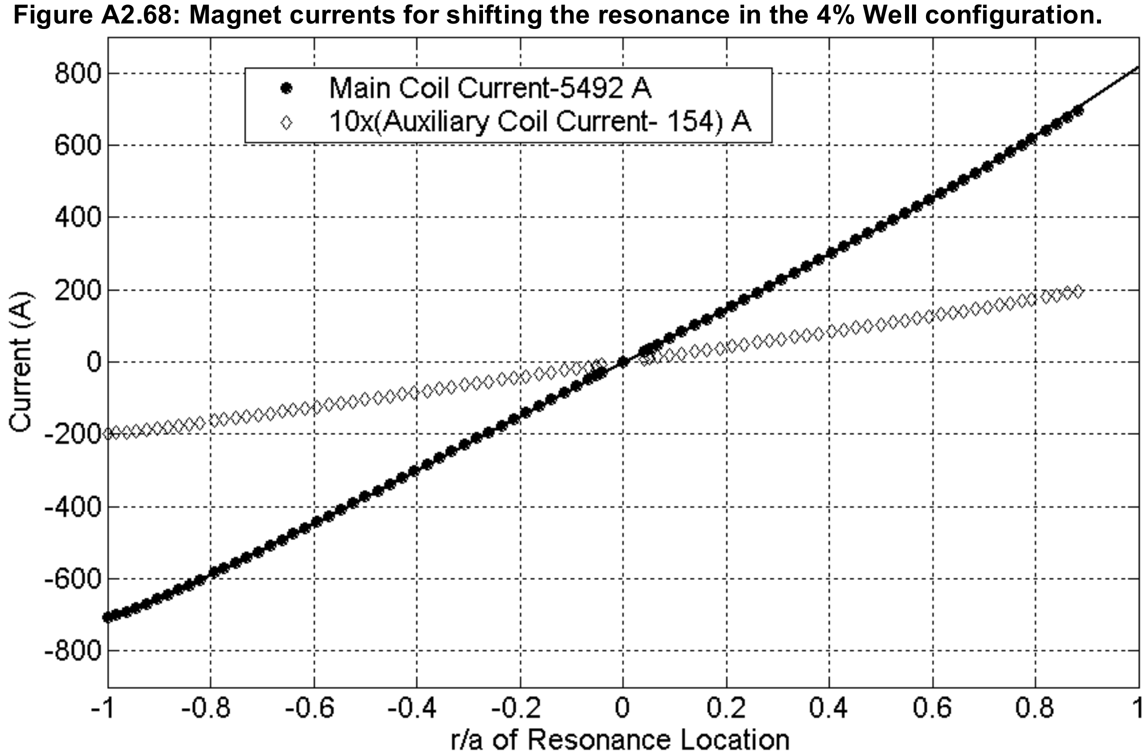

Figure A2.69: Magnet currents for shifting the resonance in the 2% Well configuration.

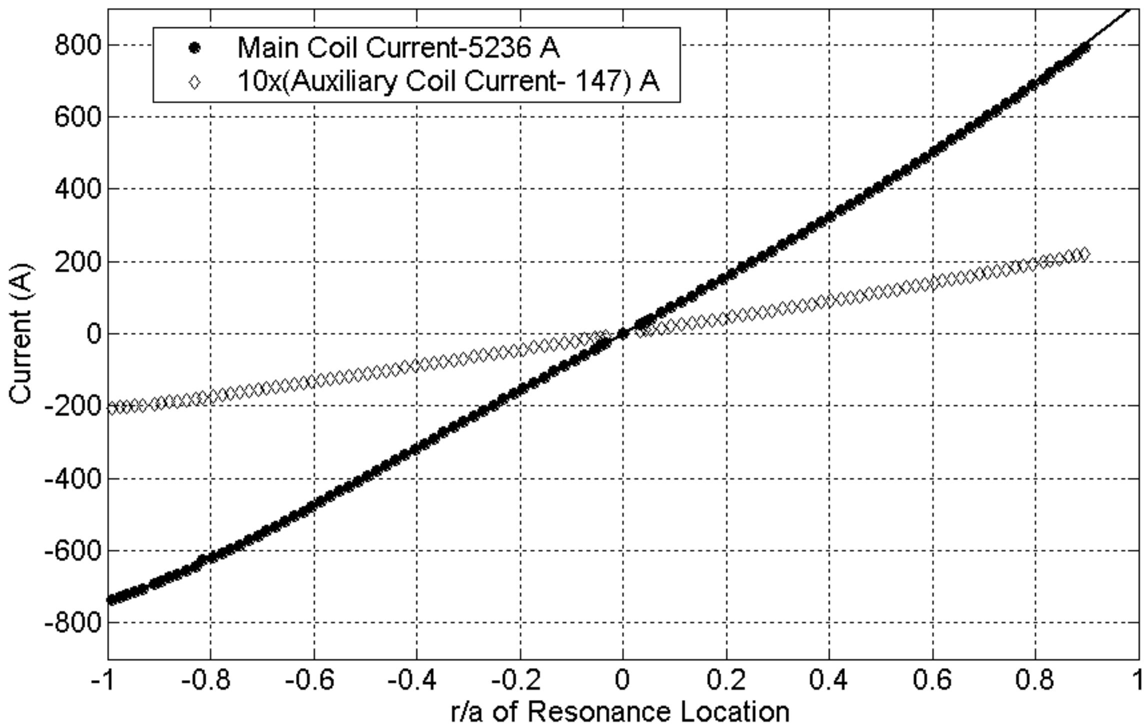

Figure A2.70: Magnet currents for shifting the resonance in the 2% Hill configuration.

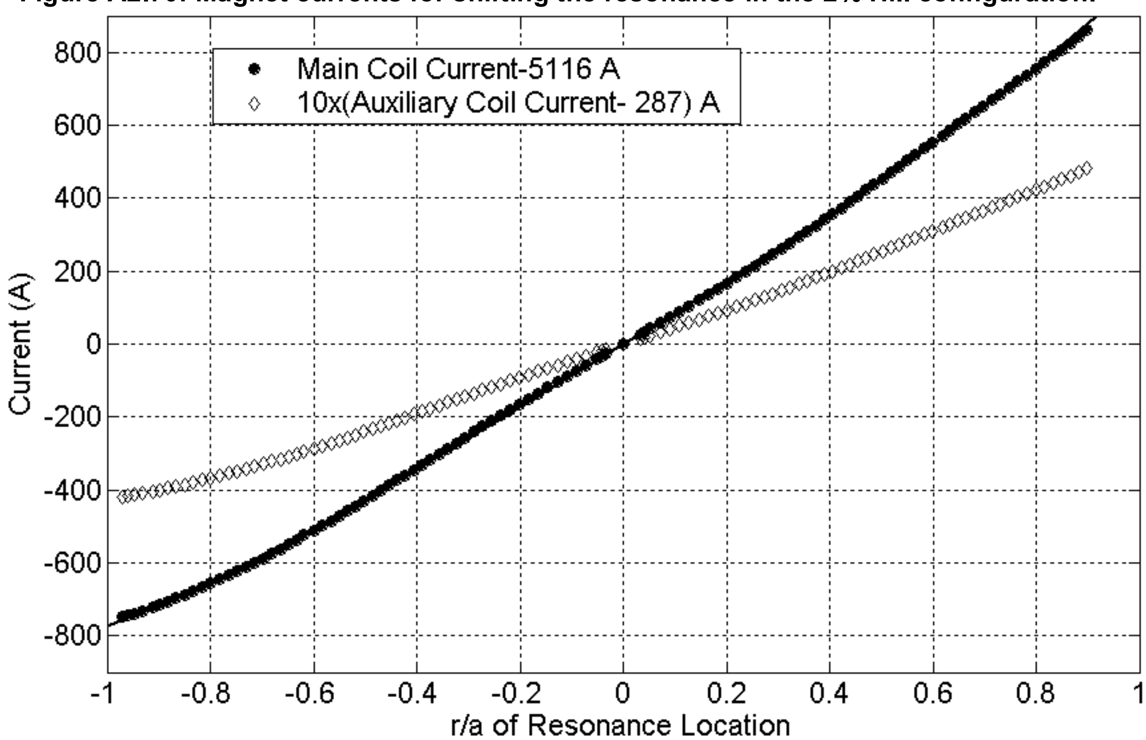

Figure A2.71: Magnet currents for shifting the resonance in the 4% Hill configuration.

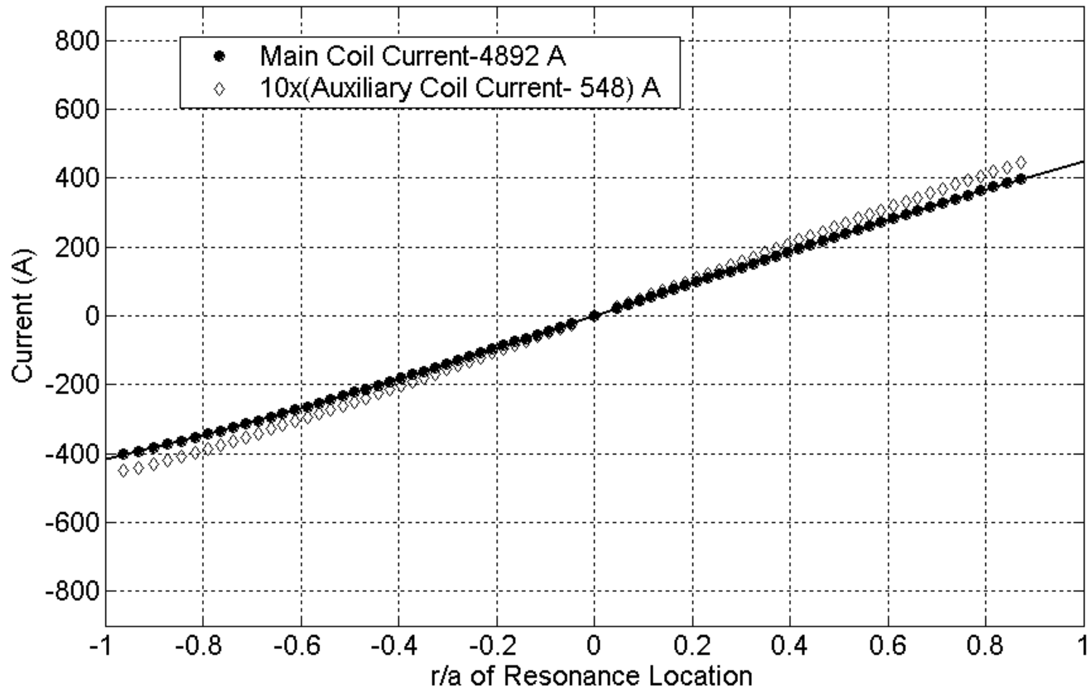

Figure A2.72: Magnet currents for shifting the resonance in the 8% Hill configuration.

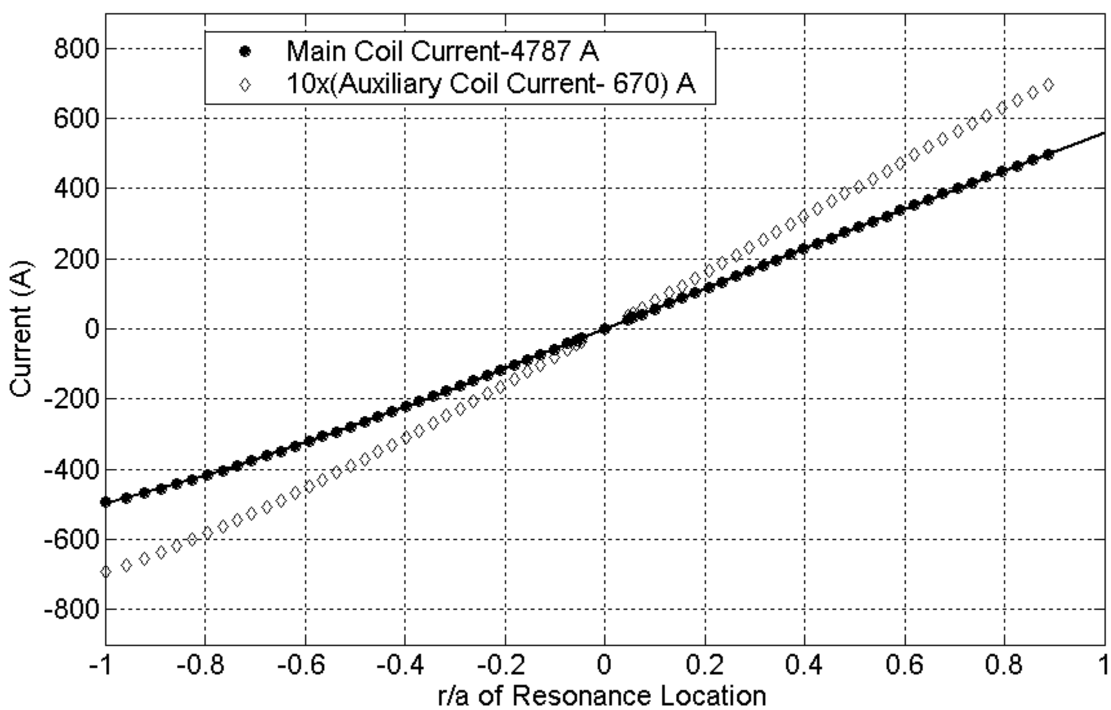

Figure A2.73: Magnet currents for shifting the resonance in the 10% Hill configuration.

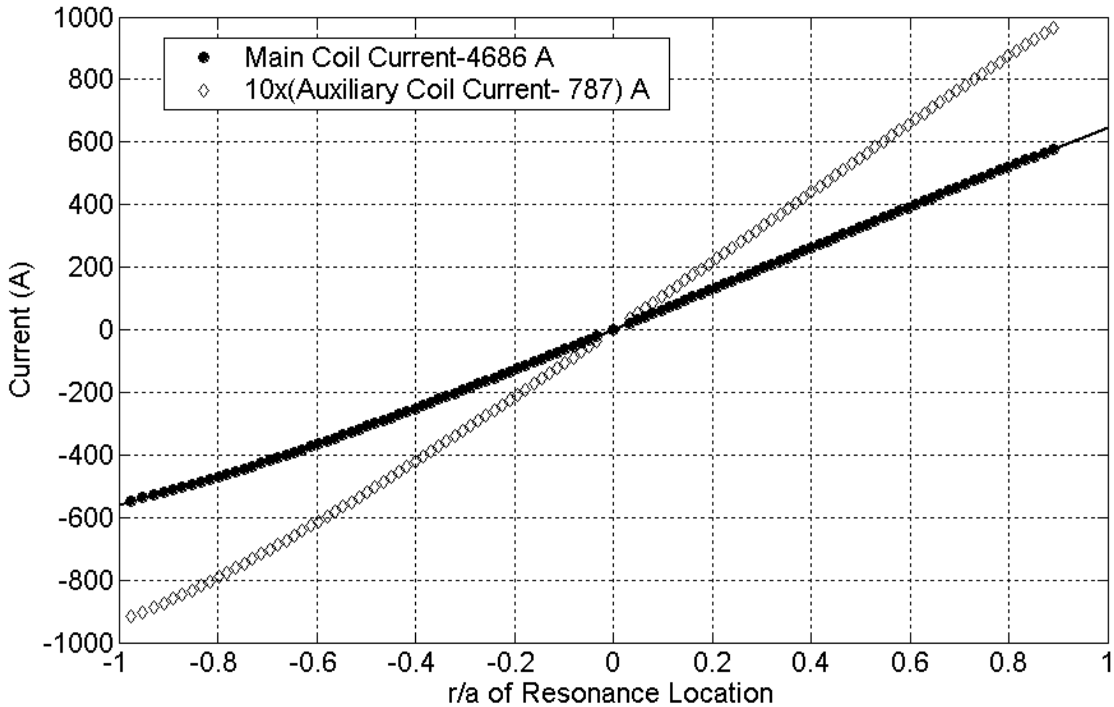

Figure A2.74: Magnet currents for shifting the resonance in the 12% Hill configuration.

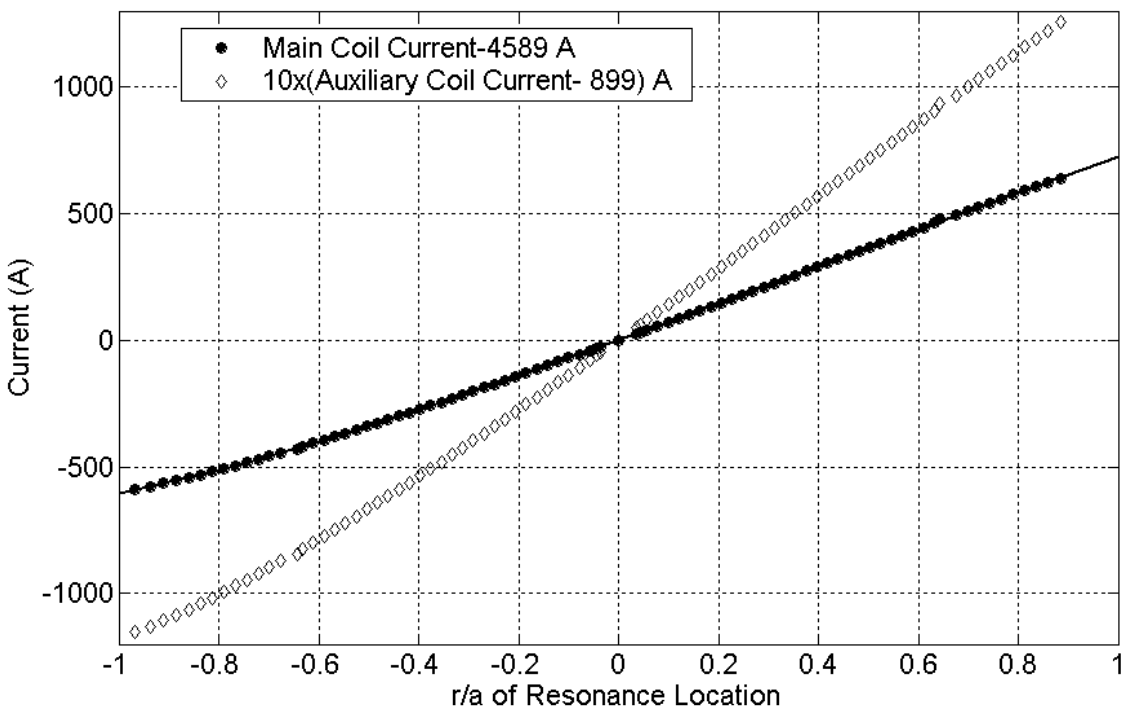

Figure A2.75: Magnet currents for shifting the resonance in the 14% Hill configuration.

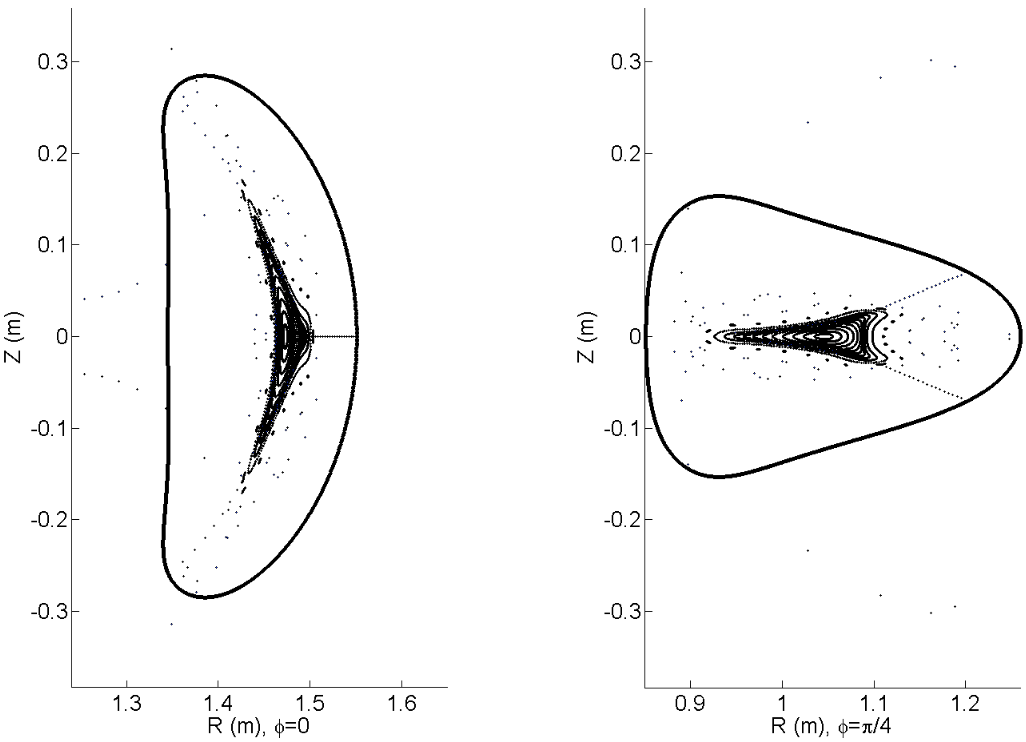

Figure A2.76: Flux Surfaces in 20% Well configuration (ɩ>4/3 inside LCFS)

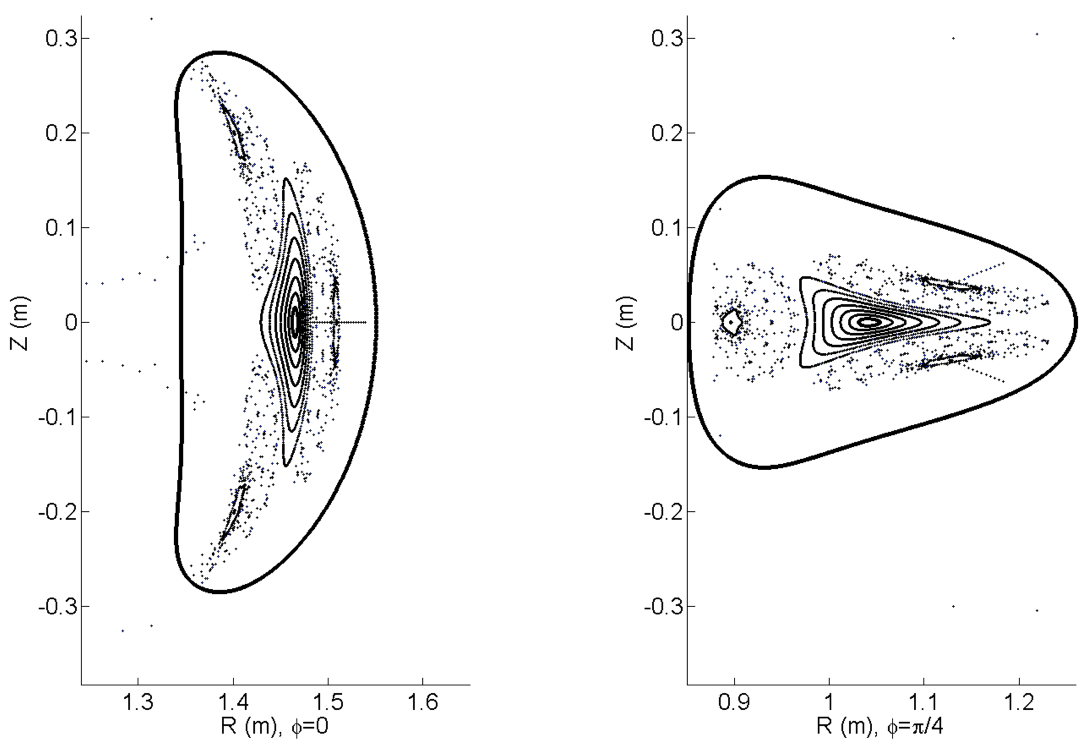

Figure A2.77: Flux Surfaces in 15% Well configuration.

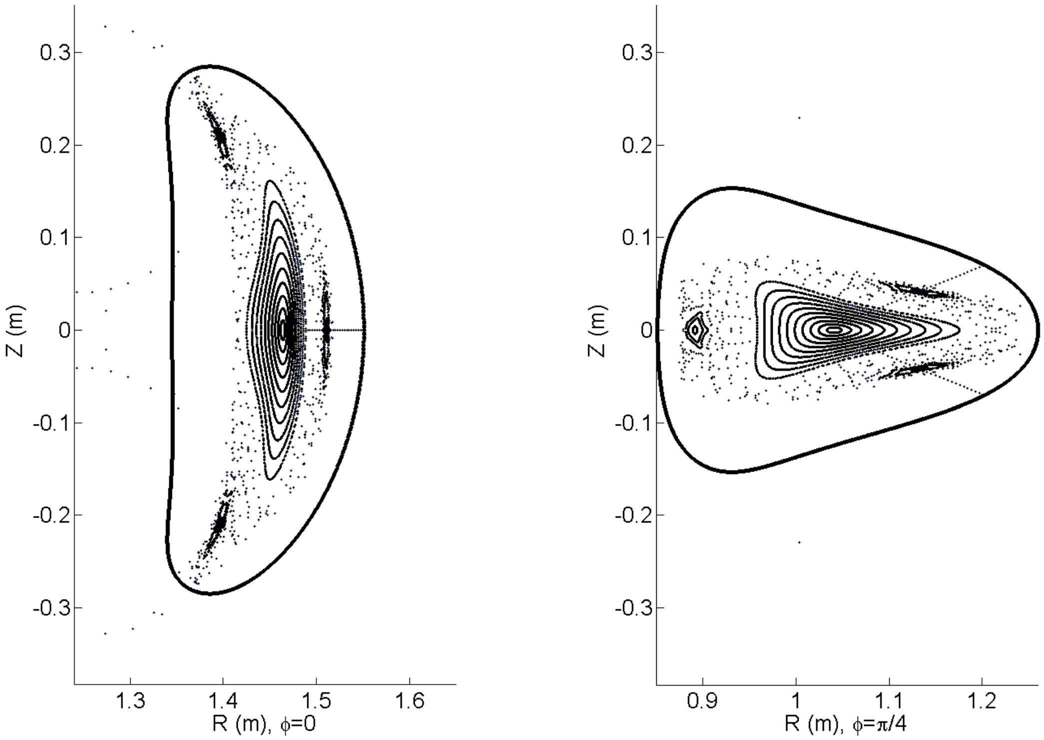

Figure A2.78: Flux Surfaces in 14% Well configuration.

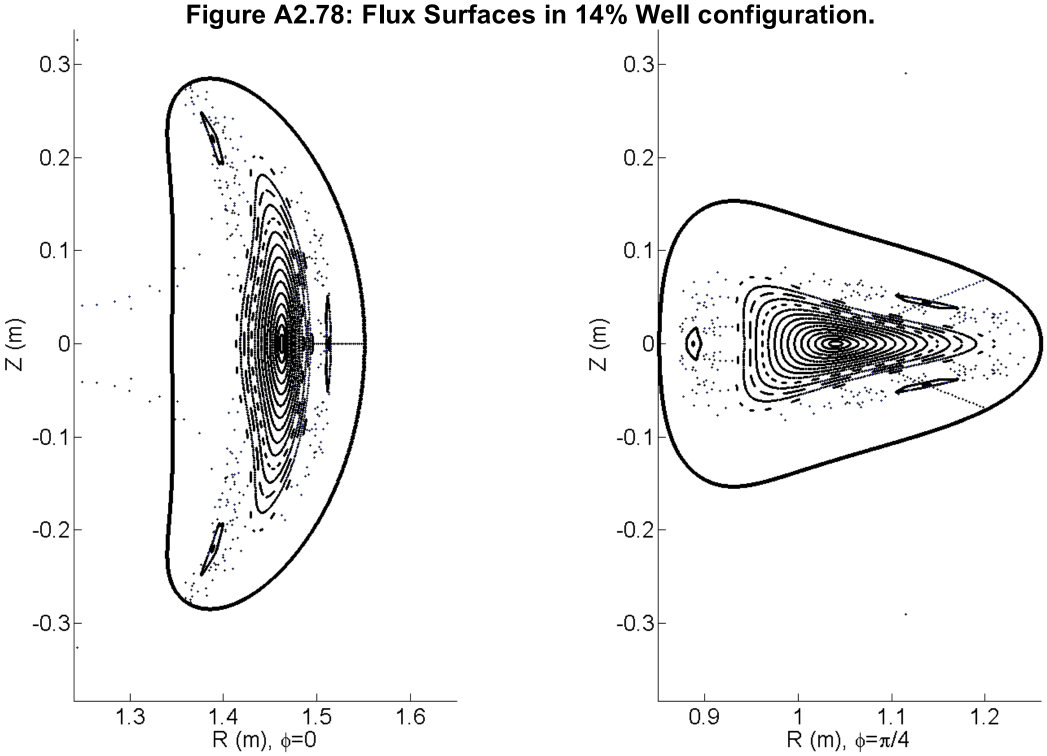

Figure A2.79: Flux Surfaces in 13% Well configuration

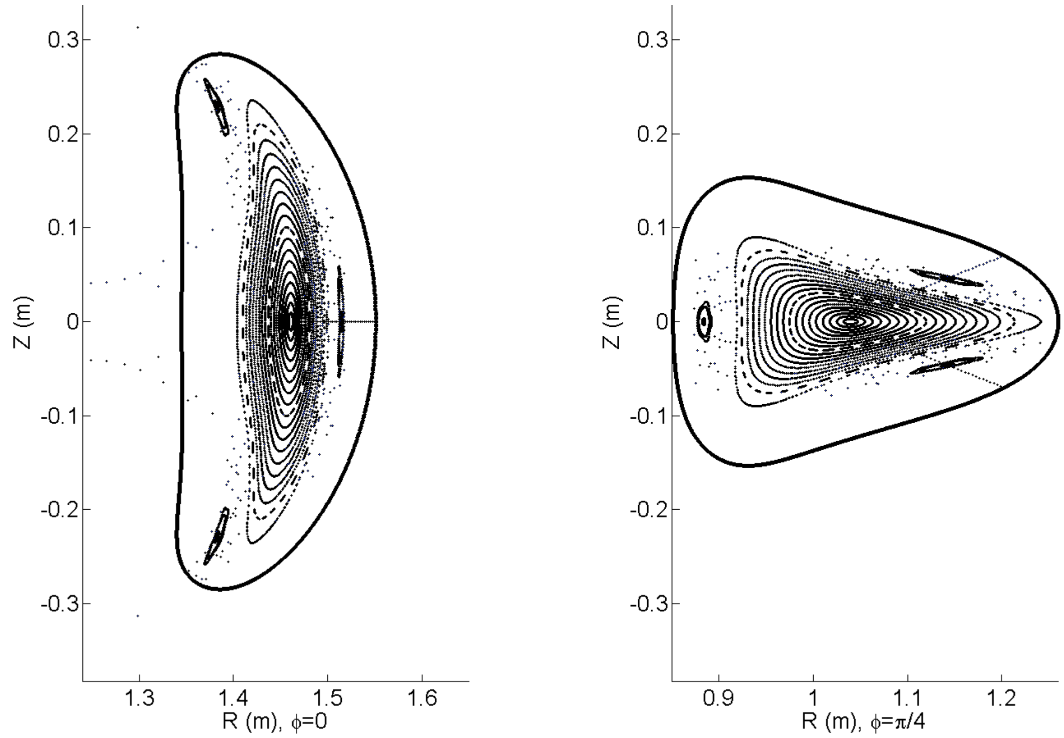

Figure A2.80: Flux Surfaces in 12% Well configuration

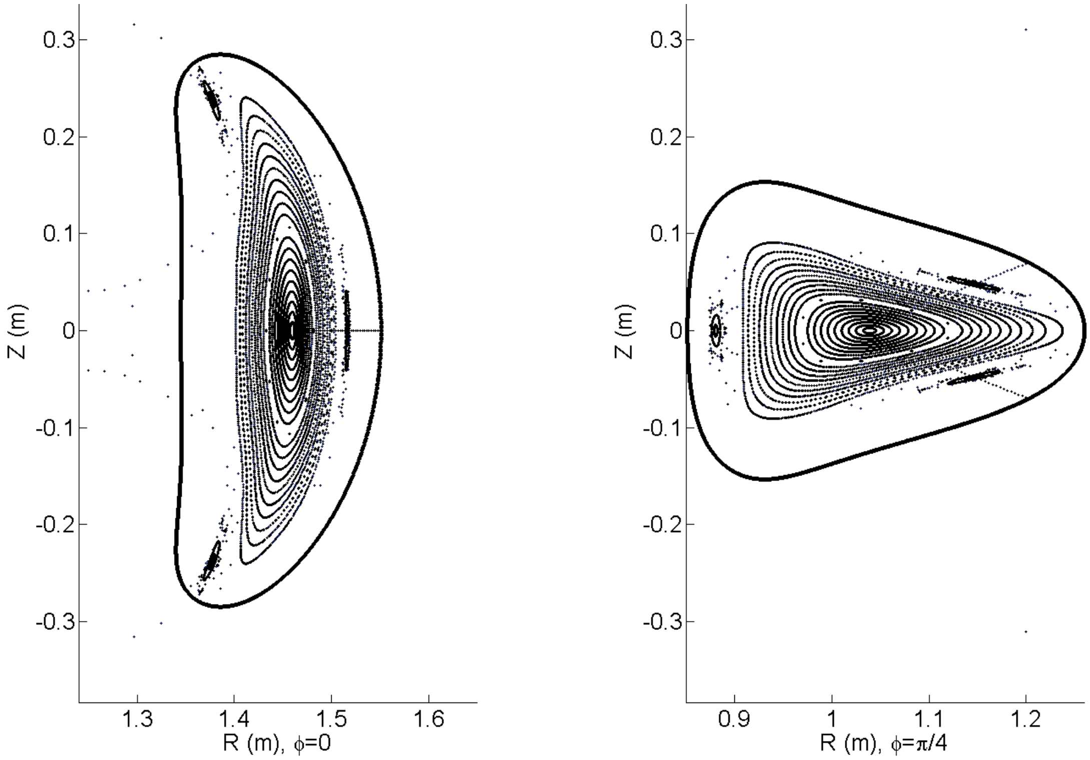

Figure A2.81: Flux Surfaces in 11% Well configuration

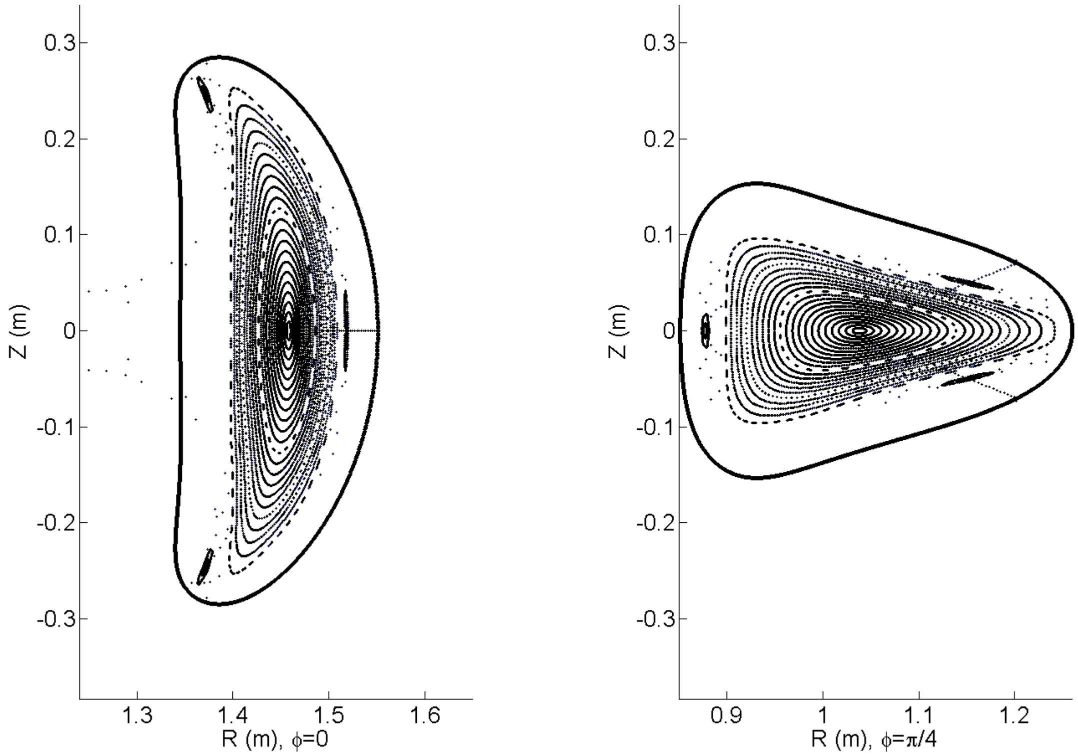

Figure A2.82: Flux Surfaces in 10% Well configuration

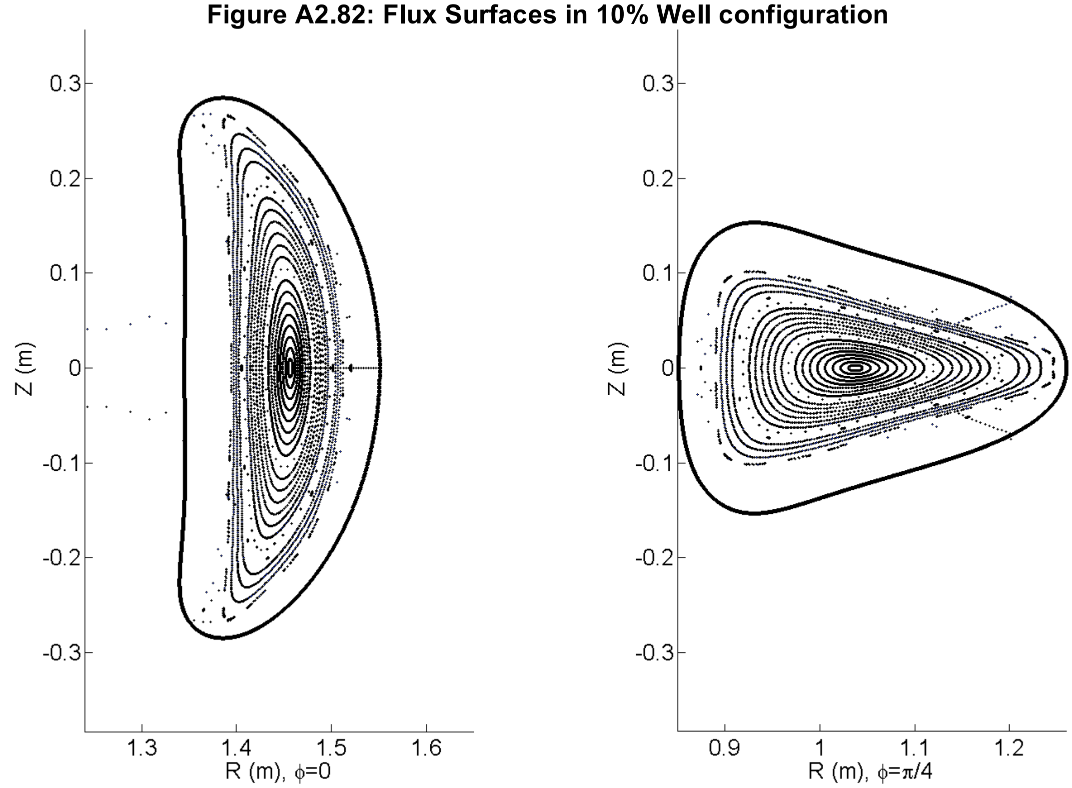

Figure A2.83: Flux Surfaces in 9% Well configuration

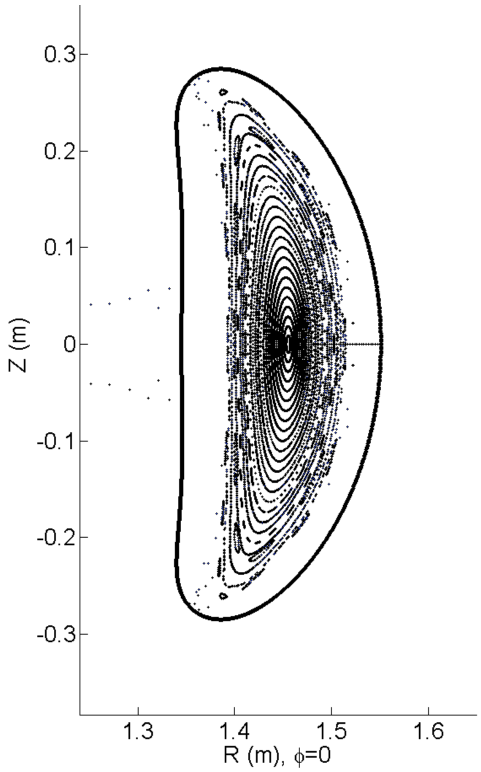

Figure A2.84: Flux Surfaces in 8% Well configuration

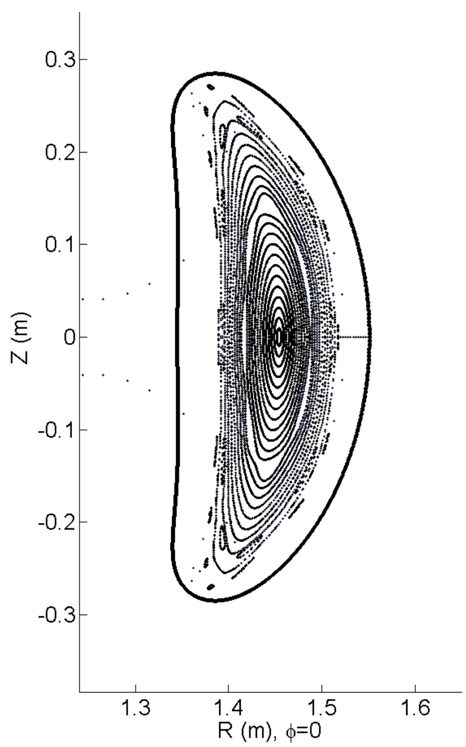

Figure A2.85: Flux Surfaces in 7% Well configuration

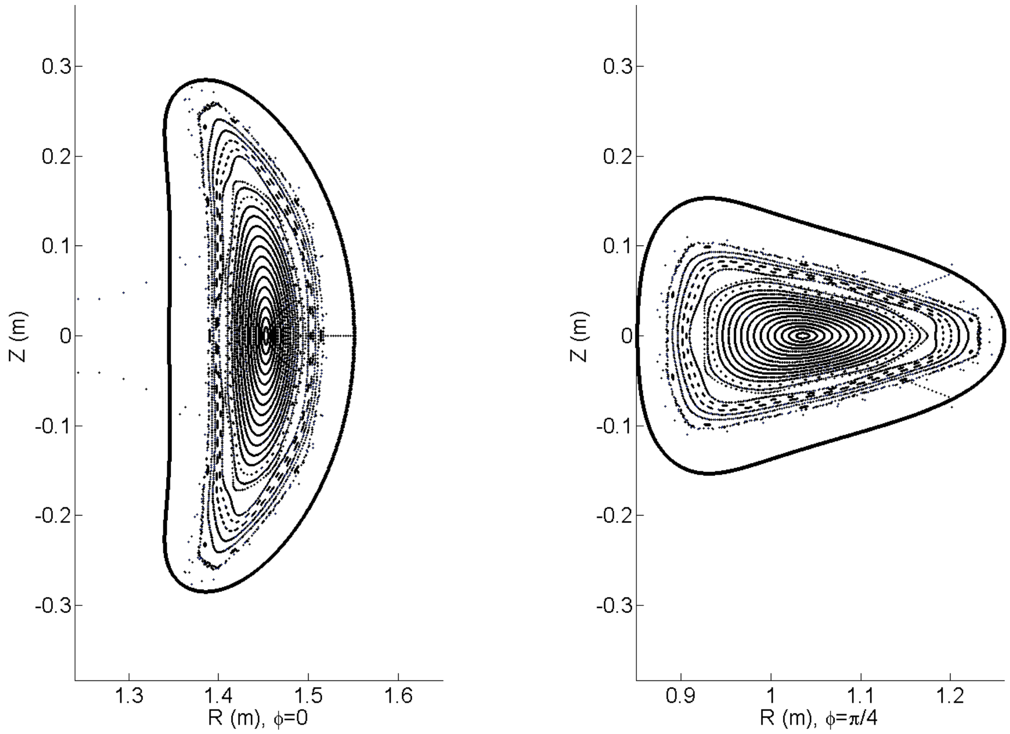

Figure A2.86: Flux Surfaces in 6% Well configuration

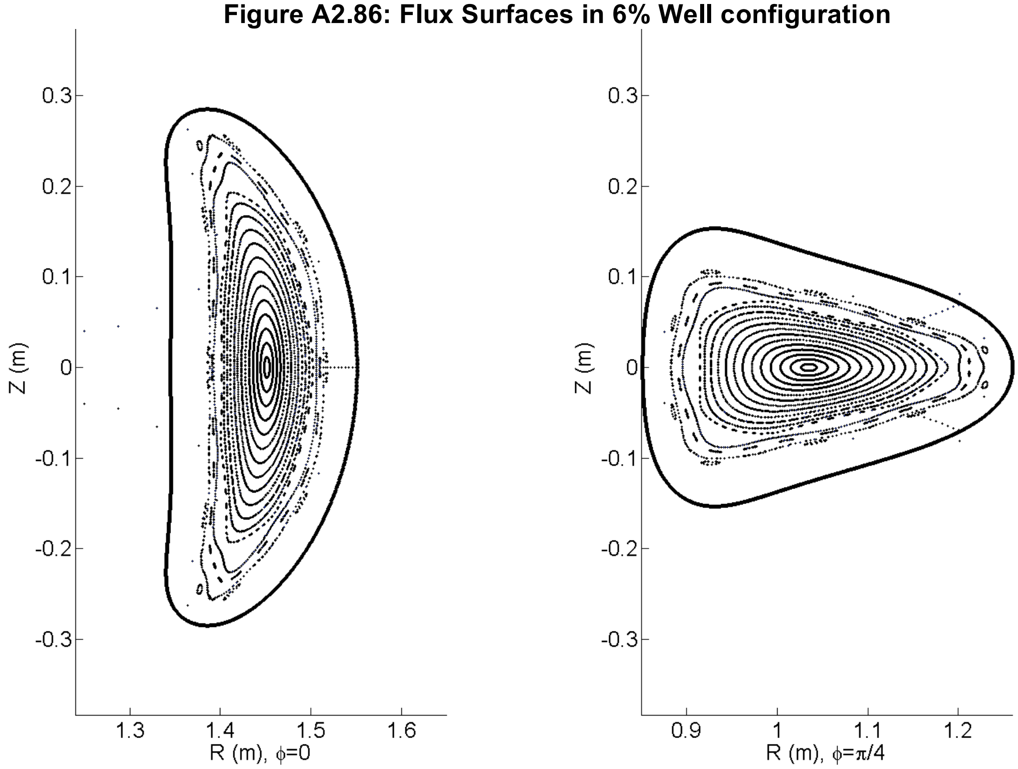

Figure A2.87: Flux Surfaces in 5% Well configuration

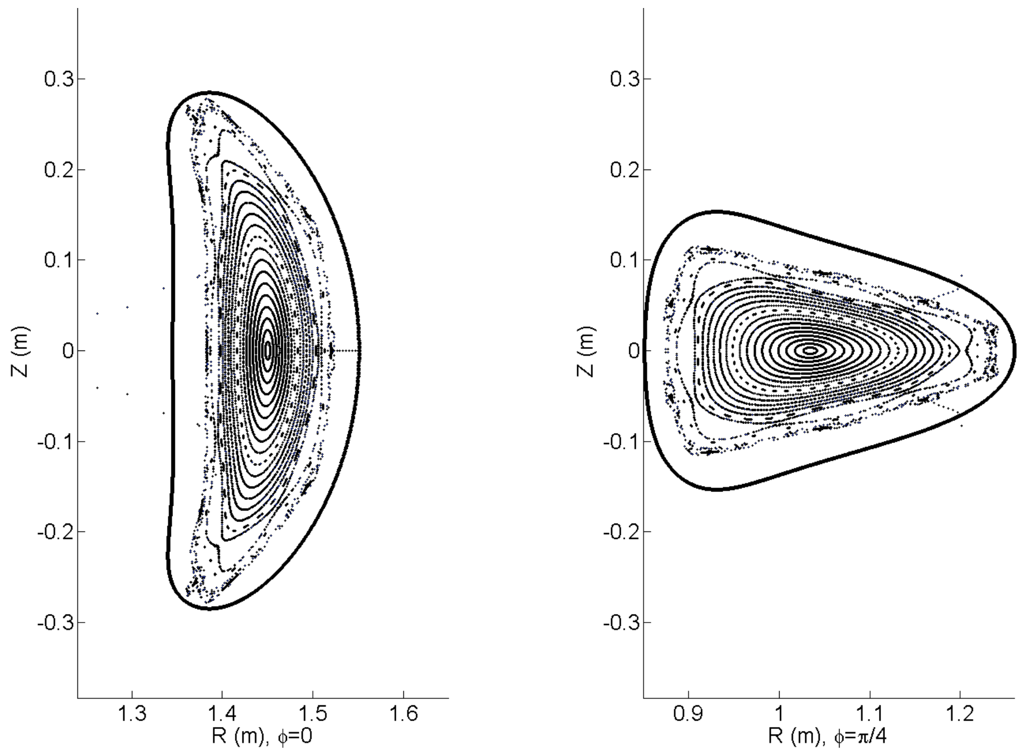

Figure A2.88: Flux Surfaces in 4% Well configuration

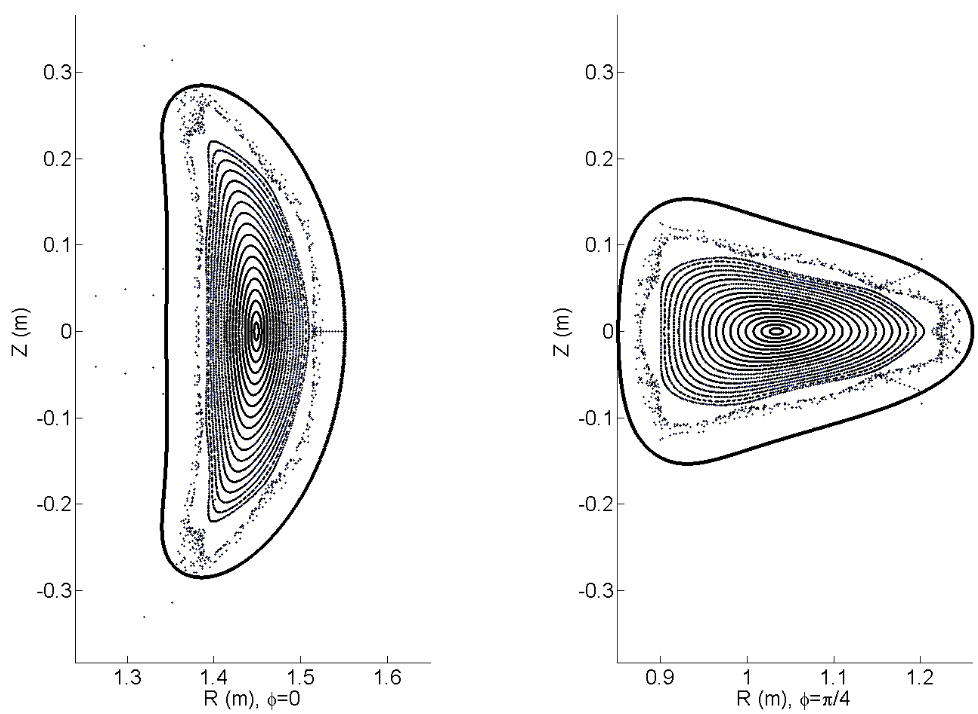

Figure A2.89: Flux Surfaces in 3% Well configuration

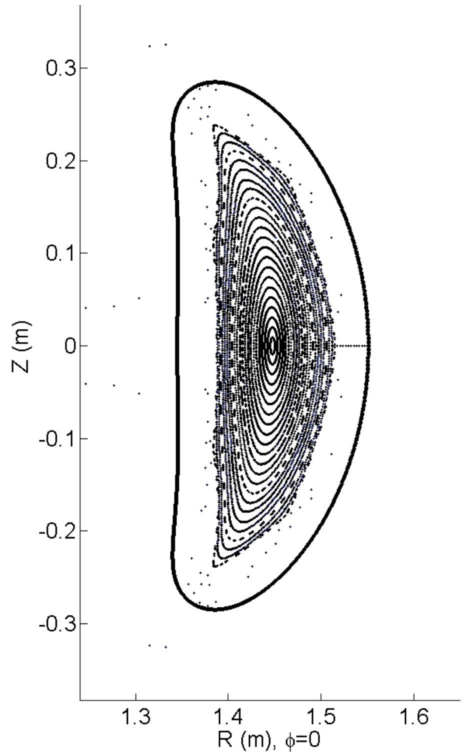

Figure A2.90: Flux Surfaces in 2% Well configuration

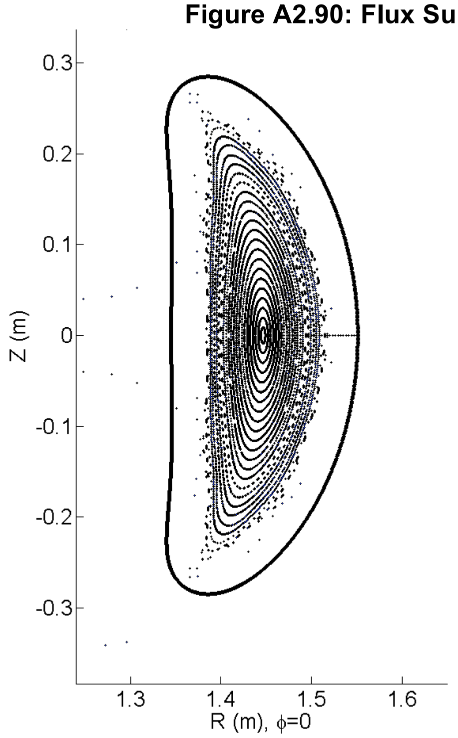

Figure A2.91: Flux Surfaces in 1% Well configuration

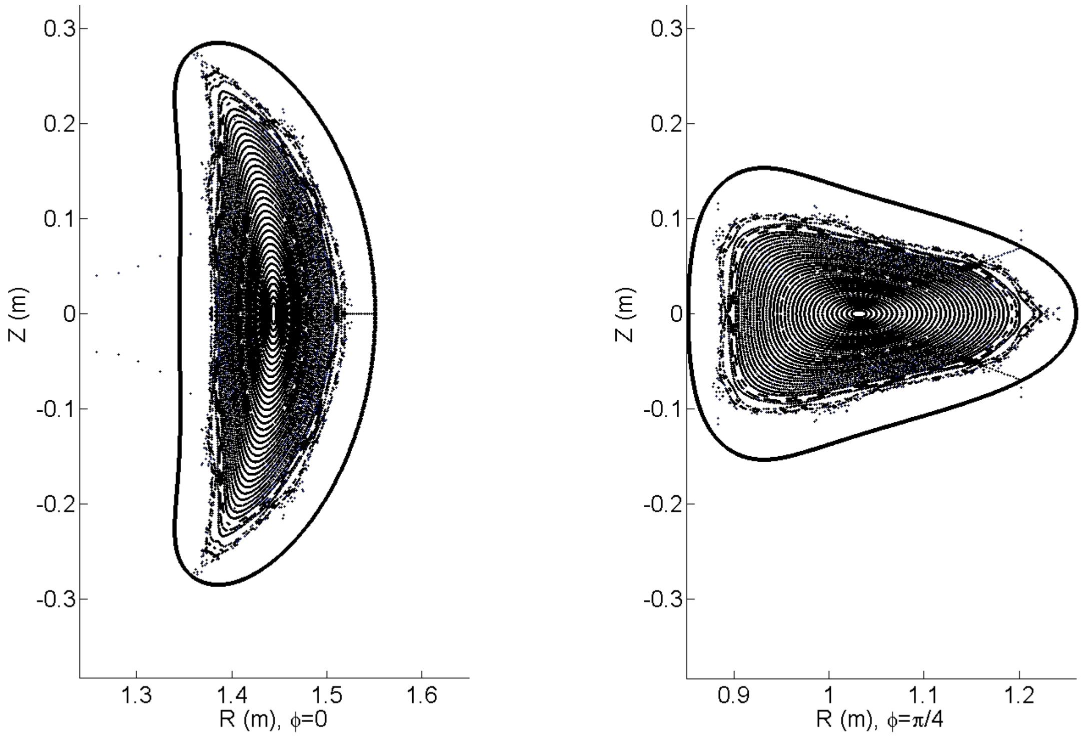

Figure A2.92: Flux Surfaces in 1% Hill configuration

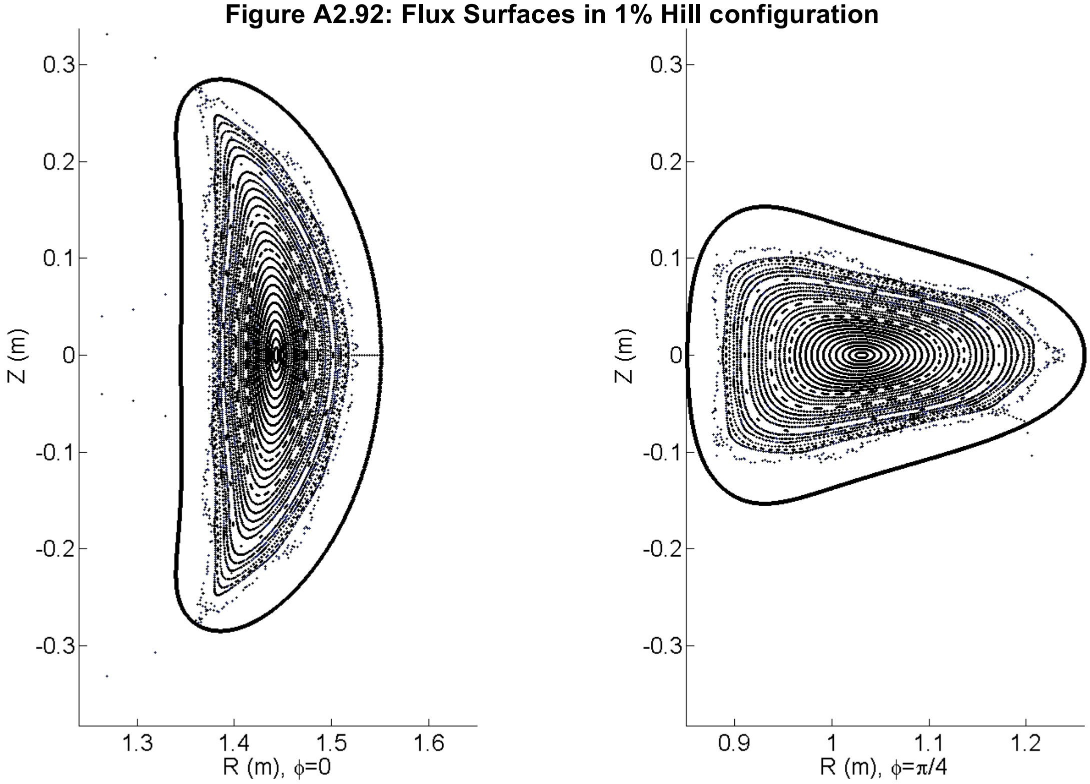

Figure A2.93: Flux Surfaces in 2% Hill configuration

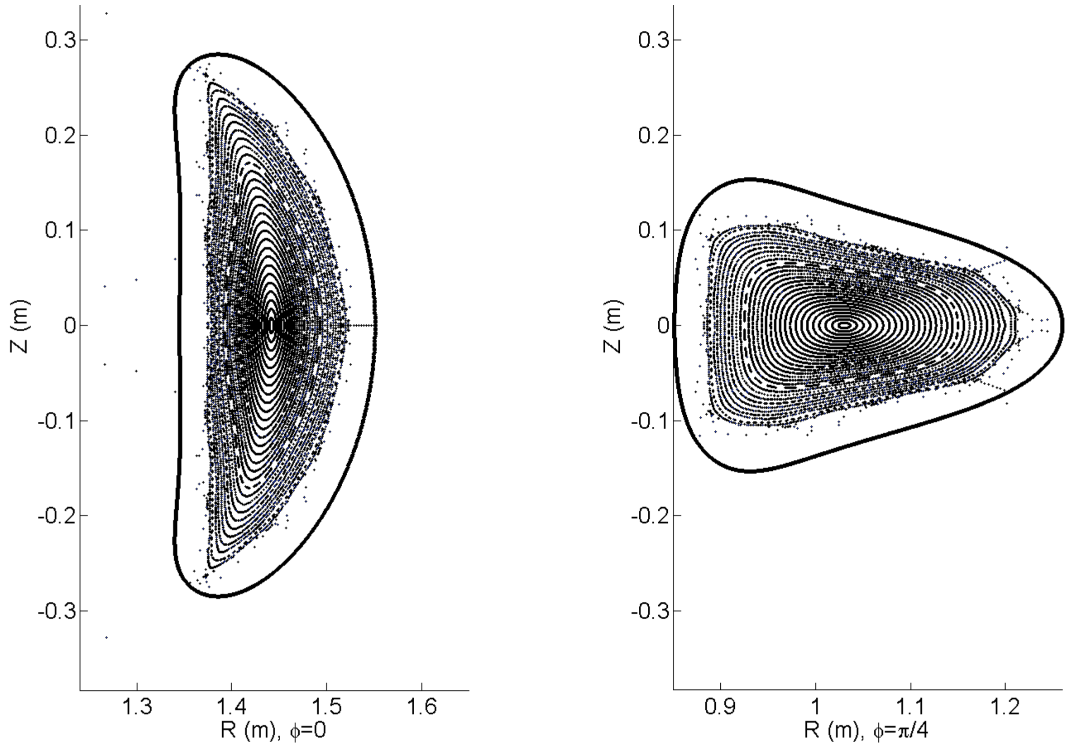

Figure A2.94: Flux Surfaces in 3% Hill configuration

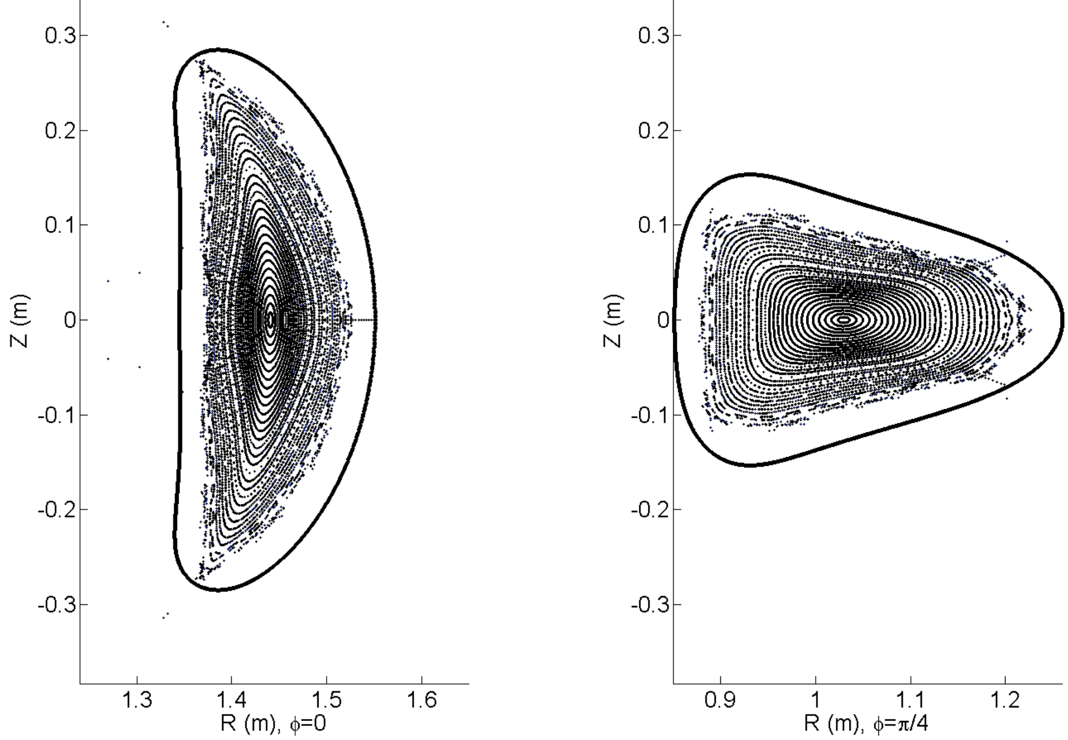

Figure A2.95: Flux Surfaces in 4% Hill configuration

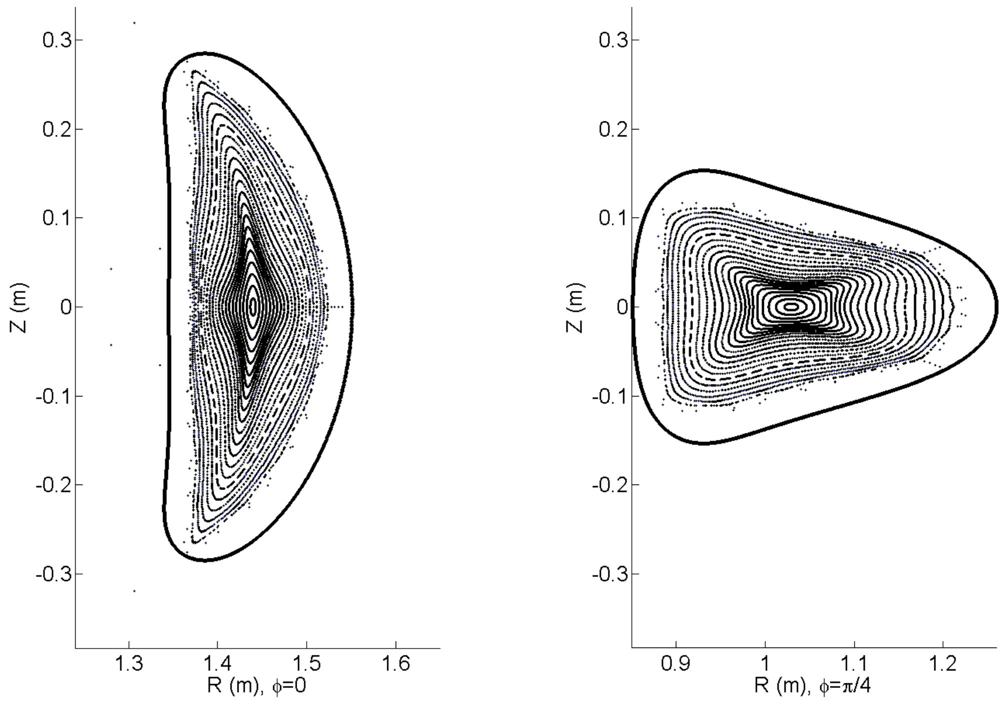

Figure A2.96: Flux Surfaces in 5% Hill configuration

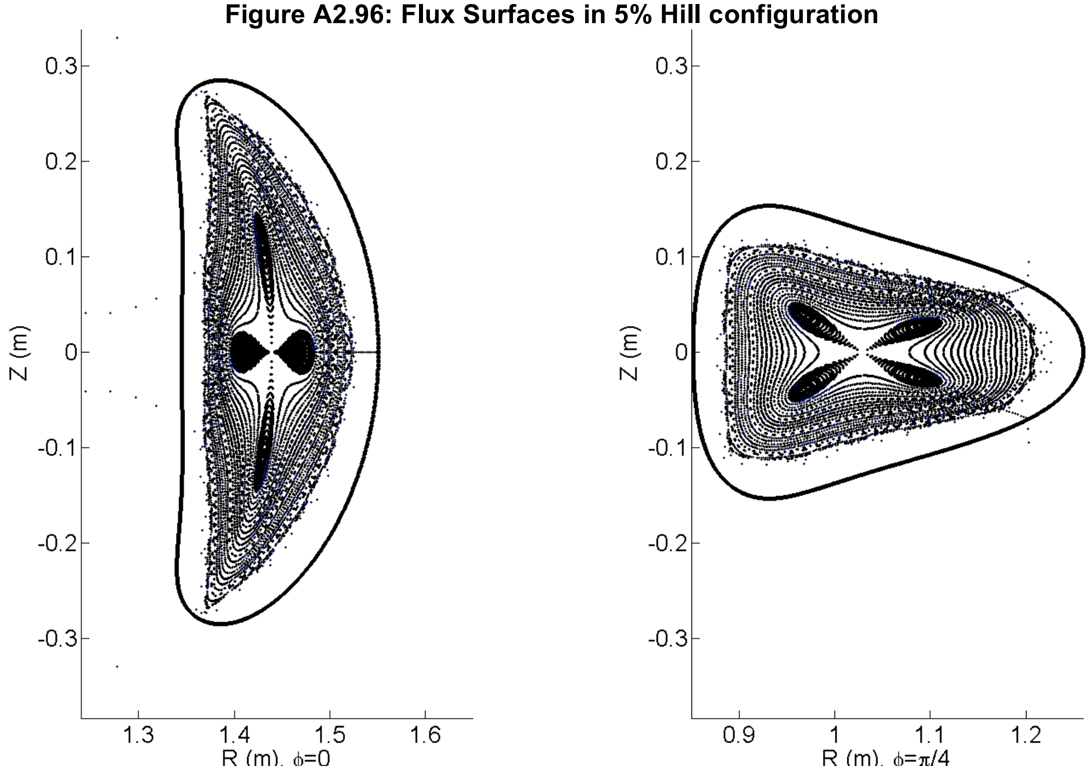

Figure A2.97: Flux Surfaces in 5.25% Hill configuration

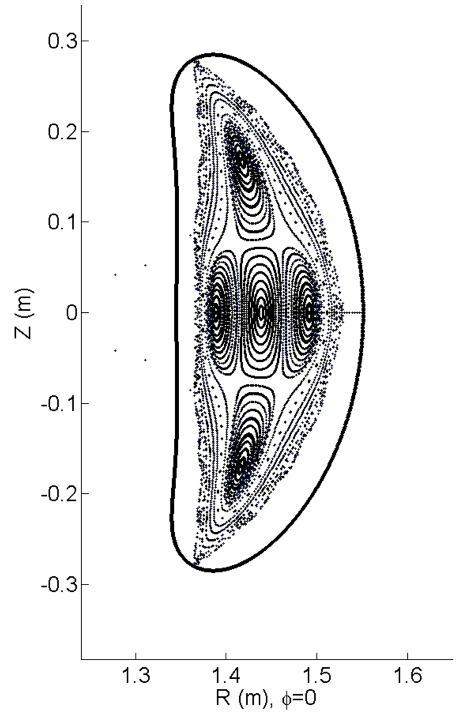

Figure A2.98: Flux Surfaces in 6% Hill configuration

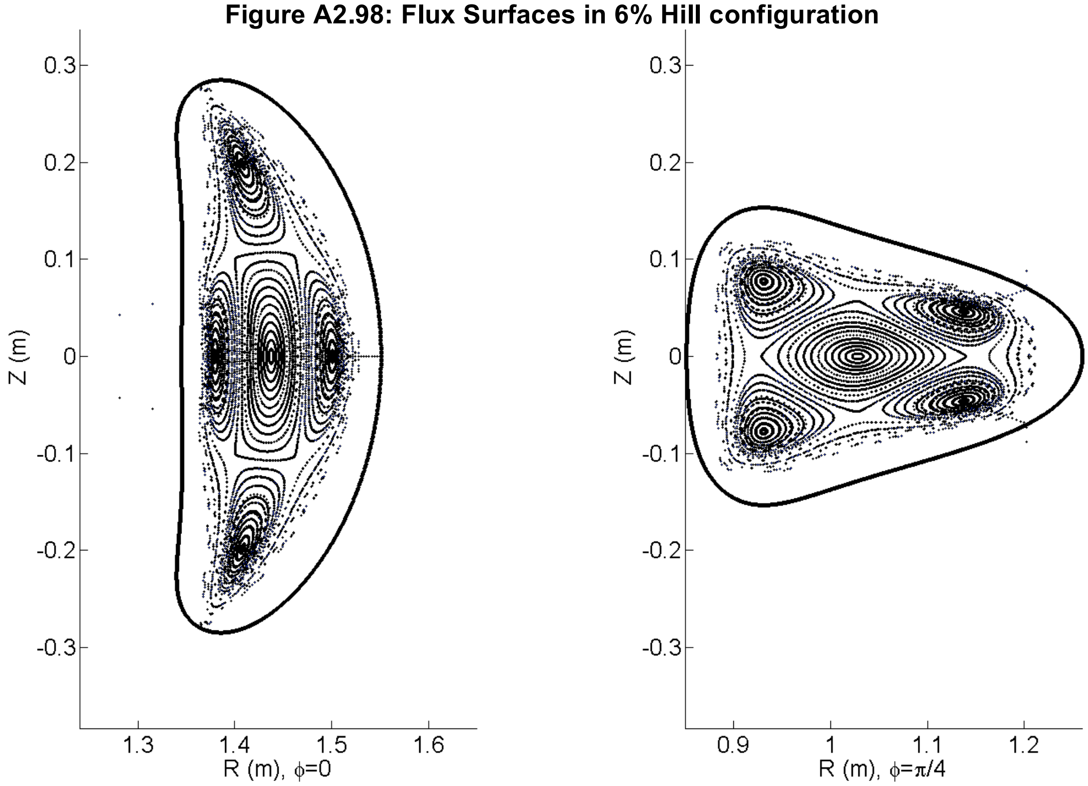

Figure A2.99: Flux Surfaces in 7% Hill configuration

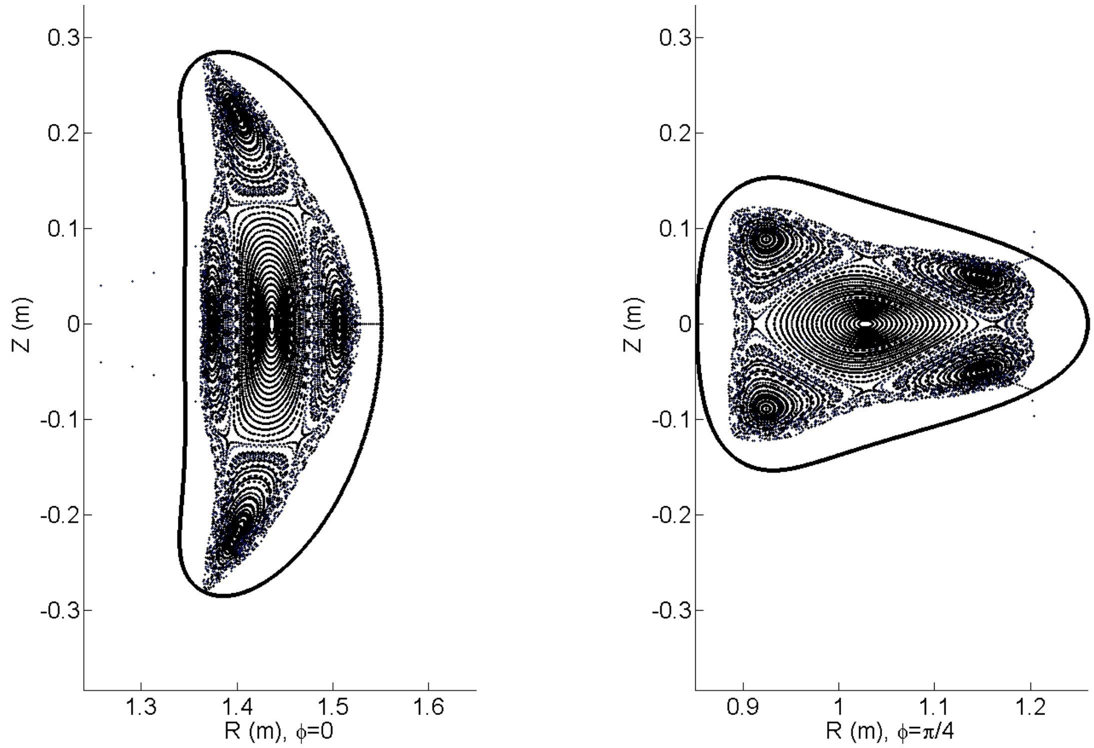

Figure A2.100: Flux Surfaces in 8% Hill configuration

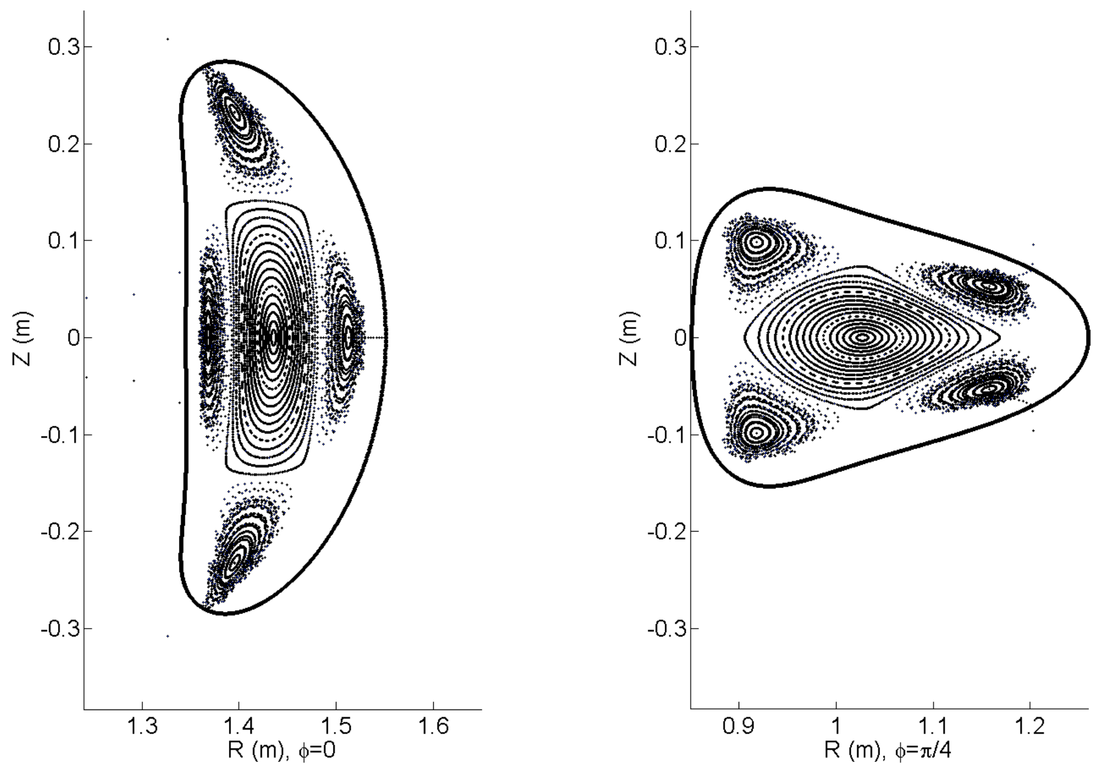

Figure A2.101: Flux Surfaces in 9% Hill configuration (ι<1 inside LCFS).

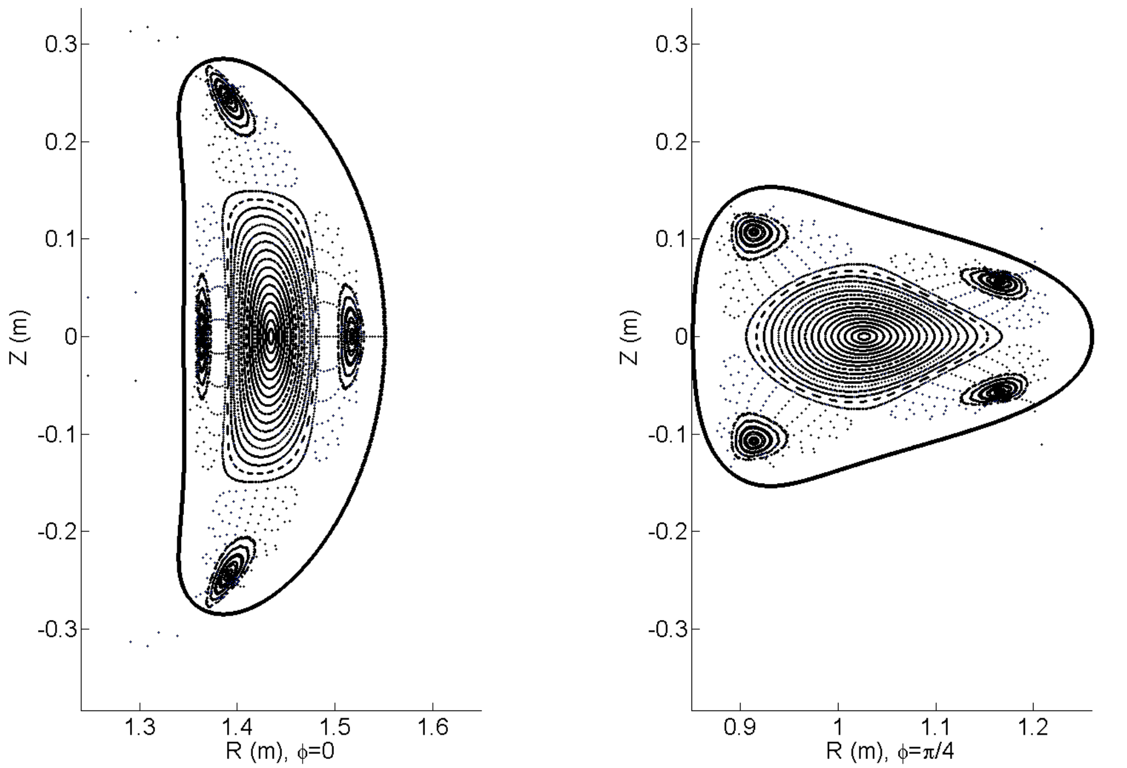

Figure A2.102: Flux Surfaces in 10% Hill configuration (ι<1 inside LCFS)

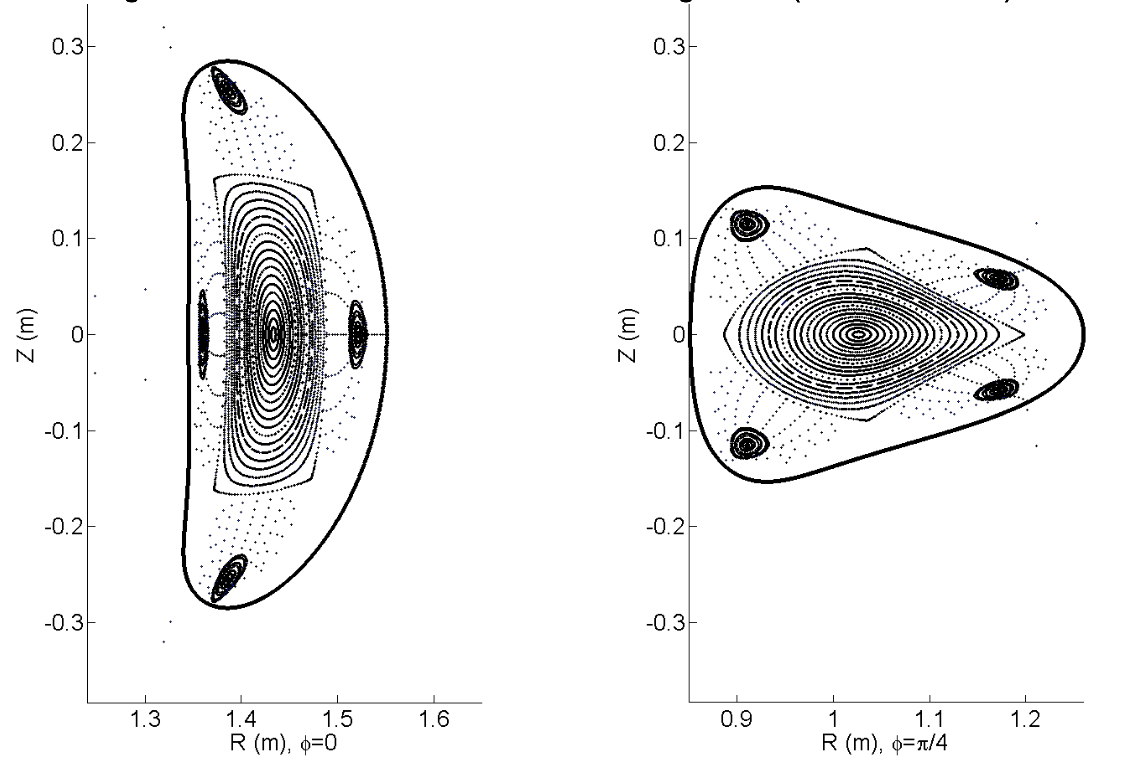

Figure A2.103: Flux Surfaces in 11% Hill configuration (ι<1 inside LCFS)

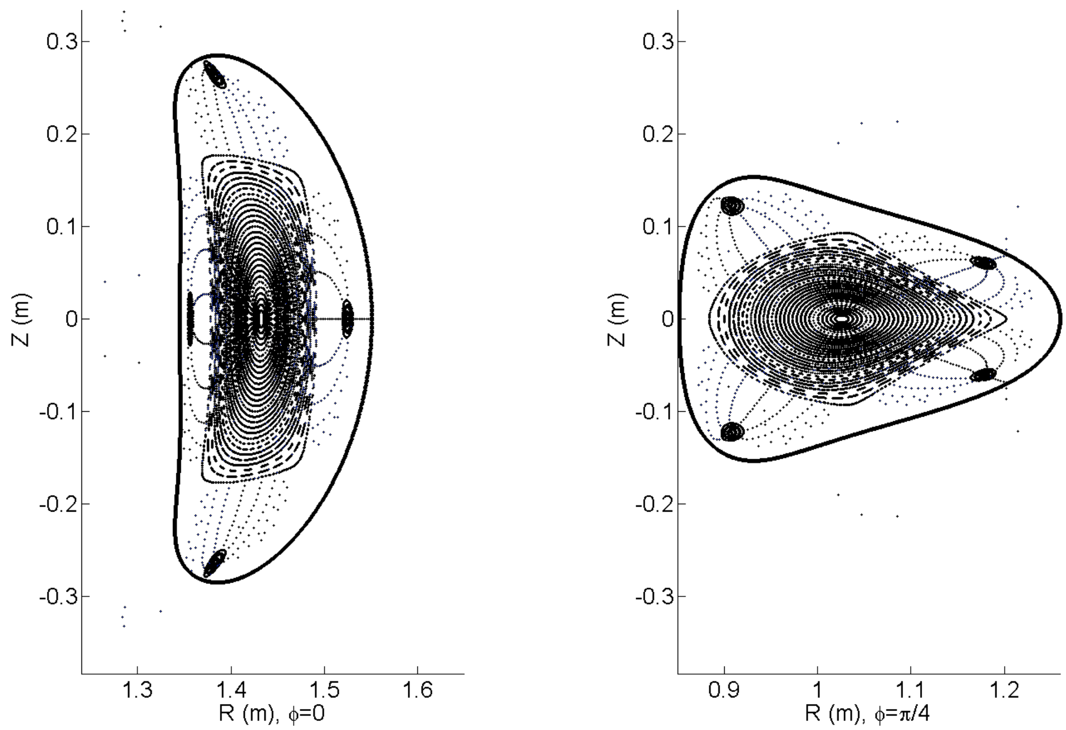

Figure A2.104: Flux Surfaces in 12% Hill configuration (ι<1 inside LCFS)

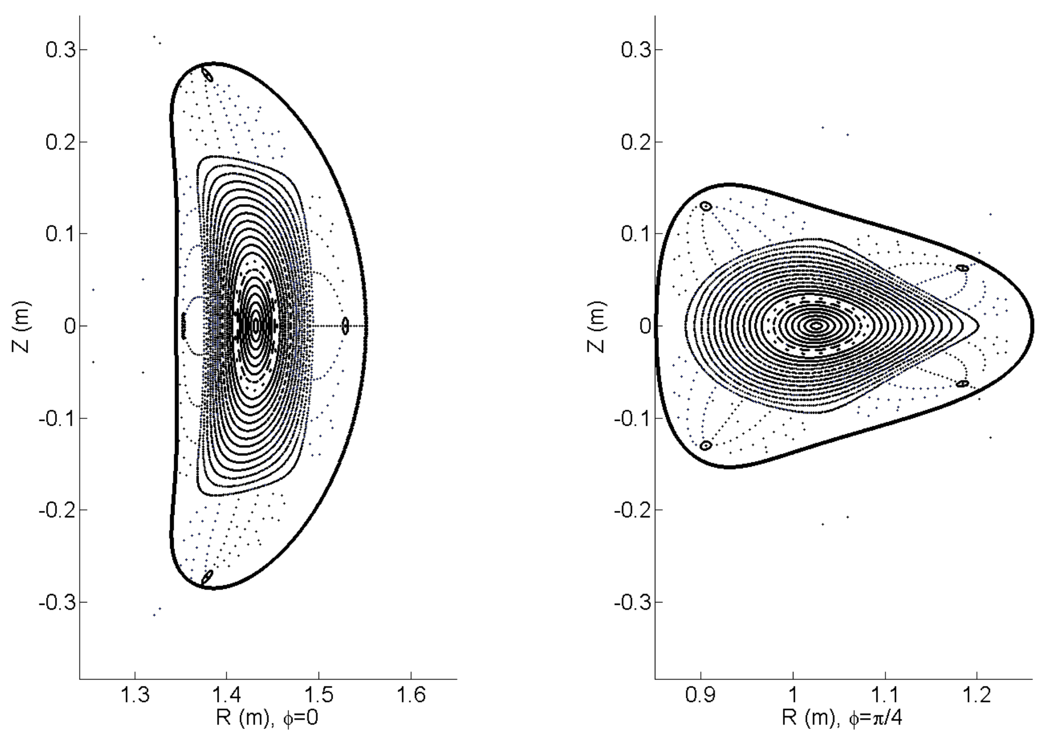

Figure A2.105: Flux Surfaces in 13% Hill configuration (ι<1 inside LCFS)

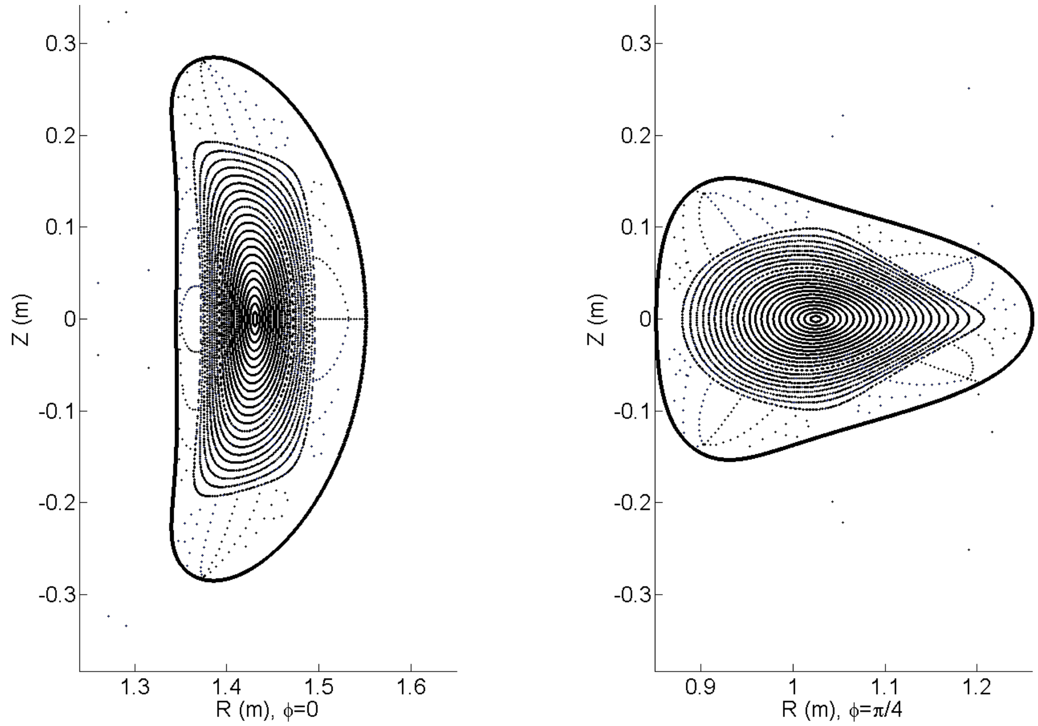

Figure A2.106: Flux Surfaces in 14% Hill configuration (ι<1 inside LCFS)

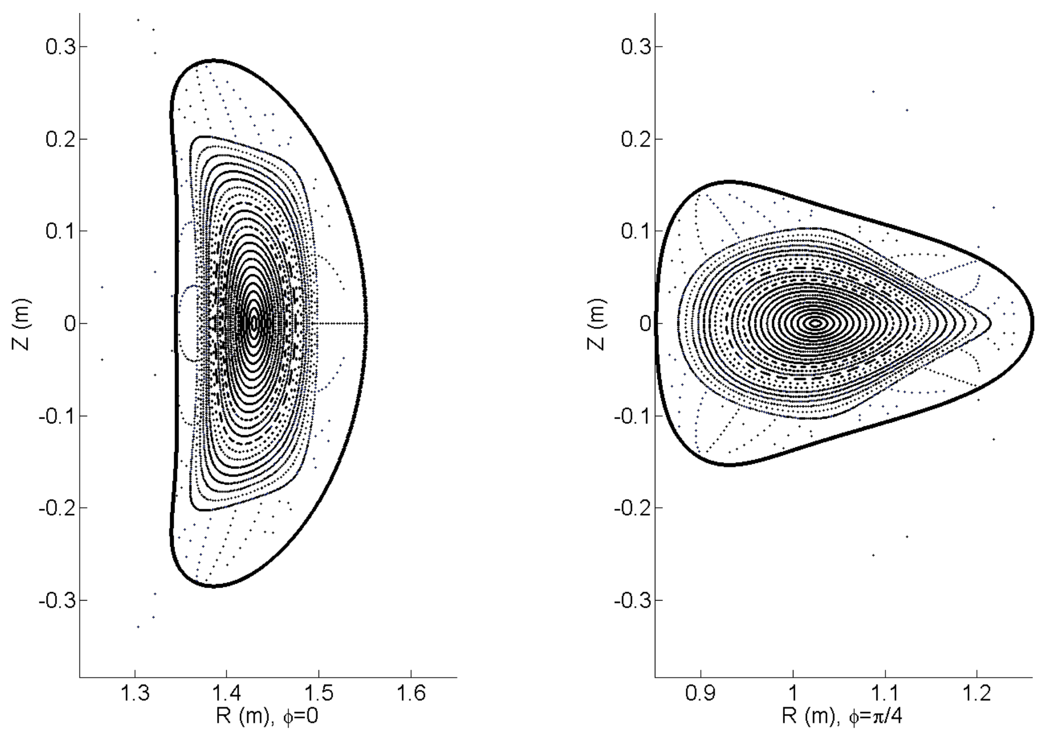

Figure A2.106: Flux Surfaces in 15% Hill configuration (ι<1 inside LCFS)

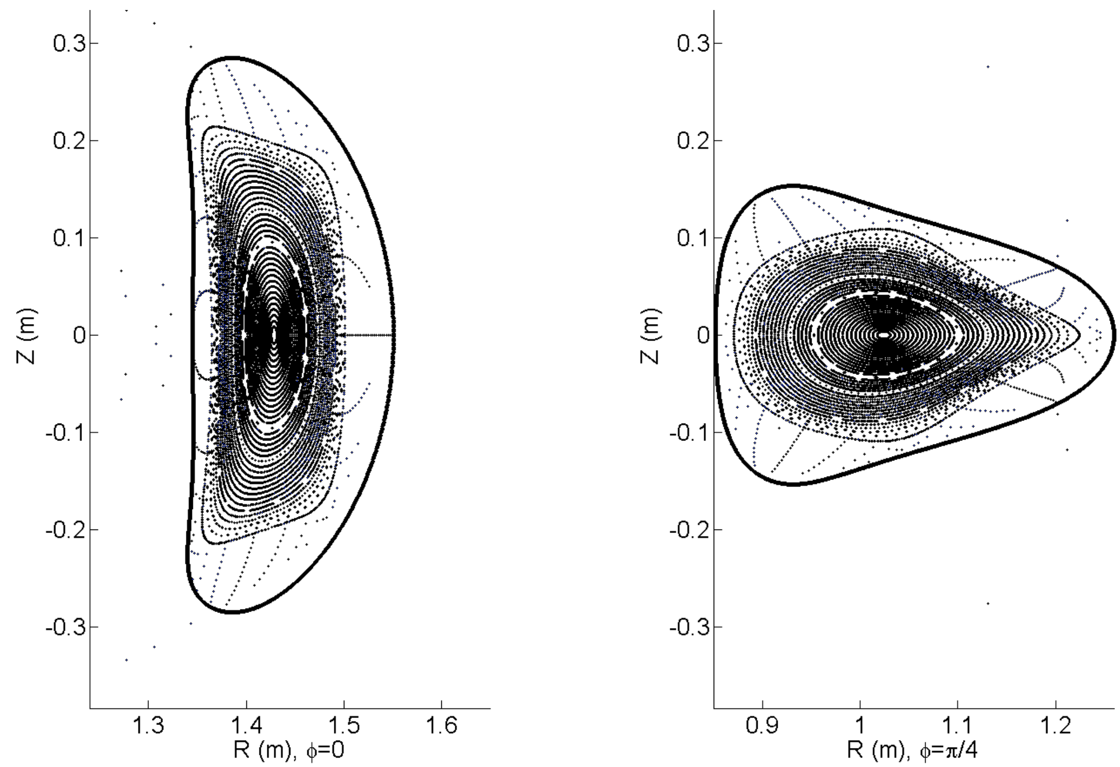

Figure A2.107: Flux Surfaces in 16% Hill configuration (ɨ<1 inside LCFS)

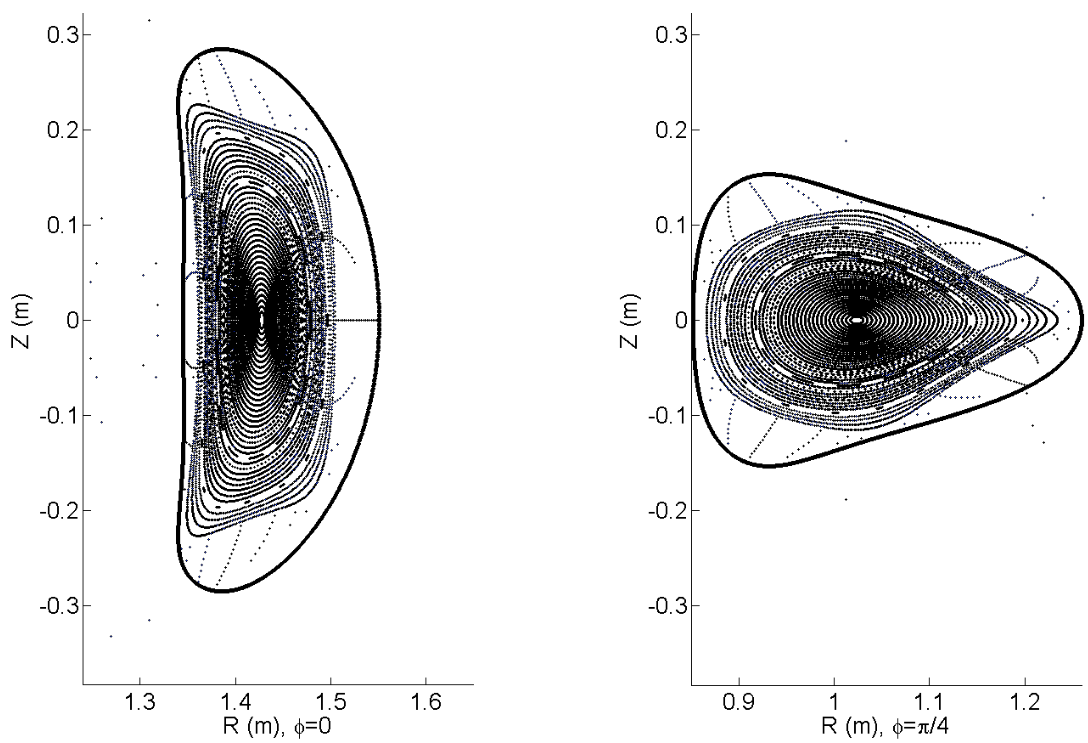

Figure A2.108: Flux Surfaces in 17% Hill configuration (ɨ<1 inside LCFS)

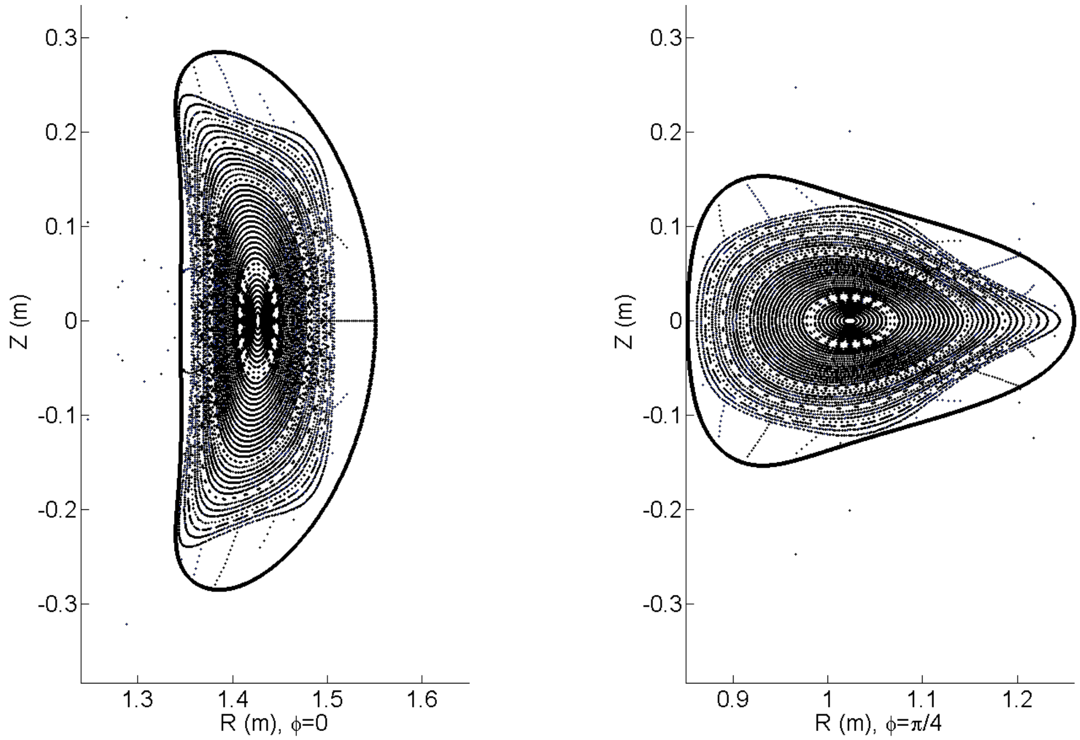

Figure A2.109: Flux Surfaces in 18% Hill configuration (ι<1 inside LCFS)

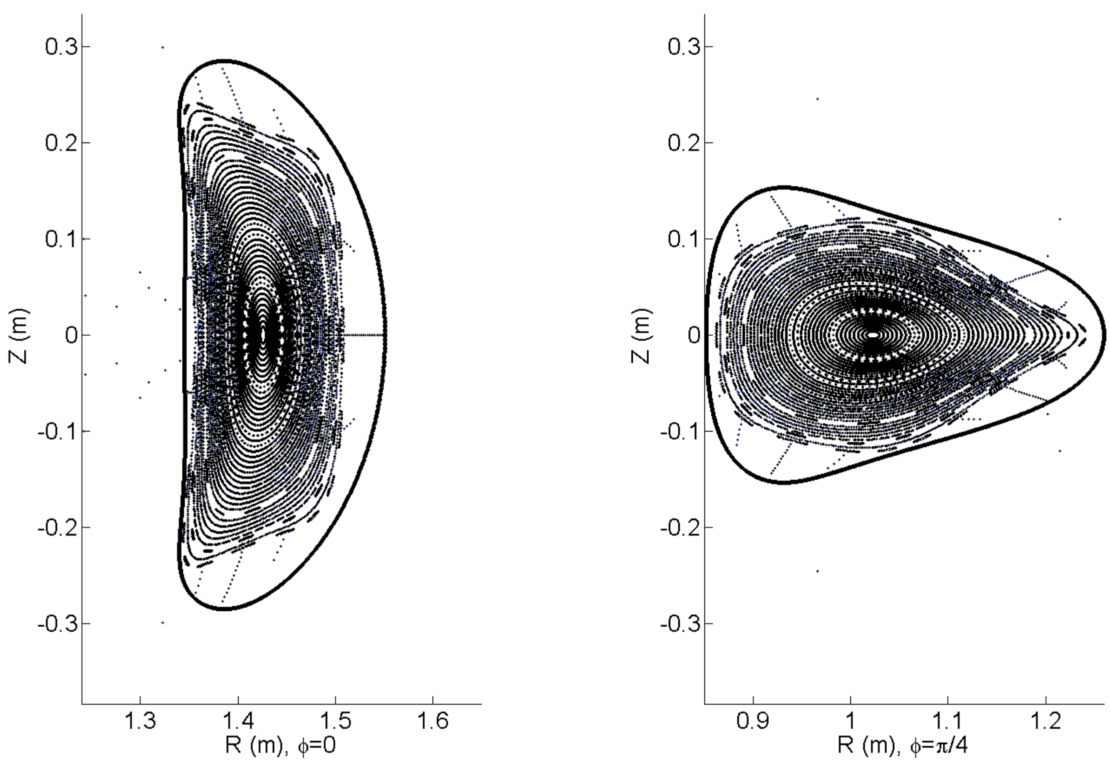

Figure A2.110: Flux Surfaces in 19% Hill configuration (ι<1 inside LCFS)

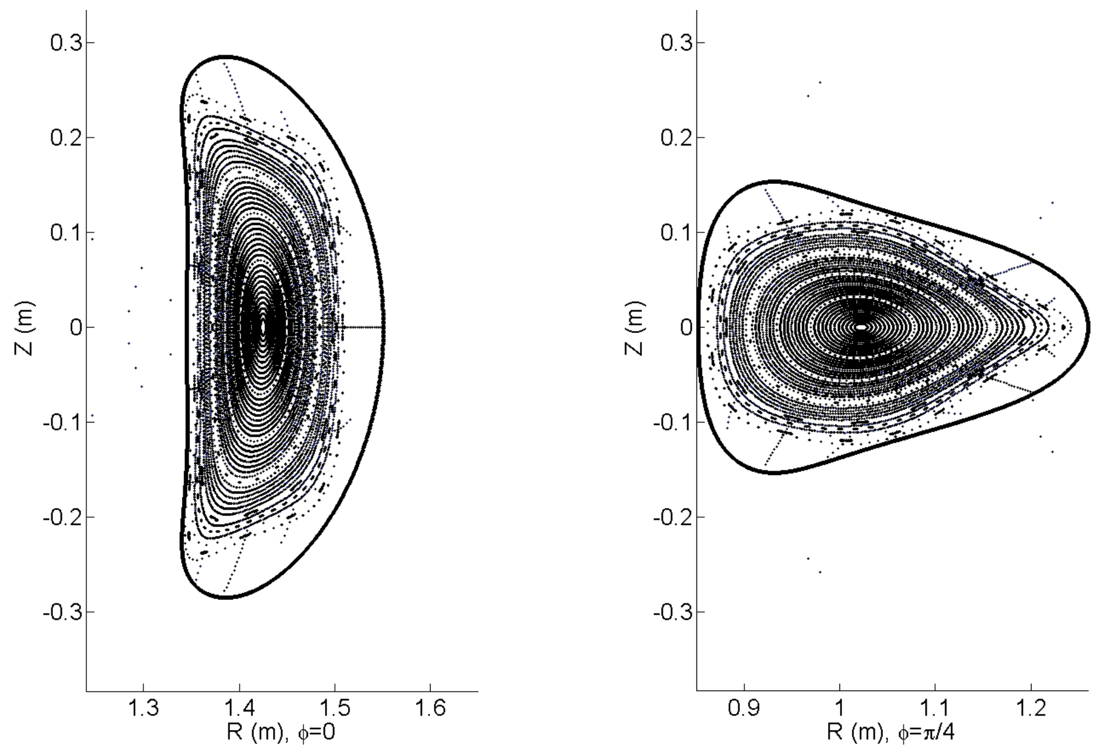

Figure A2.111: Flux Surfaces in 20% Hill configuration (ι<1 inside LCFS)

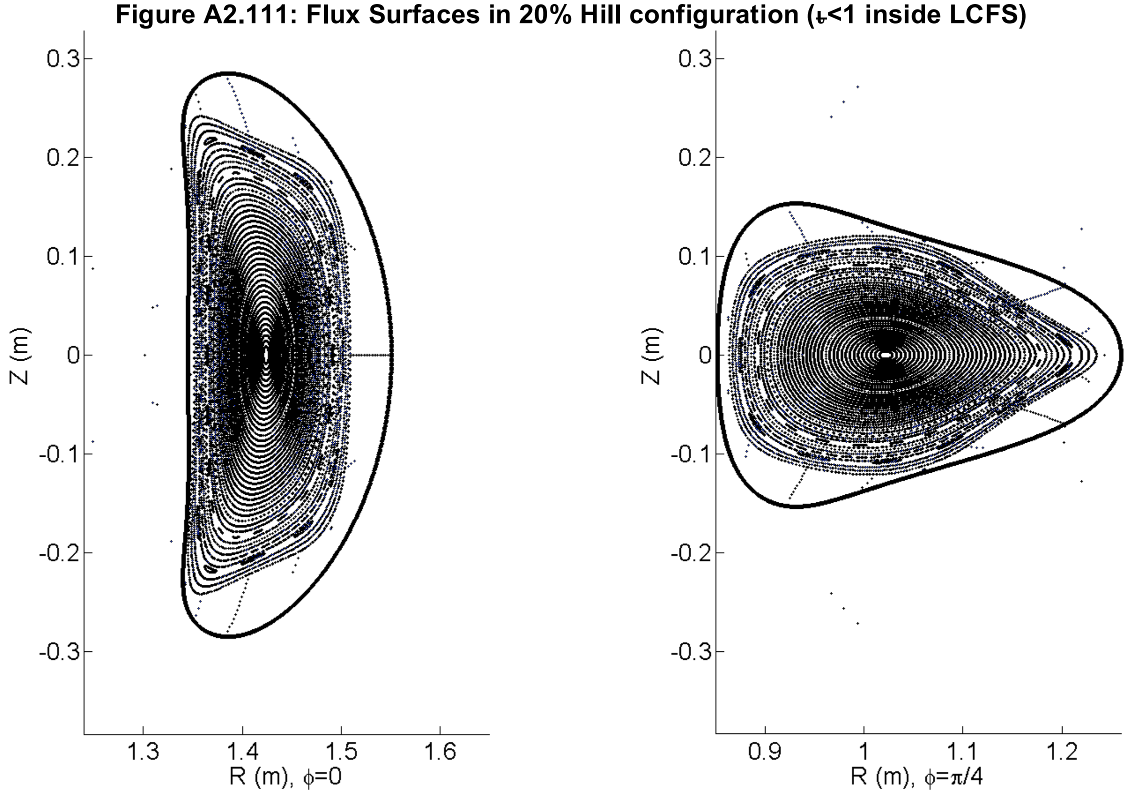

Figure A2.112: Flux Surfaces in 21% Hill configuration (ι<1 inside LCFS)

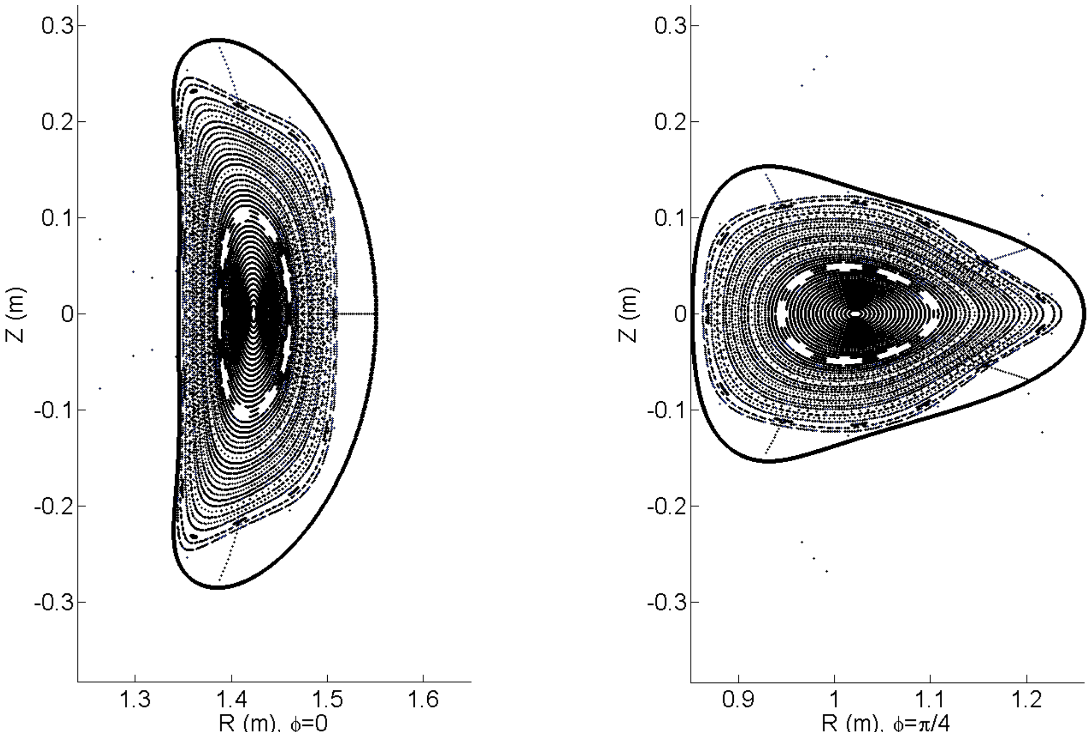

Figure A2.113: Flux Surfaces in 22% Hill configuration (ι<1 inside LCFS)

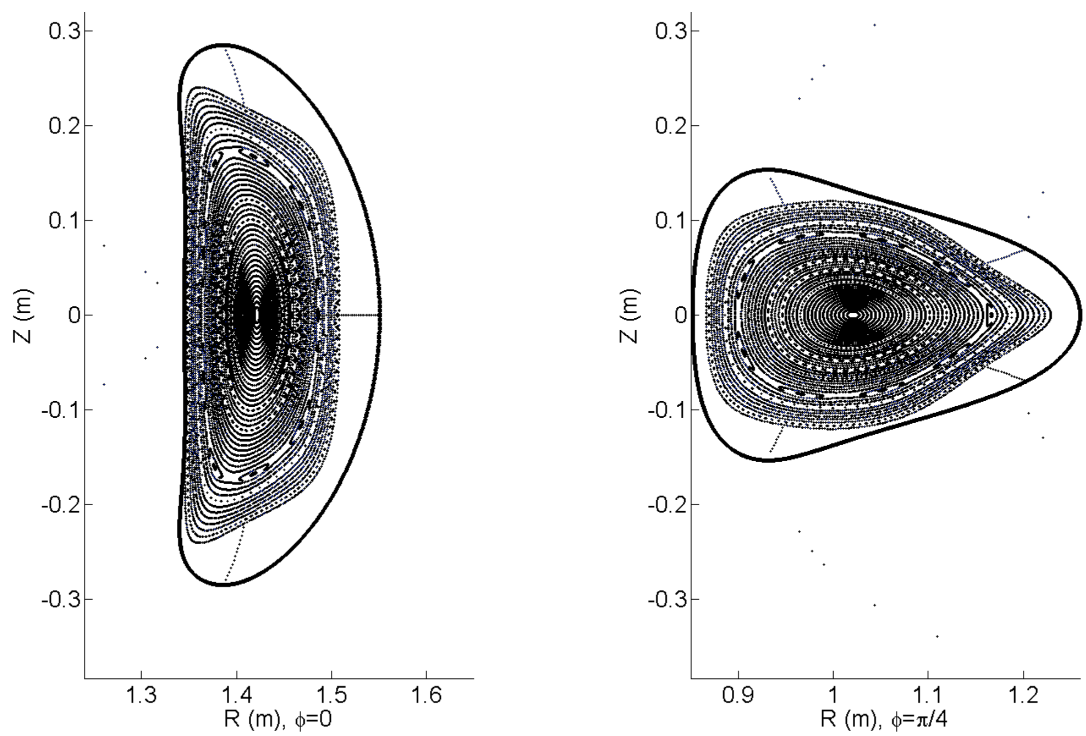

Figure A2.114: Flux Surfaces in 24% Hill configuration (ι<1 inside LCFS)

A2.4 The Type 2 and 3 Mirror configurations.

These are configurations where mirror spectral components (those with poloidal mode number m=0) are excited with toroidal mode numbers n> 4. As illustrated in Appendix 5, at fixed amp-turn percentage, these configurations are not as efficient at exciting symmetry breaking terms as the more standard Type 1 Mirror. The information on these configurations is included here as a matter of completeness.

Amp Turns %	R_{axis}, BP (m)	R_{axis}, JF (m)	R_{edge} (m)	I_{main} (A)	I_{aux} (A)
2.5	1.4446	1.0311	1.5136	5321	186
5	1.4438	1.0303	1.5138	5282	370
7.5	1.4431	1.0295	1.5122	5245	551
10	1.4423	1.0287	1.5093	5207	729
12.5	1.4416	1.0279	-1.0000	5170	905
15	1.4408	1.0270	1.5058	5134	1078
17.5	1.4401	1.0262	-1.0000	5098	1249
20	1.4394	1.0254	1.5004	5063	1418
0	1.4454	1.0320	1.5161	5361	0
-2.5	1.4461	1.0327	-1.0000	5401	-189
-5	1.4469	1.0335	-1.0000	5442	-381
-7.5	1.4478	1.0343	-1.0000	5483	-576
-10	1.4486	1.0351	-1.0000	5526	-774
-12.5	1.4494	1.0359	-1.0000	5569	-975
-15	1.4502	1.0367	-1.0000	5612	-1179
-17.5	1.4511	1.0376	-1.0000	5658	-1386
-20	1.4520	1.0383	-1.0000	5703	-1597

Table A2.17: Axis locations, plasma edge, and central resonant currents, for the Type 2 Mirror continuum.

Amp Turns %	Boundary Flux (Tm^2)	ɨ(0)	ɨ(0)	Volume ($dV/d\psi$) (m^3)	Volume (MC) (m^3)
2.5	0.0206	1.5125	1.1088	0.370	-1
5	0.0209	1.0525	1.1155	0.378	-1
7.5	0.0207	1.0536	1.1185	0.376	-1
10	0.0199	1.0560	1.1160	0.366	-1
12.5	-1.0000	-1.0000	-1.0000	-1.000	-1
15	0.0194	1.0570	1.1226	0.361	-1
17.5	-1.0000	-1.0000	-1.0000	-1.000	-1
20	0.0180	1.0593	0.1120	0.338	-1
0	0.0212	1.0500	1.1091	0.378	0.381
-2.5	-1.0000	-1.0000	-1.0000	-1.000	-1
-5	-1.0000	-1.0000	-1.0000	-1.000	-1
-7.5	-1.0000	-1.0000	-1.0000	-1.000	-1
-10	-1.0000	-1.0000	-1.0000	-1.000	-1
-12.5	-1.0000	-1.0000	-1.0000	-1.000	-1
-15	-1.0000	-1.0000	-1.0000	-1.000	-1
-17.5	-1.0000	-1.0000	-1.0000	-1.000	-1
-20	-1.0000	-1.0000	-1.0000	-1.000	-1

Table A2.18: Boundary flux, rotational transform, and volume information for Type 2 Mirror continuum of configurations.

Amp Turns %	R_{axis}, BP (m)	R_{axis}, JF (m)	R_{edge} (m)	I_{main} (A)	I_{aux} (A)
2.5	1.4451	1.0316	1.5151	5341	187
5	1.4448	1.0313	1.5129	5321	372
7.5	1.4445	1.0310	1.5135	5302	557
10	1.4443	1.0308	1.5127	5282	739
12.5	1.4440	1.0304	-1.0000	5263	921
15	1.4438	1.0301	1.5104	5244	1101
17.5	1.4435	1.0299	-1.0000	5226	1280
20	1.4433	1.0296	1.5101	5207	1458
0	1.4454	1.0320	1.5161	5361	0
-2.5	1.4456	1.0322	-1.0000	5381	-188
-5	1.4459	1.0325	1.5176	5401	-378
-7.5	1.4462	1.0328	-1.0000	5422	-569
-10	1.4465	1.0331	-1.0000	5442	-762
-12.5	1.4467	1.0334	-1.0000	5463	-956
-15	1.4470	1.0337	1.5204	5484	-1152
-17.5	1.4473	1.0340	-1.0000	5505	-1349
-20	1.4476	1.0343	-1.0000	5527	-1548

Table A2.19: Axis locations, plasma edge, and central resonant currents, for the Type 3 Mirror continuum.

Amp Turns %	Boundary Flux (Tm^2)	ɨ(0)	ɨ(0)	Volume ($dV/d\psi$) (m^3)	Volume (MC) (m^3)
2.5	0.0210	1.0499	1.1079	0.375	-1.000
5	0.0201	1.0500	1.1030	0.360	-1.000
7.5	0.0207	1.0498	1.1076	0.372	-1.000
10	0.0205	1.0499	1.1086	0.371	-1.000
12.5	-1.000	-1.000	-1.000	-1.000	-1.000
15	0.0199	1.0499	1.1035	0.361	-1.000
17.5	-1.000	-1.000	-1.000	-1.000	-1.000
20	0.0203	1.0499	1.1100	0.371	-1.000
0	0.0212	1.0500	1.1091	0.378	0.381
-2.5	-1.000	-1.000	-1.000	-1.000	-1.000
-5	0.0215	1.0507	-1.000	0.353	-1.000
-7.5	-1.000	-1.000	-1.000	-1.000	-1.000
-10	-1.000	-1.000	-1.000	-1.000	-1.000
-12.5	-1.000	-1.000	-1.000	-1.000	-1.000
-15	0.0222	1.0500	1.1077	0.378	-1.000
-17.5	-1.000	-1.000	-1.000	-1.000	-1.000
-20	-1.000	-1.000	-1.000	-1.000	-1.000

Table A2.20: Boundary flux, rotational transform, and volume information for Type 3 Mirror continuum of configurations.

[1] U. Stroth, Plasma Phys. Control. Fusion **40**, 9 (1998)